NASA Contractor Report 163103

NASA-CR-163103
19810005991

ASSESSMENT OF THE VISIBILITY IMPAIRMENT CAUSED BY THE EMISSIONS FROM THE PROPOSED POWER PLANT AT BORON, CALIFORNIA

R. W. Bergstrom
J. R. Doyle
C. D. Johnson
H. Y. Holman
M. A. Wojcik

December 1980

NAS4-2745

NASA

NASA Contractor Report 163103

ASSESSMENT OF THE VISIBILITY IMPAIRMENT CAUSED BY THE EMISSIONS FROM THE PROPOSED POWER PLANT AT BORON, CALIFORNIA

R. W. Bergstrom
J. R. Doyle
C. D. Johnson
H. Y. Holman
M. A. Wojcik

Systems Applications, Incorporated
San Rafael, California

Prepared for
Dryden Flight Research Center

National Aeronautics and
Space Administration

1980

Intentionally Left Blank

ACKNOWLEDGMENTS

Without the efforts of the following personnel in compiling the input meteorological data and coordinating with Systems Applications Incorporated the study could not have been accomplished:

Major Dennis Bielick--Air Force Flight Test Center, Edwards Air Force Base, California

L. J. Ehernberger--NASA Dryden Flight Research Center, Edwards, California

Tony VanCuren--Naval Weapons Center, China Lake, California

Intentionally Left Blank

CONTENTS

ILLUSTRATIONS

TABLES

1 INTRODUCTION

The visual impact of air pollution is currently, and potentially will be, a significant nuisance in many areas of the country. Areas of particular importance are those in which the scenic beauty of a vista within a national park, wilderness area, or other class I area is considered a natural resource. In the 1977 Clean Air Act Amendments, Congress declared as a national goal "the prevention of any future, and the remedying of any existing, impairment of visibility in mandatory class I federal areas, which impairment results from man-made air pollution." This legislation spurred research into the understanding and prediction of visibility impairment caused by air pollution.

In addition to the national goal for controlling visibility impairment, the California Air Resources Board has adopted a statewide visibility standard, establishing a minimum acceptable visual range (10 km in all areas except the Tahoe basin) for conditions in which man-made pollutants may significantly contribute to visibility impairment. The potential impact of a project on visibility is normally reviewed against this state standard. However, in certain cases, concerns about adverse economic and social effects, as well as land use compatibility, may present cause for further consideration of visibility impairment.

In the case of the proposed California Coal Project (Boron site electric generating facility), concerns arise regarding economic loss and land use compatibility with national defense operations in the upper Mojave Desert. The Mojave Desert is a region in which the clarity of the atmosphere is of particular importance. The China Lake Naval Weapons Center, Edwards Air Force Base, and NASA Dryden Flight Research Test Center utilize the good visibility of the area for their operations. The size and complexity of the these federal installations, good visibility (i.e., visual range frequently exceeding 100 km), and the existence of large, dry lake beds for aircraft operations make the area a unique and irreplaceable national defense and space testing resource.

The visibility needs of the aircraft, weapons, and space testing operations vary. However, it is estimated that a 50-mile (90 km) visual range is needed for the testing of weapons systems and that tests using sensitive cameras cannot be performed at all when visibility is as low as

33 miles (53 km) (testimony of Carl Koiner, 1980). Excellent visibility is also required for pilot training and testing at Edwards Air Force Base and the testing of experimental space vehicles at NASA Dryden. Therefore, the visibility impact of the proposed Boron site electric generating station must be evaluated in light of concerns that go beyond established federal and state visual air quality requirements and are of importance because of potential economic, social, and land use compatibility considerations.

1.1 OBJECTIVES OF STUDY

The principal objective of this study is to estimate the visibility impairment that would be caused by the proposed Southern California Edison (SCE) 1500 MWe coal-fired power plant at the Boron site in the upper Mojave Desert. The proposed plant location, the surrounding topographic features, and the boundaries of the existing federal installations are shown in figure 1. As exhibited here, the potential for visibility impairment to operations within the federal installations involves a number of possible plume transport directions. In estimating the potential for visibility impairment, we first consider the frequency of occurrence of meteorological conditions that could result in transport of the plume to the viewing area. We then perform a generic evaluation of the visibility impairment that might be caused by facilities of a similar or smaller size located in the upper Mojave Desert. We perform this analysis to provide representative estimates of the potential for visibility impairment given the meteorological conditions, background ambient air quality, and background visual range of this desert region. Finally, we estimate plume visibility impairment for two specific viewing conditions to provide an assessment of the possible impacts of the proposed facility.

1.2 THE CAUSES OF VISIBILITY IMPAIRMENT

As indicated schematically in figure 2, visibility impairment is caused by the following interactions in the atmosphere:

- Light scattering
  - By molecules of air
  - By particles
- Light absorption

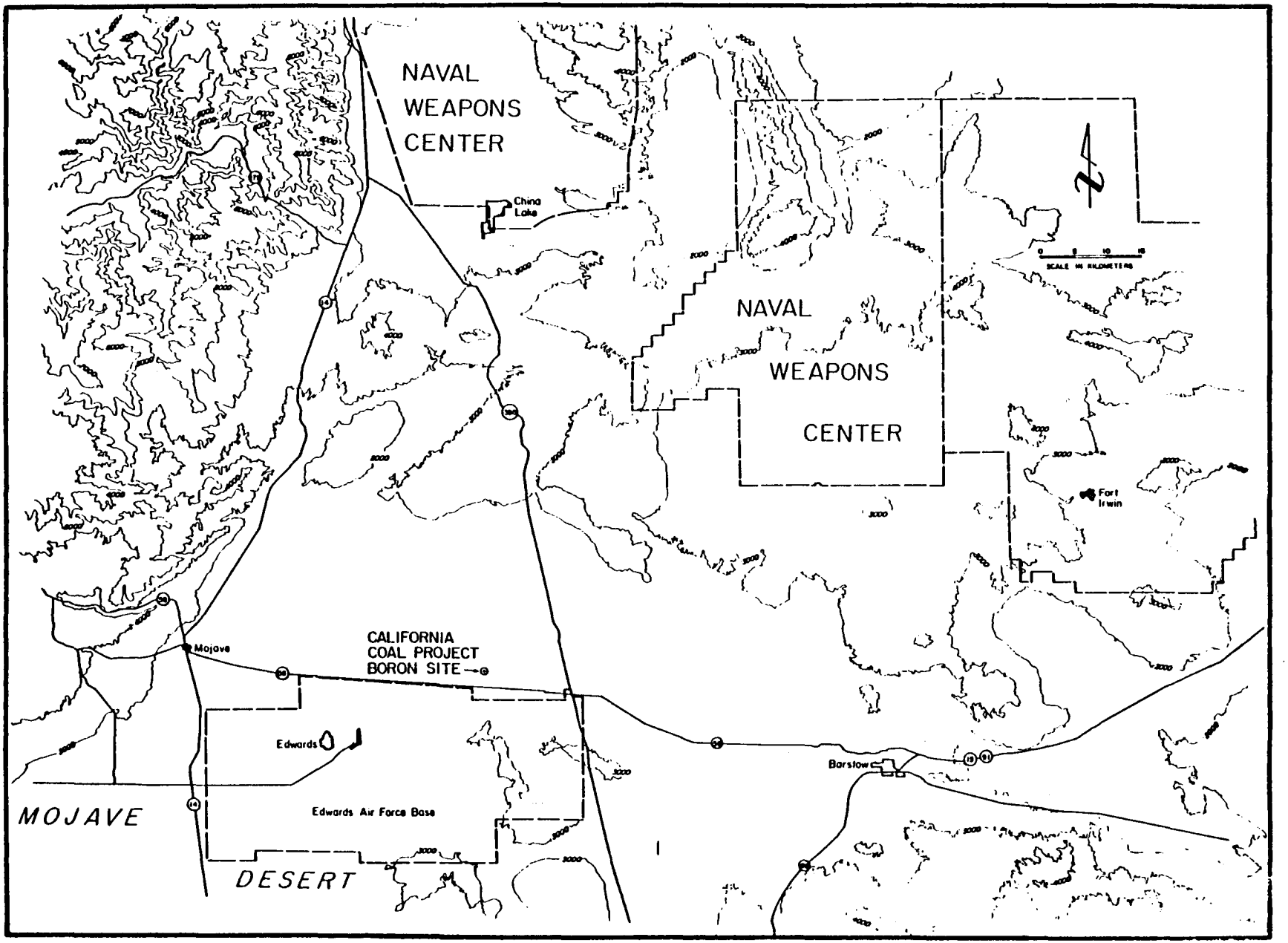

FIGURE 1. MAP OF THE STUDY AREA

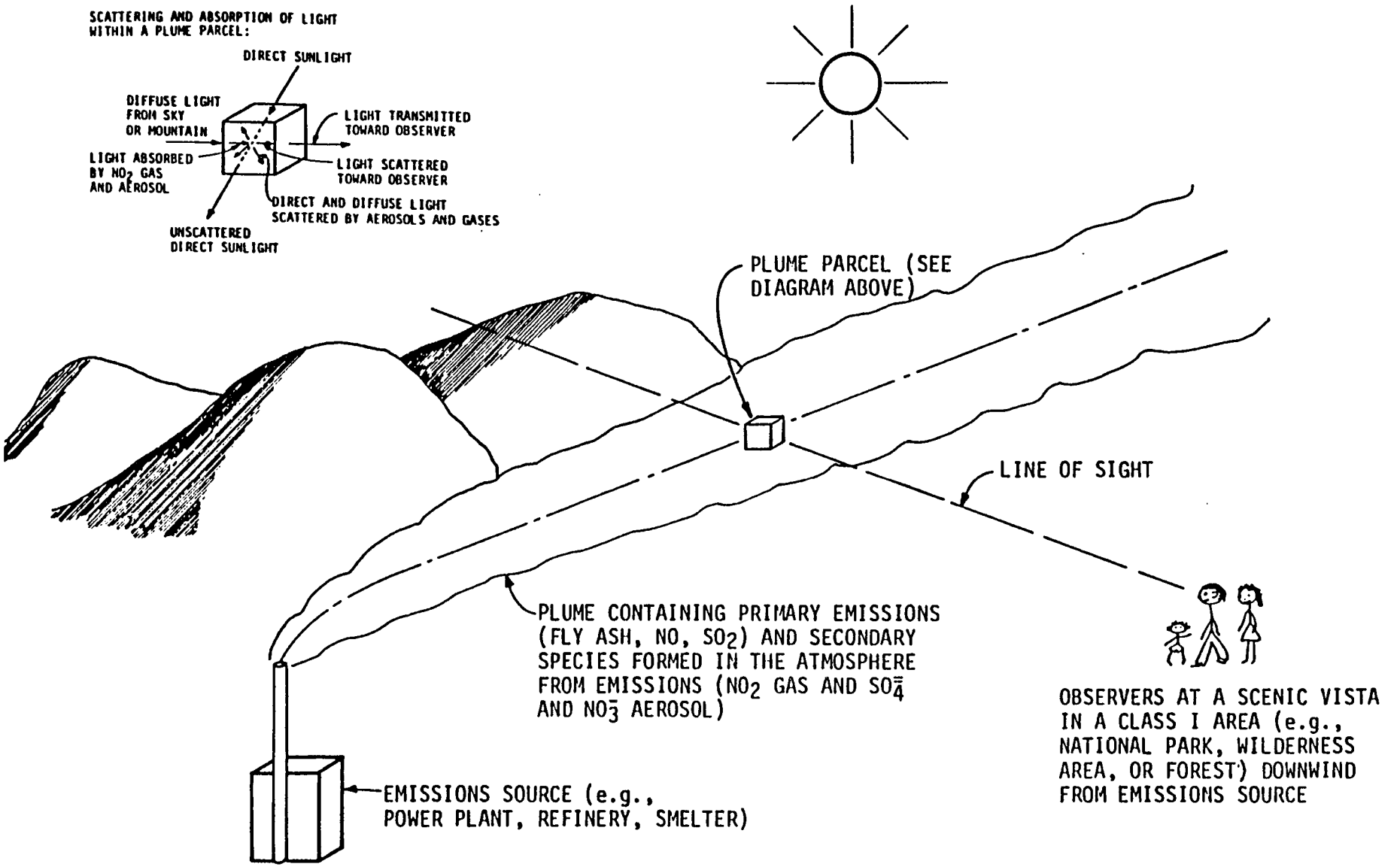

FIGURE 2. SCHEMATIC OF VISIBILITY IMPAIRMENT CAUSED BY AIR POLLUTION IN CLASS I AREAS

- By gases

- By particles.

The scattering of light by very small particles such as gaseous molecules of air (Rayleigh scattering), which causes the blue color of the atmosphere, is dominant when the air is relatively free of aerosols and light-absorbing gases. Fine solid or liquid particulates, whose diameters range from 0.1 to 1.0 μm (the most effective size per unit mass in scattering light), account for most atmospheric light scattering. Light scattering by larger particles is the most important mechanism of visual range reductions. Light absorption by gases is particularly important in the discussion of visibility impairment because nitrogen dioxide, a major constituent of power plant plumes, absorbs light. Nitrogen dioxide is reddish-brown because it absorbs strongly at the blue end of the visible spectrum while it allows light at the red end to pass through. Light absorption by particles becomes important when black soot (elemental carbon) or any other strong absorber of visible light is present. However, most atmospheric particles are not significantly visible light absorbers.

Man-made contributions to visibility impairment result from the emission of primary particulate matter (such as fly ash, acid or water droplets, soot and other combustion-derived organics, and fugitive dust) and of pollutant precursors that are converted in the atmosphere to the following secondary species:

> Nitrogen dioxide (NO_2) gas, from emissions of nitric oxide (NO).

> Sulfate ($SO_4^=$) particles, from SO_x emissions.

> Nitrate (NO_3^-) particles, from NO_x emissions.

> Organic particles, from hydrocarbon and NO_x emissions.

Coal-fired power plants emit primary particles of fly ash and combustion-generated particulates to the atmosphere. Before highly efficient particulate control technology was commonly employed, primary particulate matter, such as smoke, windblown dust, and soot, was a major contributor to visibility impairment. If coal-fired plants are equipped with efficient precipitators or other abatement equipment, the emissions rate of primary particles may be small. However, some emissions escape the control equipment; this contributes to ambient particulate concentrations and hence to general visibility impairment. If the emissions rate of primary particulates is sufficiently large, the plume itself may be visible.

In the past, as a result of their high rate of emissions of primary particulate matter, many older coal-fired power plants generated visibly conspicuous plumes. Both new plants and old plants still in operation have benefited from more efficient particulate abatement equipment and a more advanced state of the art. At this point, it is common to specify and achieve particulate removal efficiency in excess of 99 percent. In addition, with the installation of flue gas desulfurization systems (scrubbers) and boiler combustion modifications, emissions of sulfur dioxide and nitrogen oxide have also been reduced. As a result, the visual impact of power plant plumes has been sharply reduced, as evidenced by the nearly invisible plumes of modern coal-fired power plants. Unfortunately, however, the contribution to visibility impairment of secondary pollutants--nitrogen dioxide gas and sulfate, nitrate, and organic aerosol--is becoming increasingly evident.

Since nitrogen dioxide absorbs light selectively, it can discolor the atmosphere, causing a yellow or brown plume when it is present in sufficient concentrations. Almost all of the nitrogen oxide emitted from power plant stacks is nitric oxide, a colorless gas, but chemical reactions in the atmosphere can oxidize a substantial portion of the colorless NO to the reddish brown NO_2. Because they range in size between 0.1 and 1.0 μm in diameter, which is the most efficient size per unit mass for light scattering, secondary sulfate, nitrate, and organic particles have a dominating effect on visual range in many situations. Submicron particles (with diameters in the range from 0.1 to 1.0 μm) are 10 times more effective in light scattering than the same mass of coarse (>1 μm) particles.

The effect of the intervening atmosphere on the visibility and coloration of a viewed object (e.g., the horizon sky, a mountain, or a cloud) can be calculated by solving the radiation transfer equation along the line of sight. Visibility impairment can be quantified by comparing the intensity or the coloration of two objects (e.g., a distant mountain against the horizon sky). The effect of the intervening atmosphere on the viewed object's light intensity, as a function of wavelength $[I(\lambda)]$, can be determined if the concentration and characteristics of air molecules, aerosol, and nitrogen dioxide along the line of sight are known.

The assessment of the visual impact of an emissions source involves the prediction of the concentrations of substances resulting from the emissions and the calculation of the resulting effect on the radiative transfer in the atmosphere.

1.3 REPORT ORGANIZATION

This report is divided into three main sections. The first, chapter 2, is an overview of the visibility model and an analysis of the meteorological conditions that supply the inputs to the model. The second part, chapter 3, is an analysis of the visibility impact that might occur from the proposed power plant under a range of possible meteorological and emissions conditions. In this section we show that substantial visual impacts would occur for a large range of conditions. The third part is an analysis of two specific observer locations and the impact of the plume on target perceptibility. We indicate in this section that the impact on target perceptibility is a function of observer-plume-target geometry as well as sun angle and target reflectance. Impacts could range from complete masking of the target to a 10 percent reduction in color perceptibility.

2 TECHNICAL APPROACH AND ASSUMPTIONS

In this chapter we discuss the general model features and the approach and assumptions used in this study.

2.1 THE VISIBILITY MODEL

This discussion briefly summarizes the main features of SAI's visibility models. The technical details of the models are presented in the appendix , which is reproduced from SAI's recent report to the EPA, "User's Manual for the Plume Visibility Model (PLUVUE)" (Johnson et al., 1980).

Modeling of visibility impairment requires mathematical descriptions for the following physical and chemical atmospheric processes in succession:

> Emissions.

> Pollutant transport, diffusion, and removal.

> Chemical reactions and physical transformations of precursors in the atmosphere.

> Light scattering and absorption properties of aerosols and gases resulting from precursors.

> Radiative transfer through aerosols and gases along different lines of sight.

Two different types of models have been developed by SAI. The Gaussian plume model used in this study is designed to calculate the visual impact of emissions from a single point source at downwind distances on the order of 100 km. The regional grid model is designed to calculate the visual impact resulting from multiple sources over several days within a 1000 km x 1000 km region.

Distinctly different problems are handled by plume and regional visibility models. At distances as far as approximately 100 km from a point source such as a power plant, a plume itself may be perceptible because it is colored differently or is darker or brighter than the background. In such cases, the visual impact is not the result of a reduction in visual range (though this may occur), but rather of atmospheric discoloration in a well-defined plume. Beyond about 100 km downwind, however, individual plumes become uniformly dispersed in the vertical direction within the mixed layer and are no longer distinguishable as plumes. On a regional scale, visual impact is caused by a general haziness, due to reduced visual range, and a uniformly colored haze.

The plume model used in this study is an improved version of the one originally developed for the EPA (Latimer et al., 1978), which was used by Southern California Edison for its visibility assessment of the Boron site (Bury et al., 1980). The major improvement is the inclusion of more detailed secondary particle formation.

Sulfuric acid and sulfates are produced by the oxidation of sulfur dioxide in one of two general processes:

> Homogeneous oxidation of SO_2 by free radicals, probably OH•, which are generated by photochemical activity.

> Heterogeneous absorption of SO_2 on water droplets and on catalytic metal ions or unsaturated hydrocarbon particles.

For clean background areas, such as those often found in the Mojave Desert near the Boron site, the heterogeneous formation of $SO_4^=$ is limited due to the absence of catalytic pollutants. However, the westerly flow of pollutants from the Los Angeles region into the southwest desert region can provide sufficient levels of pollutants in the area of interest during certain periods of the year (principally summer months) so that the heterogeneous formation of sulfate might not be considered negligible.

The formation processes governing the production of nitrate aerosols are more difficult to isolate and identify than those believed to affect sulfate formation in the atmosphere. However, nitrates, like sulfates, are believed to be subject to a variety of homogeneous as well as heterogeneous reactions.

In the visibility model, the homogeneous sulfate and nitrate formation rates are calculated in a manner similar to that used to calculate NO-to-NO_2 conversion (see Latimer et al., 1978). The principal causes of SO_2-to-$SO_4^=$ and NO_2-to-HNO_3 conversions are homogeneous pollutant reactions involving the hydroxyl (OH•) free radical. Calculations of the

formation rate from these reactions are based on steady-state plume OH• concentration. This steady-state plume OH• concentration is calculated by balancing the rate of OH• production with the rate of OH• destruction. (The details of this formulation are presented in the appendix. In addition, a pseudo-first-order rate constant was used to characterize the heterogeneous formation of sulfate.

2.2 CHARACTERIZING THE MAGNITUDE OF VISIBILITY IMPAIRMENT

The final step in the modeling is the quantification of visibility impairment once the spectral light intensity, $I(\lambda)$, has been calculated for the specific lines of sight of an observer at a given location in an atmosphere with known aerosol and pollutant concentrations. Visibility impairment--including reduction in visual range, the visibility of plumes and haze layers, and atmospheric discoloration--is caused by changes in light intensity as a result of light scattering and absorption in the atmosphere.

Visibility impairment can be classified, in terms of visual effects, in the following manner:

> Coloration of objects.

  - Brightness.

  - Hue and saturation.

> Contrast and color differences between two objects.

  - Black object and horizon sky (to calculate visual range).

  - Haze layers.

  - Plume background.

The magnitude of impairment can be characterized by the reduction in visual range from some reference value, by a reduction in contrast between an object and the horizon sky at a known distance from the observer, or by a shift in coloration or light intensity of the sky or distant objects, such as clouds or terrain features, compared with what is perceived on a "clear" day. In all cases, the magnitude of visibility impairment can be characterized by the change in light intensity or coloration of an object (or part of the sky) compared with that of some reference object. For example, a distant mountain is visible because the intensity and

coloration of light from the mountain is different from that of the horizon sky.

Four parameters are generally used to characterize visibility impairment of a power plant plume:

> Percentage reduction in visual range

> Blue-red ratio

> Plume contrast

> ΔE (perceptibility).

2.2.1 Visual Range

Visual range is defined as the farthest distance at which a black object can be perceived against the horizon sky. The threshold of perception of differences between the light intensity of two objects has been characterized by a liminal contrast. The value of the liminal contrast is commonly taken to be 0.02, as first suggested by Koschmieder in 1924 (Middleton, 1952). However, the liminal contrast is a function of the observer and his state of mind (e.g., fatigue, attentiveness) as well as the intensity of the background lighting. Under the best conditions, the liminal contrast may be as low as 0.005 (Committee on Colorimetry, Optical Society of America, 1963). The Federal Aviation Administration assumes a value of 0.055. Based on an experiment using 10 observers and a total of 1000 observation hours, Middleton (1952) reported a median of 0.03 and a mode of 0.02 for the liminal contrast. For the purposes of standardization, it is reasonable to describe the perception of a "standard observer" and to select and use a single value for the liminal contrast. We used the Koschmieder value (0.02) for our calculations.

The observation of distant targets, such as mountains or airplanes, is not the same as strictly defined visual range--i.e., the farthest distance at which a black object is distinguishable from the horizon sky by a standard observer where liminal contrast is 0.02. This is true not only because of the variability in the contrast threshold, but also because distant targets, such as mountains, are usually not perfectly black. The situation in which a camera is used to photograph an aircraft, which can be represented as a black object (e.g., painted black or viewed in its own shadow), may present a more reasonable use of visual range. This situation is one of the areas of interest in this study.

The contrast between two objects at a particular wavelength is defined as:

$$C(\lambda) = \frac{I_1(\lambda) - I_2(\lambda)}{I_2(\lambda)} \quad . \qquad (1)$$

If the two objects are the same color (i.e., $(I_1[\lambda]/I_2[\lambda]$ is constant over $0.4 < \lambda < 0.7$ μm), then the contrast at all wavelengths will be the same. However, if the objects have different colors, then C is a function of wavelength. For the calculation of visual range, we evaluate the contrast at a wavelength of 0.55 μm, which is at the middle of the visible spectrum and is the wavelength to which the human eye is most sensitive. The intrinsic contrast of a black object ($I_1 = 0$) against the horizon sky ($I_2 = I_h$) is -1; the visual range is the distance at which this contrast is reduced by the light scatter and absorption of the intervening atmosphere to -0.02. Thus, visual range can be evaluated by computing contrast iteratively as a function of distance from the observer until it drops to -0.02. This approach is necessary if one is dealing with a nonhomogeneous atmosphere.

For a homogeneous atmosphere, however, the calculation of visual range is analytic, using the Koschmieder relationship:

$$r_v = \frac{3.912}{b_{ext}} \quad . \qquad (2)$$

The percentage reduction in visual range is calculated as follows:

$$1 - \frac{r_v}{r_{v0}} \cdot 100 \text{ percent} \quad , \qquad (3)$$

where r_v is the visual range for views through the plume center and r_{v0} is the visual range without the plume (ambient background visual range). In most situations, the percentage reduction in visual range is directly proportional to the integral of the plume light scattering and absorption coefficients along the line of sight and is independent of the background visual range. The percentage reduction in visual range is indicative of the haziness of objects observed through the plume. Until it is diffused, the plume will affect only a few of the observer's lines of sight; therefore, calculated visual range reduction pertains only to specific lines of sight through the plume center (perpendicular to the plume centerline) and not to prevailing visibility. The magnitude of visual range reduction is not necessarily related to the perceptibility of the plume or to atmospheric discoloration. A significant reduction in visual range could occur without a perceptible plume or atmospheric discoloration.

2.2.2 Contrast of Haze Layers and Plumes

Contrast can be used to characterize the perceptibility of a haze layer or a plume against a background--the sky, a cloud, or a distant mountain. A plume would be visible if the absolute value of the contrast between it and the background were greater than a threshold or liminal contrast. Thus, the contrast of the plume against a mountain is calculated as follows:

$$C_p = \frac{I_p - I_m}{I_m} > 0 \quad . \tag{4}$$

The plume is also visible against the horizon sky, perhaps mainly because of the color change but also because of contrast:

$$C_p = \frac{I_p - I_h}{I_h} < 0 \quad . \tag{5}$$

The magnitude and the sign of the contrast of a haze layer or plume against a background is therefore a useful way to characterize visibility impairment. Positive contrasts refer to plumes brighter than the background, whereas negative contrasts refer to plumes darker than the background. We do not have any experimental data for liminal contrast (the barely perceptible threshold contrast) in the case of a plume against a background. The same liminal contrast used to define visual range (0.02) could be used to define plume visibility. However, it seems likely that the liminal contrast for plumes is greater than 0.02, because in many cases the boundary between a plume and the background is not distinct owing to the nature of plume dilution.

2.2.3 Blue-Red Ratio

Contrast of plumes can be evaluated at several different wavelengths; we use 0.55 μm for the evaluation of plume contrast. However, plume contrast may be greater at the blue end of the visible spectrum. Latimer and Samuelsen (1975, 1978) used the ratio of plume to background intensities at the blue end (λ = 0.4 μm) and at the red end (λ = 0.7 μm) as a means of characterizing the wavelength-dependent plume contrast and plume coloration with respect to the background. This blue-red luminance ratio is defined as

$$R = \frac{I_p(0.4\ \mu m)/I_h(0.4\ \mu m)}{I_p(0.7\ \mu m)/I_h(0.7\ \mu m)} = \frac{C_p(0.4\ \mu m) + 1}{C_p(0.7\ \mu m) + 1} \quad . \tag{6}$$

The use of the blue-red ratio in conjunction with the plume contrast at 0.55 μm is a simple way of characterizing plume color. When $R > 1$, the plume is more blue than the background; when $R < 1$, the plume is redder (or more yellow-brown); when $R = 1$, with C_p (0.55 μm) > 0, the plume is a brighter white than the horizon; and with C_p (0.55 μm) < 0, the plume is a darker gray. We discuss more sophisticated methods of quantifying color in the next subsection.

2.2.4 Color

The color associated with a given spectral light intensity distribution results from processes occurring in the human eye. The retina has three different frequency sensors that convert signals into color sensations by means of the brain. The system operates so that an object that reflects half blue light and half yellow light is identified not as yellow-blue, but rather as a new color, green. This attribute of the eye-brain system gives rise to another mode of detecting an object, that of color change or discoloration. Thus, an object can be perceived because it has a different brightness at a particular wavelength from that of the background (contrast) or because it has a different color (so-called color contrast). Gases and particles in the atmosphere can give rise to coloration by their scattered light (blue sky or white clouds) or by altering the color of objects seen through them (brown coloration caused by NO_2).

The chromaticity diagram was developed to quantify the concept of color. In such a diagram, the spectral distribution of light is weighted with three functions corresponding to the detectors in the eye. For any distribution of light, there are three numbers that define a point in space. Next, the projection of the point onto a unit plane ($x + y + z = 1$) is computed. The result is a two-dimensional surface called a chromaticity diagram (see figure 3). Monochromatic light forms the outside of the surface, and white light is located in the center. Any color can thus be represented by its chromaticity coordinates (x,y), which are defined by:

$$x = \frac{X}{X + Y + Z} \quad ; \quad y = \frac{Y}{X + Y + Z} \quad , \tag{7}$$

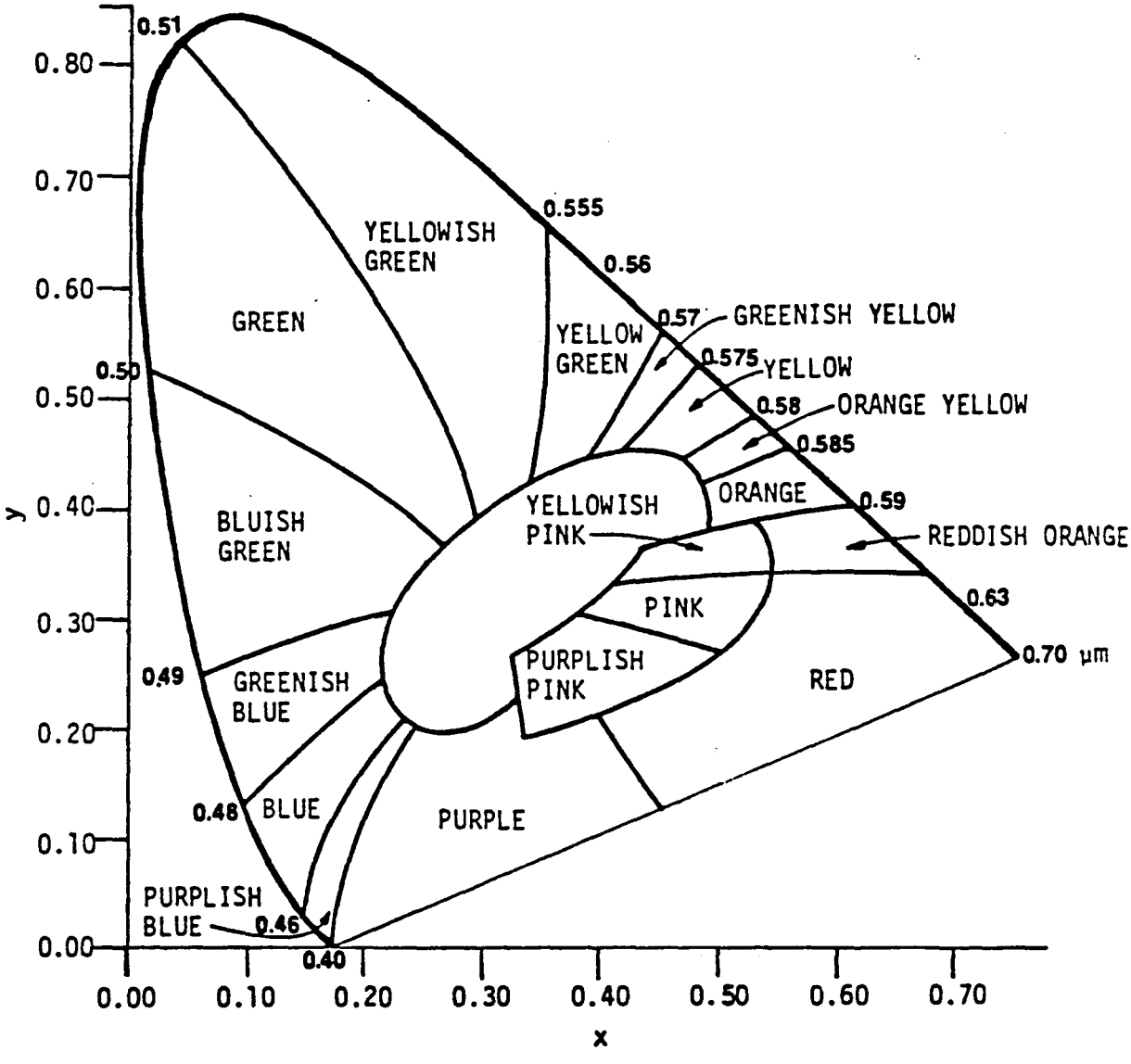

FIGURE 3. CHROMATICITY DIAGRAM

where

$$X = \int_{\lambda} I(\lambda)\ \bar{x}\ d\lambda \quad ,$$

$$Y = \int_{\lambda} I(\lambda)\ \bar{y}\ d\lambda \quad ,$$

$$Z = \int_{\lambda} I(\lambda)\ \bar{z}\ d\lambda \quad ,$$

and I (λ) is the wavelength distribution of light and x, y, z are the three weighting functions. The weighting functions (called tristimulus values) are shown in figure 4.

Horvath (1971) and Husar and White (1976) computed chromaticity coordinates of atmospheric scattered or transmitted light and showed that the light would be distinguishable from white light for various sun angles, aerosol properties, and NO_2 concentrations. Since the chromaticity diagram does not differentiate between differences in intensity (e.g., between yellow and brown or between white, gray, and black), chromaticity coordinates must be used in conjunction with a descriptor of light intensity for a complete specification of color. Thus, if we establish a color solid by taking the two-dimensional chromaticity diagram and adding a third dimension perpendicular to this plane to represent brightness, we have a means of completely specifying by three coordinates the color and its intensity.

Figure 5 is a drawing of such a color solid. The brightness in such a coordinate system is usually specified by the value of Y or by a parameter (L*), which is directly proportional to the subjective perception of brightness and is related to Y as follows:

$$L^* = 25\ Y^{1/3} - 17 \quad .$$

L* is used in quantifying color differences and is simply the parameter called "value" in the Munsell color system multiplied by 10.

The Munsell color system is the most widely used means of specifying colors. In this system, colors are arranged in order by value (brightness), hue (the shade of color--for example, yellow, red, green, blue), and chroma or saturation (the degree of departure of a given hue from a neutral gray of the same value). By specifying a given hue, value, and chroma, one can obtain a sample color chip from the Munsell Book of Color that corresponds to the specification. By this means, the objective specification of color (L*,x,y) can be related to the subjective perception of color by visually examining the color paint chip. ASTM Standard D 1535-68 (American Society for Testing and Materials, 1974) is the reference method

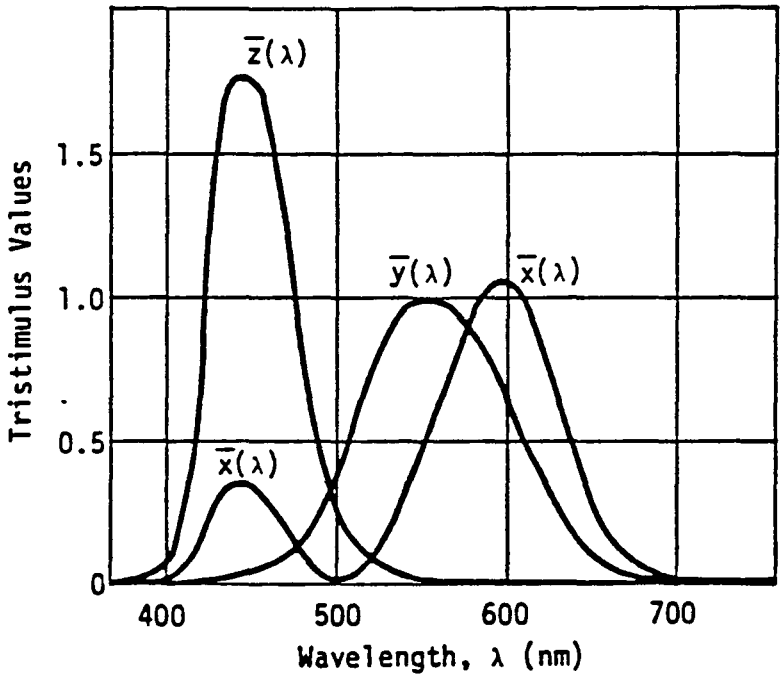

Source: Judd and Wyszecki (1975).

FIGURE 4. SPECTRAL TRISTIMULUS VALUES $\bar{x}(\lambda)$, $\bar{y}(\lambda)$, $\bar{z}(\lambda)$

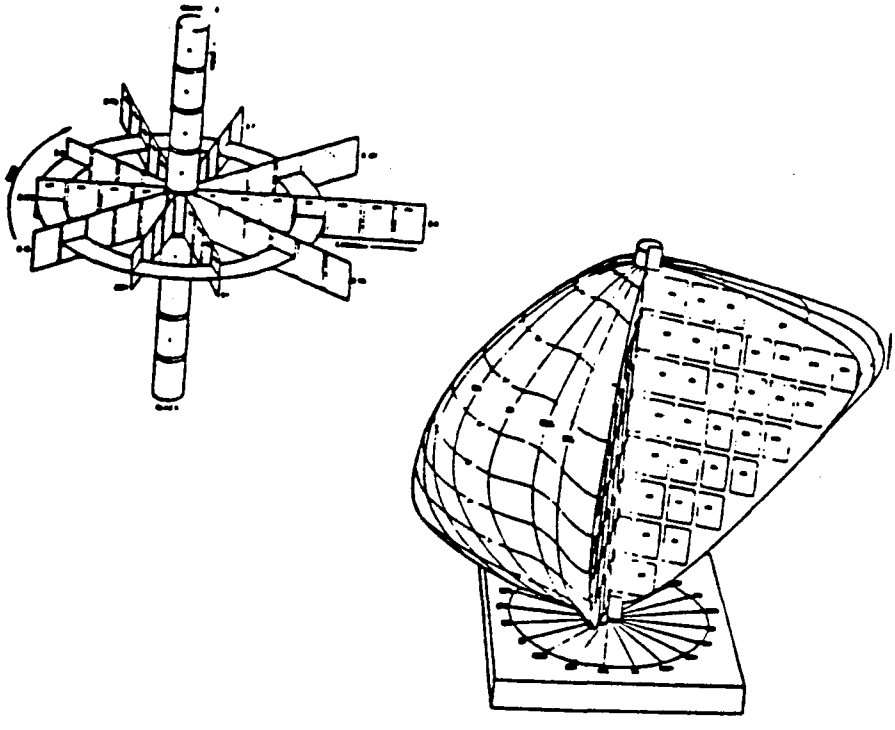

Source: Munsell Color Company.

FIGURE 5. REPRESENTATIONS OF A COLOR SOLID

for converting objective color specifications (L*,x,y) to the Munsell hue, value, and chroma notations by which a colored paint sample can be selected. We have used this method to convert light intensity (Y or L*) and chromaticity coordinates (x,y) calculated by the plume and regional visibility models to Munsell notation to be used by a commercial artist in illustrating atmospheric discoloration (Latimer et al., 1978).

2.2.5 Plume Perceptibility

The final step in the quantification of plume perceptibility is the specification of color differences--differences both in color and brightness. In 1976 the Commission Internationale de l'Eclairage (CIE) adopted two color-difference formulas by which the perceived magnitude of color differences can be calculated. Color differences are specified by a parameter ΔE, which is a function of the change in light intensity of value (ΔL^*) and the change in chromaticity ($\Delta x, \Delta y$). This parameter, ΔE, can be considered as a distance between two colors in a color space. The color space is defined such that equal distances (ΔE) between any two colors correspond to equally perceived color changes. This suggests that a threshold (ΔE_0) can be found to determine whether a given color change is perceptible.

Since the CIE could not decide between two different proposed formulas for ΔE, both were adopted in 1976 as standard means by which color differences can be specified. These color differences, which are labeled $\Delta E(L^*U^*V^*)$and $\Delta E(L^*a^*b^*)$, are calculated by the plume visibility code. We have elected to plot $\Delta E(L^*a^*b^*)$. Values of ΔE greater than 20 indicate a strong discoloration, ΔEs between 5 and 20 represent weak discoloration, and those of 2.5 to 5 (or less) indicate that a plume would probably not be perceptible. It is currently uncertain as to what the specific thresholds of perceptibility are in terms of values of blue-red ratio, plume contrast, and ΔE.

Figure 6 summarizes these qualitative interpretations of the quantitative specifications of visibility impairment. This figure provides a key to the results presented in section 3.

The SAI plume visibility code was designed to answer the question, "Are the visual effects of a given source perceptible by a human observer?" For this study a slightly different question also appears to be appropriate: "Do the visual effects caused by a given source result in a perceptible change in the detectability of a given target?" This question is addressed by determining the contrast difference (at a single wavelength or across all wavelengths) between an object and its background for conditions with and without the plume between observer and object. A

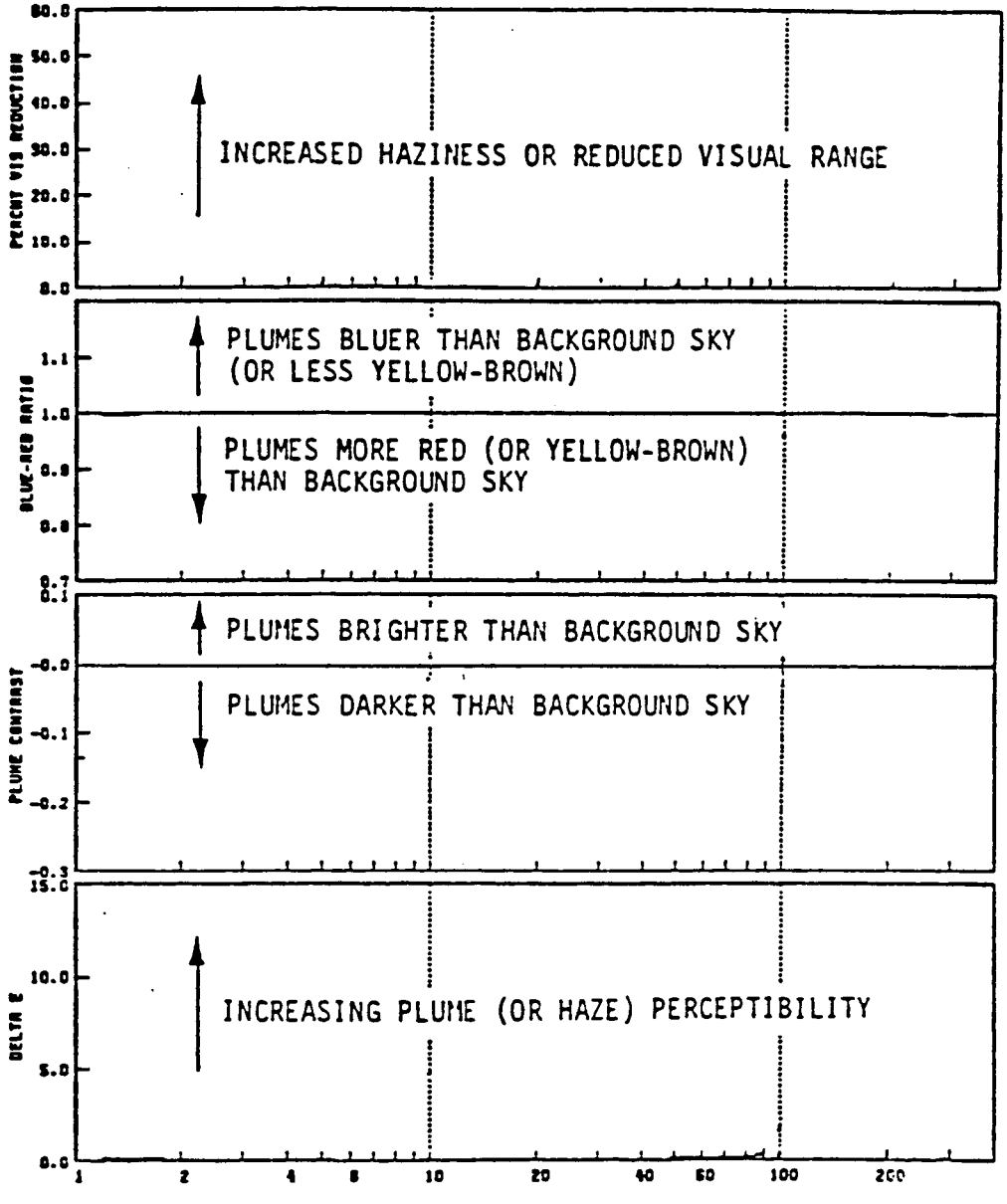

FIGURE 6. KEY TO PARAMETERS USED TO CHARACTERIZE VISIBILITY IMPAIRMENT

measure of this visual effect can be represented by the change in perceptibility, $\Delta(\Delta E)$, of a white, gray, or black object. This calculation is discussed in section 4.

2.3 CHARACTERIZING THE FREQUENCY OF OCCURRENCE OF VISIBILITY IMPAIRMENT

Plume visual impact is a complicated phenomenon, the magnitude of which is a function of many variables. These include

- Power plant emissions rates (particulate, SO_2, NO_x).
- Wind speed.
- Wind direction.
- Atmospheric stability.
- Persistence of meteorological conditions.
- Background ozone concentration.
- Background visual range.
- Topographical effects on plume transport and diffusion.
- Ultraviolet solar intensity.
- Time of day.
- Orientation of observer, plume, and sun.
- Viewing background (whether it is a sky, cloud, or terrain background, and whether the terrain is snow-covered, sunlit, or in shadow).

Because of the large number of variables important to a visual impact calculation, a computer model must be applied several times to assess the magnitude and frequency of occurrence of visual impact. As discussed, visual impact is considered to be visual range reduction (which results in the reduction of contrast between the sky and terrain objects), plume and object or target appearance (which results from contrast and color differences between the plume or object and the viewing background), and atmospheric discoloration. It would be ideal to calculate hourly impacts over the course of a year or more using hourly values of the above variables. However, such an extensive data base is rarely available for

use. Even if it were available, the computing costs involved would be prohibitive. It is therefore preferable to select a few representative values of each of these variables in order to represent a range of visual impact (i.e., the magnitude and frequency of occurrence) over a given period of time, such as a season or year.

2.3.1 Relative Location of Emissions Source

To determine the potential for visibility impairment caused by emissions from the power plant of interest, its location relative to important topographic features and areas that may be adversely affected must be established. Figure 7 shows elevation contours that could block the transport of the plume from the proposed Boron site to the areas of potential impact (e.g., Edwards Air Force Base and China Lake Naval Weapons Center). To assess the possibility that the terrain may block transport to certain areas (i.e., channel the plume away from areas of integral viewing significance), a screening analysis was performed to compare plume height with terrain elevations.

A representative stack height was calculated by adding to the physical stack height the plume rise for neutral conditions and a wind speed of 4 m/s (9 miles per hour):

$$H = h_{stack} + \Delta h \quad . \tag{9}$$

The neutral plume rise was calculated using the following Briggs plume rise formula (Briggs, 1969, 1971, 1972):

$$\Delta h = 1.6\ F\ 1/3\ (3.5\ X^{*})\ 2/3\ u^{-1} \quad , \tag{10}$$

where

ΔH = plume rise,

uH = average speed in the layer through which the plume rises = 4 m/s,

F = buoyancy flux

$$= g \frac{\dot{V}}{\pi} \left(1 - \frac{T_{ambient}}{T_{stack}} \right) \cdot (T \text{ in } {}^{0}\text{Kelvin}) \quad ,$$

g = gravitational acceleration = 9.8 m/s^2,

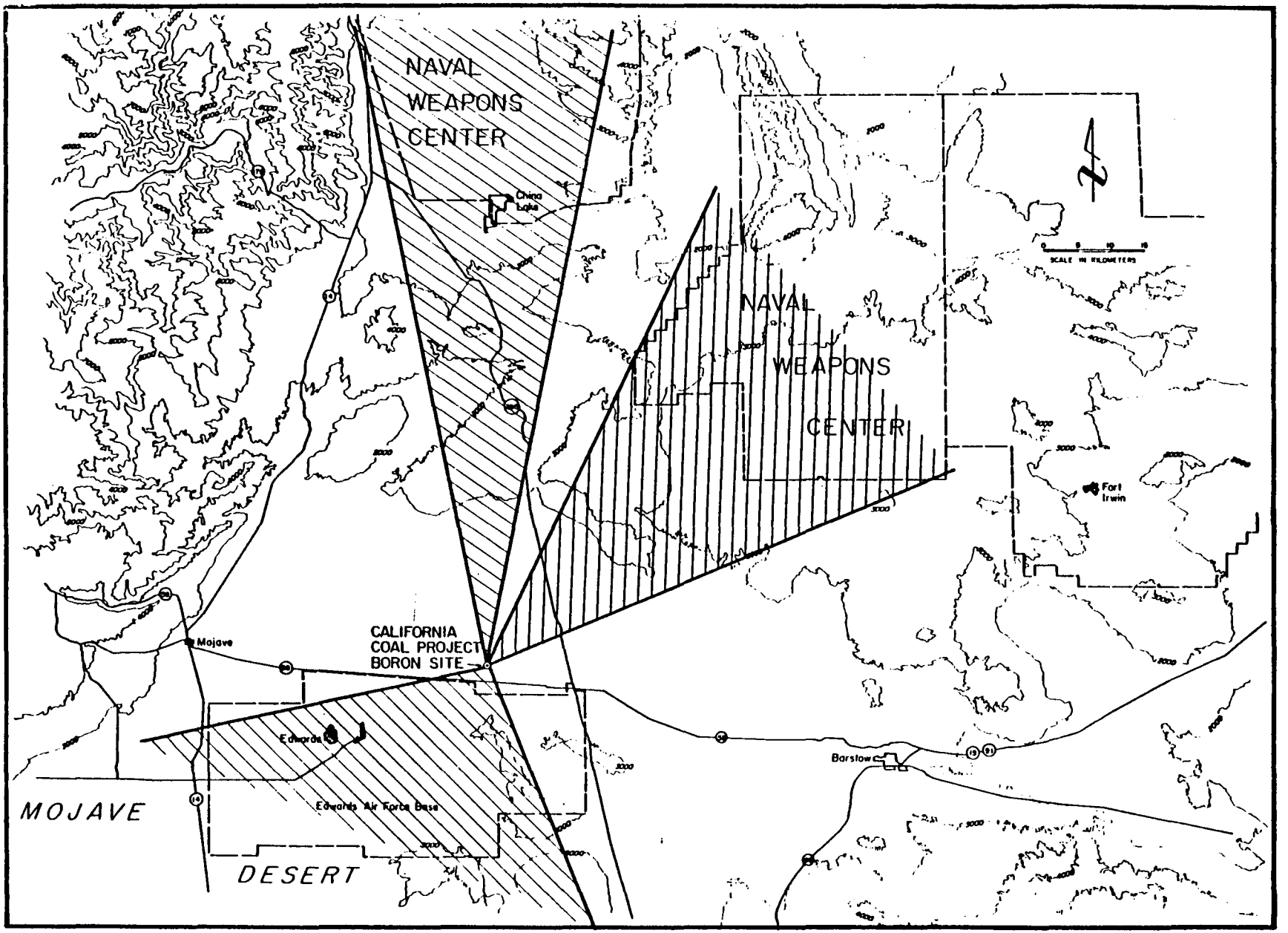

FIGURE 7. STUDY AREA SHOWING PLUME TRAJECTORIES AFFECTING OBSERVER LINES OF SIGHT

$\dot{V}$ = flue gas volumetric flow rates, and

$$\chi^* = = \begin{cases} 14F^{5/8}, & \text{if } F < 55 \\ 34F^{2/5}, & \text{if } F \geq 55 \end{cases}$$

The resulting effective stack height is estimated under this screening analysis as 383 meters (1226 feet) (h_{stack} = 152 m, Δh = 231 m). The ground elevation of the source is approximately 762 meters above sea level (2500 ft msl), and thus the height of the plume above sea level is estimated at approximately 3726 feet. Comparison of this value with the terrain elevations shown in figure 7 indicates that the elevated terrain ranging from 3000 to 4000 feet directly north of the plant site could possibly block or channel transport of the plume to the China Lake Naval Weapons Center. Transport of the plume to the Mojave-B complex of the Naval Weapons Center, northeast of Boron, is less likely to be blocked by the intervening terrain that ranges from 2000 to 3000 feet msl. Terrain is clearly not a concern for transport of the plume south and southwest into Edwards Air Force Base.

The distance over which the plume must be transported in order to have an impact on observer locations is also a factor in the visibility analysis. Both the advection and dispersion of pollutants emitted from a single source become increasingly difficult to simulate with any accuracy as distance from the source increases. This difficulty results from the fact that dispersion parameters have been estimated only for relatively short distances and are generally believed to be conservative at distances of 50 km or less from the source. Also, wind and atmospheric conditions measured at a single location may not be applicable to points downwind, especially in complex terrain settings. A further complication is that the distance a plume may be transported under certain "worst-case" meteorological conditions (e.g., low wind speed and stable conditions) is limited by the persistence of such conditions. This limitation on transport distance under assumed "worst-case" meteorological conditions is treated later in determining the frequency of occurrence of visibility impairment at each downwind distance.

The distances required to transport the power plant plume from the Boron site to each of the federal military installations varies considerably. In the case of Edwards Air Force Base, transport of the plume 10 to 20 km is sufficient to establish a number of potential observer-plume-object viewing conditions that could have a significant impact. For the China Lake Naval Weapons Center (due north of the Boron site) the plume has to be transported across elevated terrain approximately 65 km downwind of the source. The closest point of the other Naval Weapons Center installation (Randsburg Wash, north-northeast of the Boron site) is

approximately 45 km from the proposed site. Therefore, in regard to distance from the source, operations at Edwards would be affected the most significantly, followed by operations in the Randsburg Wash area of the Naval Weapons Center, and the China Lake area operations, the most remote from the source, the least affected. Of course, distance and the other important factors previously mentioned will be considered more explicitly in the model assessment of the potential visibility impairment at each of these sites.

2.3.2 Meteorological Conditions

The joint frequency of occurrence of meteorological conditions at the effective stack height is used to estimate the "worst-case" meteorological conditions that will be exceeded on a number of days per year in the area associated with visual impacts.

The important meteorological parameters are

- Wind speed
- Wind direction
- Atmospheric stability.

Wind speed affects plume visual impact strongly because plume centerline concentrations and plume line-of-sight integrals are inversely proportional to wind speed. Greater impact would be expected during light-wind, stagnation conditions than during strong-wind, well-ventilated conditions.

Wind direction affects plume visual impact because the direction of the plume parcel transport affects the orientation of the plume with respect to the observer. If the plume is transported directly toward an observer, the observer's lines of sight directly along the plume center will be significantly affected. If the observer's line of sight is oblique to or along the plume axis, visual impact will be greater than if the line of sight is normal to the plume axis. Also, the direction of plume transport affects the distance between the observer and the plume material.

The atmospheric stability of the upper air controls the rate at which source emissions are mixed with ambient air. During stable conditions, diffusion is limited, particularly in the vertical direction, so plumes remain as ribbon-like layers. Plume discoloration is most apparent during such stable conditions, because the integral of NO_2 and particulate con-

centrations along the line of sight is greater. During well-mixed (neutral or unstable) conditions, plumes are rapidly diffused and not likely to be visible as plumes per se.

Stability also has an effect on chemical conversion within a plume. The conversion of nitric oxide (NO) to nitrogen dioxide (NO_2) is diffusion-limited in stable plumes, as is the formation of sulfate and nitrate, because background ozone that effects NO_2 formation is depleted in the plume.

It is essential to consider the persistence as well as the frequency of occurrence of these conditions. For example, plume discoloration will generally be most intense during light-wind, stable conditions. However, the transport time to the viewing area increases as the wind speed decreases. As the transport time approaches and exceeds 12 hours, it is increasingly probable that the plume will be broken up by convective mixing and by changes in wind direction and speed; thus, it will not be visible as a plume or a discolored layer. However, since increased haze often occurs because of secondary aerosols that take time to form in the atmosphere, visual range reduction may be more significant when transport times to the area of concern are long. Largest increases in general haze (visual range reduction) resulting from an emissions source often occur if there is stagnation caused by synoptic meteorological conditions or topographic factors, or if there is trapping of emissions caused by upslope on downslope flow reversals.

It should be noted that visual range reduction will not necessarily be less with increasing distance between the plume and the observer. However, the aesthetic effects of visual range reduction are expected to be reduced as the plume-observer distance increases, because only the more distant objects are affected and fewer lines of sight are impacted.

Ideally, we would prefer to have a meteorological data base with detailed spatial and temporal coverage. However, upper-air data at 900 mb atmospheric pressure (~ 4000 ft msl) collected at Edwards Air Force Base at 4:00 a.m. were considered most applicable to this study and were the principal meteorological data used. These data consist of vertical temperature gradients from which dispersion coefficients are inferred, along with measurements of wind direction and speed. Joint frequency distributions of each stability class, wind speed, and wind direction combinations for each season of the year and the whole year were calculated from the data collected during the period 1952 to 1967. The data at approximately plume height were used for this analysis. The data were categorized under both the Pasquill-Gifford and TVA atmospheric stability class systems. Most plume models use Pasquill-Gifford (PG) dispersion coefficients (σ_y, σ_z) to characterize downwind plume dispersion, though these coefficients

are based on releases at ground level and measurements of dilution at short downwind distances. Measurements from a variety of sources, including the TVA and the Navajo Generating Station in northern Arizona, suggest that buoyant, elevated emissions from power plants diffuse more rapidly initially and less rapidly subsequently than indicated by the PG dispersion coefficients. However, these alternative dispersion coefficient systems are neither recommended nor endorsed officially by the EPA. Therefore, we have used both the PG and TVA dispersion coefficients in this study to determine the sensitivity of the results to these alternative input parameters. Figures 8 and 9 show the σ_y and σ_z, respectively, for PG and TVA categories.

It should be emphasized that the vertical diffusion (σ_z) of a plume and the wind speed (u) are the most important diffusion parameters for visibility impact assessments, because the optical thickness of a plume for horizontal lines of sight is inversely proportional to the product $\sigma_z u$ (see the appendix, equation A-13). Specification of horizontal diffusion (σ_y) is less important than vertical diffusion.

Accordingly, the worst-case dispersion conditions can be ranked in order of decreasing severity by evaluating the product $\sigma_z \cdot u$ where σ_z is the PG or TVA vertical dispersion coefficient for a given stability class and downwind distance x, and u is the average wind speed. The dispersion conditions are ranked in ascending order of the value $\sigma_z u$ (i.e., the higher the product of $\sigma_z u$, the less severe the dispersion conditions) for each downwind distance of interest. The joint frequency of occurrence of each meteorological condition (e.g., stability class, wind speed) and wind direction of interest is then used to determine the cumulative frequency of occurrence of conditions worse than or equal to the condition modeled. Table 1 summarizes the results of such an analysis based on the joint frequency tables prepared from atmospheric data collected at Edwards Air Force Base. Six different meteorological conditions have been considered:

> TVA-3, 2 m/s wind speed

> TVA-3, 4 m/s wind speed

> TVA-4, 2 m/s wind speed

> TVA-4, 4 m/s wind speed

> PG-E, 2 m/s wind speed

> PG-E, 4 m/s wind speed.

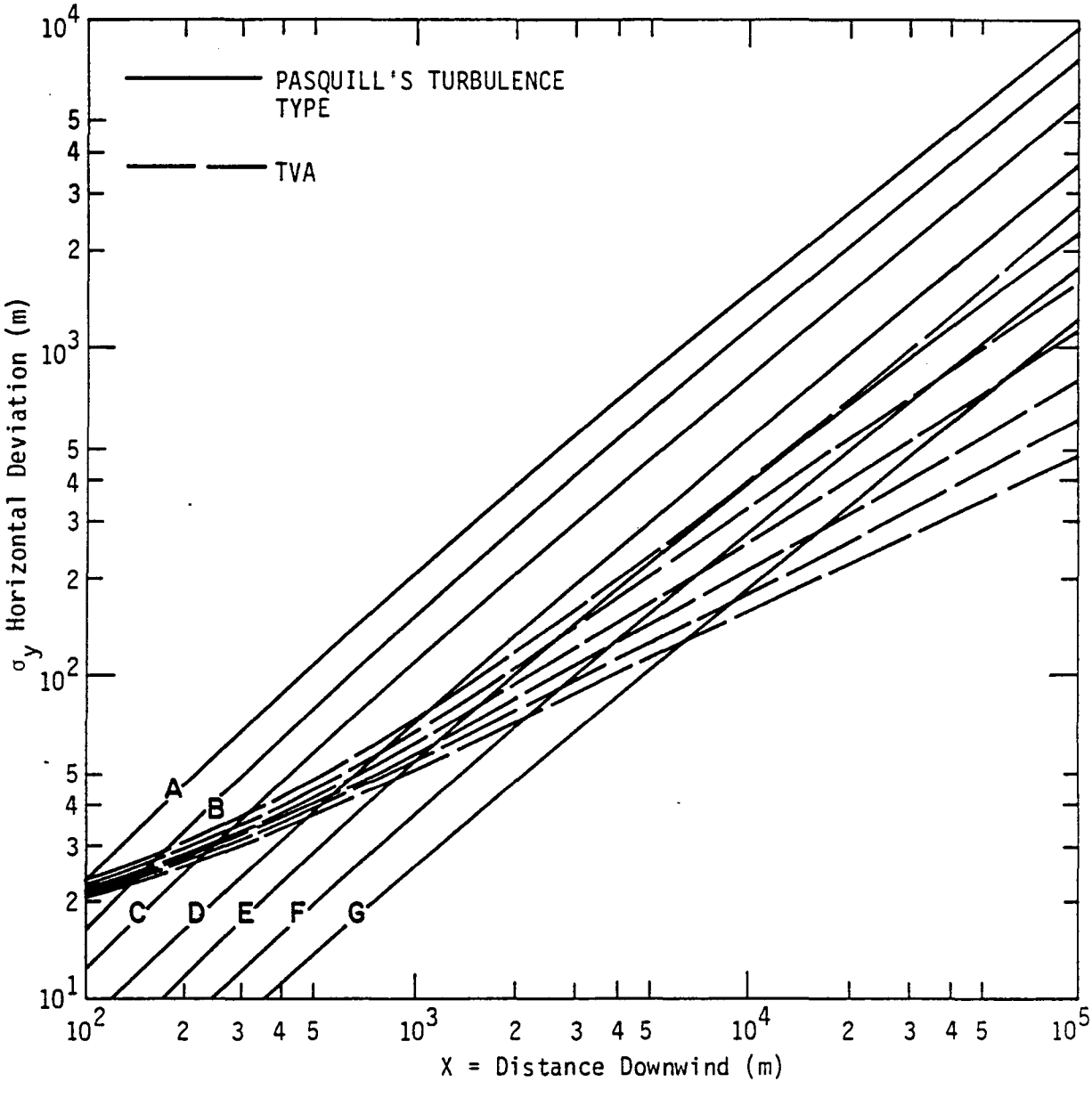

FIGURE 8. LATERAL DISPERSION COEFFICIENT, σ_y, AS A FUNCTION OF DOWNWIND DISTANCE

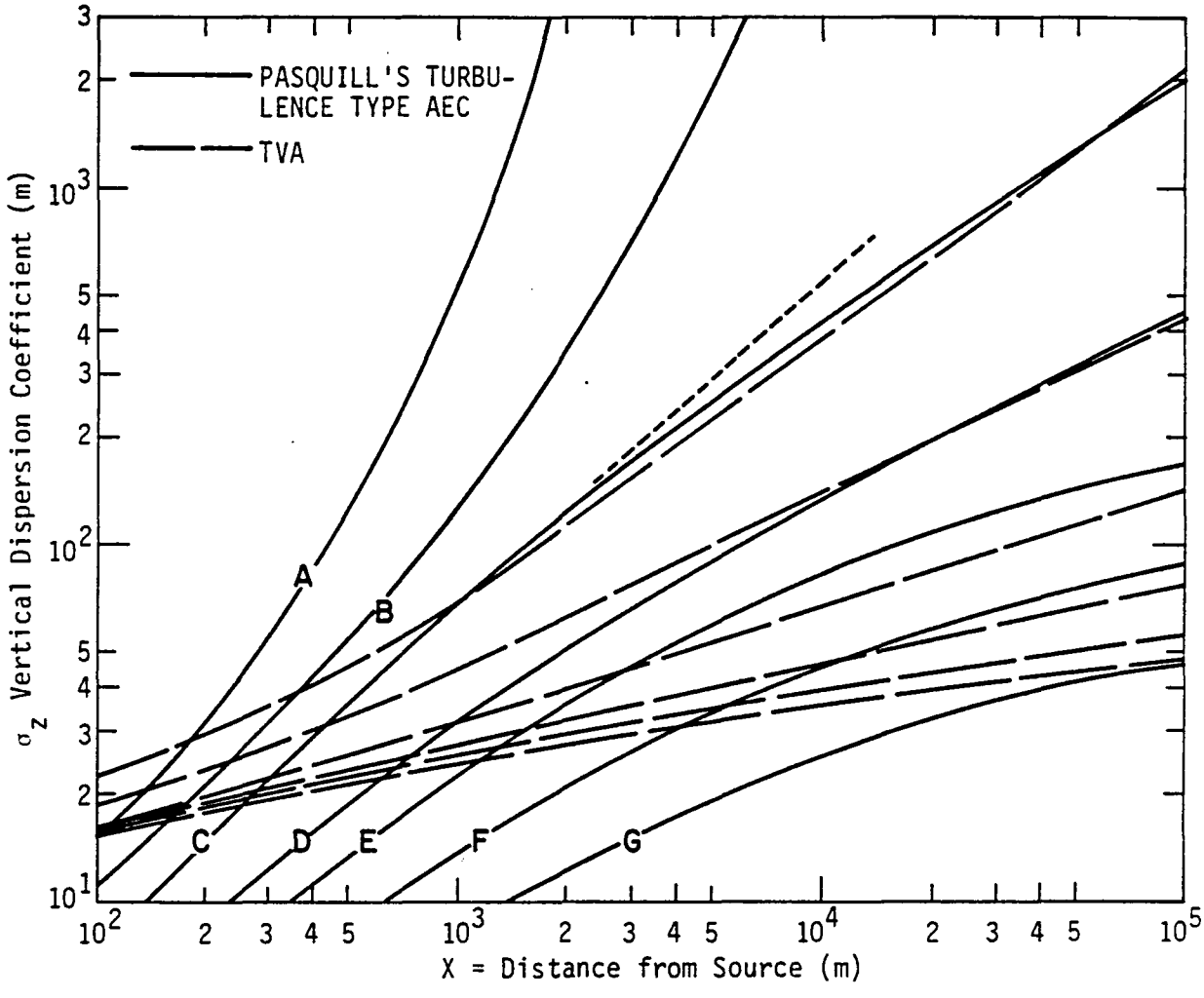

FIGURE 9. VERTICAL DISPERSION COEFFICIENT, σ_z, AS A FUNCTION OF DOWNWIND DISTANCE

TABLE 1. CUMULATIVE FREQUENCY OF OCCURRENCE OF ATMOSPHERIC DISPERSION DURING MORNING HOURS
(percent of year or season)

(a) More Severe or Equal to TVA-3 Stability with 2 m/s Wind Speed

Source-Receptor Transport Distance* (km)	Full Year			Winter (3 months)			Summer (3 months)		
	Wind Direction			Wind Direction			Wind Direction		
	NNW-ENE	S	SSW-WSW	NNW-ENE	S	SSW-WSW	NNW-ENE	S	SSW-WSW
10	6.5	0.2	2.2	14.4	0.0	2.1	5.4	0.2	1.7
20	6.5	0.2	2.3	14.4	0.0	2.4	5.4	0.2	1.7
40	7.1	0.2	3.3	15.6	0.0	3.0	5.6	0.2	1.9
60	3.7	0.2	3.0	9.9	0.0	1.8	1.1	0.2	1.6
80	3.7	0.2	3.0	9.9	0.0	1.8	1.1	0.2	1.6

(b) More Severe or Equal to TVA-3 Stability with 4 m/s Wind Speed

Source-Receptor Transport Distance* (km)	Full Year			Winter (3 months)			Summer (3 months)		
	Wind Direction			Wind Direction			Wind Direction		
	NNW-ENE	S	SSW-WSW	NNW-ENE	S	SSW-WSW	NNW-ENE	S	SSW-WSW
10	10.9	0.5	7.2	23.4	0.3	6.6	9.8	0.2	6.4
20	10.9	0.5	7.2	23.4	0.3	6.6	9.8	0.2	6.4
40	10.9	0.5	7.5	23.4	0.3	6.9	9.8	0.2	6.6
60	5.3	0.4	6.4	14.1	0.0	4.5	1.9	0.2	6.2
80	5.3	0.4	6.4	14.1	0.0	4.5	1.9	0.2	6.2

TABLE 1 (Continued)

(c) More Severe or Equal to TVA-4 Stability with 2 m/s Wind Speed

Source-Receptor Transport Distance* (km)	Full Year Wind Direction			Winter (3 months) Wind Direction			Summer (3 months) Wind Direction		
	NNW-ENE	S	SSW-WSW	NNW-ENE	S	SSW-WSW	NNW-ENE	S	SSW-WSW
10	5.3	0.1	1.5	10.8	0.0	1.8	4.6	0.0	1.0
20	5.3	0.1	1.5	10.8	0.0	1.8	4.6	0.0	1.0
40	5.3	0.1	1.5	10.8	0.0	1.8	4.6	0.0	1.0
60	0.7	0.0	0.6	1.5	0.0	0.6	0.1	0.0	0.7
80	0.7	0.0	0.6	1.5	0.0	0.6	0.1	0.0	0.7

(d) More Severe or Equal to TVA-4 Stability with 4 m/s Wind Speed

Source-Receptor Transport Distance* (km)	Full Year Wind Direction			Winter (3 months) Wind Direction			Summer (3 months) Wind Direction		
	NNW-ENE	S	SSW-WSW	NNW-ENE	S	SSW-WSW	NNW-ENE	S	SSW-WSW
10	8.7	0.3	4.1	17.4	0.0	4.5	9.2	0.2	2.8
20	8.7	0.3	4.2	17.4	0.0	4.8	9.2	0.2	2.8
40	7.4	0.2	3.9	16.5	0.0	3.9	5.8	0.2	2.7
60	2.8	0.1	2.7	7.2	0.0	2.7	1.3	0.2	2.4
80	2.8	0.1	2.7	7.2	0.0	2.7	1.3	0.2	2.4

TABLE 1 (Concluded)

(e) More Severe or Equal to Pasquill-Gifford E Stability with 2 m/s Wind Speed

Source-Receptor Transport Distance* (km)	Full Year			Winter (3 months)			Summer (3 months)		
	Wind Direction			Wind Direction			Wind Direction		
	NNW-ENE	S	SSW-WSW	NNW-ENE	S	SSW-WSW	NNW-ENE	S	SSW-WSW
10	8.4	0.3	2.4	15.7	0.0	3.3	3.5	0.2	1.3
20	8.4	0.3	2.4	15.7	0.0	3.3	3.5	0.2	1.3
40	6.1	0.2	2.1	13.6	0.0	2.1	1.2	0.2	1.3
60	1.7	0.1	1.2	5.1	0.0	0.9	0.2	0.2	0.6
80	1.7	0.1	1.2	5.1	0.0	0.9	0.2	0.2	0.6

(f) More Severe or Equal to Pasquill-Gifford Stability with 4 m/s Wind Speed

Source-Receptor Transport Distance* (km)	Full Year			Winter (3 months)			Summer (3 months)		
	Wind Direction			Wind Direction			Wind Direction		
	NNW-ENE	S	SSW-WSW	NNW-ENE	S	SSW-WSW	NNW-ENE	S	SSW-WSW
10	11.9	0.4	6.2	25.2	0.3	7.8	3.8	0.2	5.3
20	11.9	0.4	6.2	25.2	0.3	7.8	3.8	0.2	5.3
40	11.1	0.4	5.8	21.1	0.3	6.0	3.8	0.2	5.1
60	4.4	0.2	4.6	10.5	0.3	3.6	0.5	0.2	4.4
80	4.4	0.2	4.6	10.5	0.3	3.6	0.5	0.2	4.4

* Atmospheric conditions in which average wind speed would not result in transport over specified distance within 12 hours (assumed persistence) are excluded from frequency calculations.

the annual and winter and summer cumulative frequency of occurrence of atmospheric dispersion conditions more severe than or equal to these six conditions is presented for wind directions of interest (see figure 2) for a number of downwind distances. These frequency estimates will be used to predict the number of days that a given observer location or locations may experience significant visibility impairment.

For this analysis we have assumed it unlikely that steady-state plume conditions will persist for more than 12 hours. Thus, at a given downwind distance and wind speed, if more than 12 hours is required to transport a plume parcel from the emissions source, we assume that the plume material is more dispersed than a standard Gaussian plume model would predict. This enhanced dilution results from daytime convective mixing and wind direction and speed changes. Thus, in table 1 we do not add to the cumulative frequencies the frequency of a meteorological condition in which the wind speed is too low to transport the plume over the specified distance within 12 hours. For example, a wind speed of 1.0 m/s can transport a plume parcel only 43.2 km in 12 hours and thus is not considered in estimating the cumulative frequencies at 60 or 80 km.

2.3.3 Background Ozone

An important input parameter to the visibility model is background ozone concentration, that is, the concentration of ozone outside the plume. Ozone reacts directly with the colorless nitric oxide (NO) emitted from power plants to form a brownish gas, nitrogen dioxide (NO_2), the principal plume colorant:

$$NO + O_3 \rightarrow NO_2 + O_x \quad . \tag{11}$$

Ozone is also important indirectly in the oxidation of plume NO_2 and SO_2, because ultraviolet radiation photolyzes ozone to form the hydroxyl radical ($OH\cdot$) that reacts with NO_2 and SO_2 to form nitric acid and sulfate aerosol, as discussed in the appendix.

Approximately five years of ozone concentration data are available from the China Lake Naval Weapons Center. A total of 1500 days of ozone data from the period February 1975 through September 1979, including all four seasons, were used for this study to estimate background ozone concentrations.

Since we are concerned with background ozone concentrations at plume altitude, 500 to 800 m above ground, we must interpret ground-level ozone concentration data with care. In their analysis of long-term ozone concentration data at remote U.S. sites, Singh, Ludwig, and Johnson (1978)

reported that there is a significant diurnal variation in ozone concentrations at the surface owing to the surface depletion of ozone. They reported a significant reservoir of ozone in the free troposphere varying in concentration from about 30 ppb in the winter to about 60 ppb in the summer. The tropospheric ozone is rapidly mixed to the ground during the daytime; this causes surface concentrations near the the free tropospheric value. However, at night and in early morning, ozone is no longer mixed to the ground because of the development of a ground-based stable layer. During this period, ground-level ozone concentrations gradually decrease as a result of a surface depletion mechanism. In relatively remote unpolluted regions like the upper Mojave Desert, one would not expect a significant anthropogenic source of ozone. Rather, surface ozone appears to be affected by downward mixing from the free troposphere. In figure 10, the vertical ozone structure and diurnal and seasonal variations in ozone concentration are shown schematically.

Because of the importance of ozone concentrations at plume altitude in our visibility calculations, it is appropriate to use the daily maximum value of the surface concentration to represent the daily average concentration at plume altitude (see figure 11). For example, the maximum surface concentration shown in figure 11(a) is probably more representative of average concentrations at plume altitude than is a diurnal average surface concentration. Therefore, we have used daily maximum concentrations to represent average concentrations at plume altitude. (Figure 11 presents histograms of daily maximum ozone concentrations based on all data and winter and summer ozone data collected at the China Lake Naval Weapons Center.) The seasonal variation in ozone concentration is similar to that observed by Singh, Ludwig, and Johnson (1978). The median ozone concentrations are 0.037 ppm for all year, 0.022 ppb for the winter months, and 0.034 ppb for the summer months. The ozone values are probably lower for China Lake than for Edwards Air Force Base, because the former is more remote than Edwards.

2.3.4 Background Visual Range

The background visual range is also an important input parameter, because the extent to which a plume or object will be perceptible to an observer at a given distance from the plume depends on the clarity (i.e., the visual range) of the atmosphere between the observer and the plume. Thus, the change in perceptibility of an object with and without an intervening plume will be greater on clear days (i.e., days with higher background visual range) than on hazy days.

In this study nephelometer measurements of the light scattering coefficient made at China Lake were used to estimate background visual

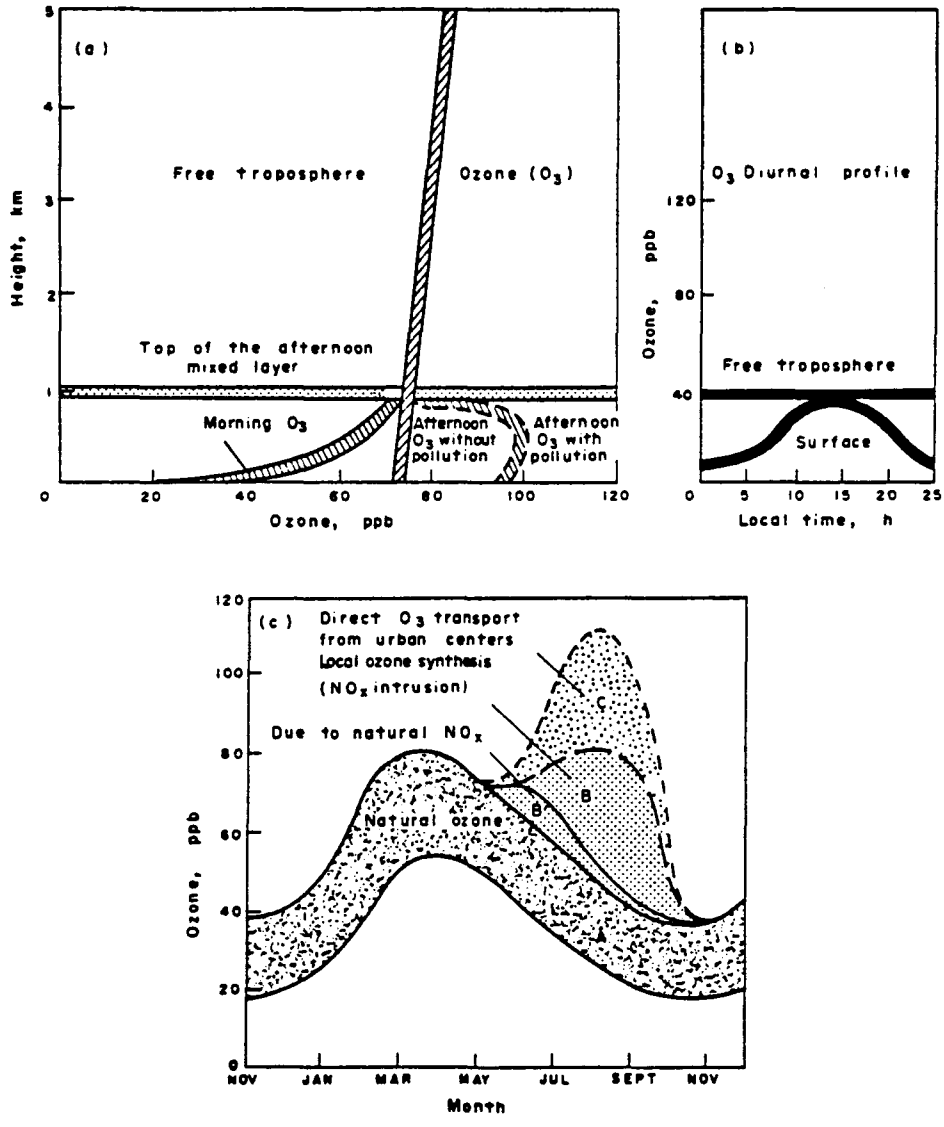

Source: Singh, Ludwig, and Johnson (1978).

FIGURE 10. A SCHEMATIC OF THE VERTICAL O_3 STRUCTURE AND ITS DIURNAL AND SEASONAL VARIATIONS AT REMOTE SITES

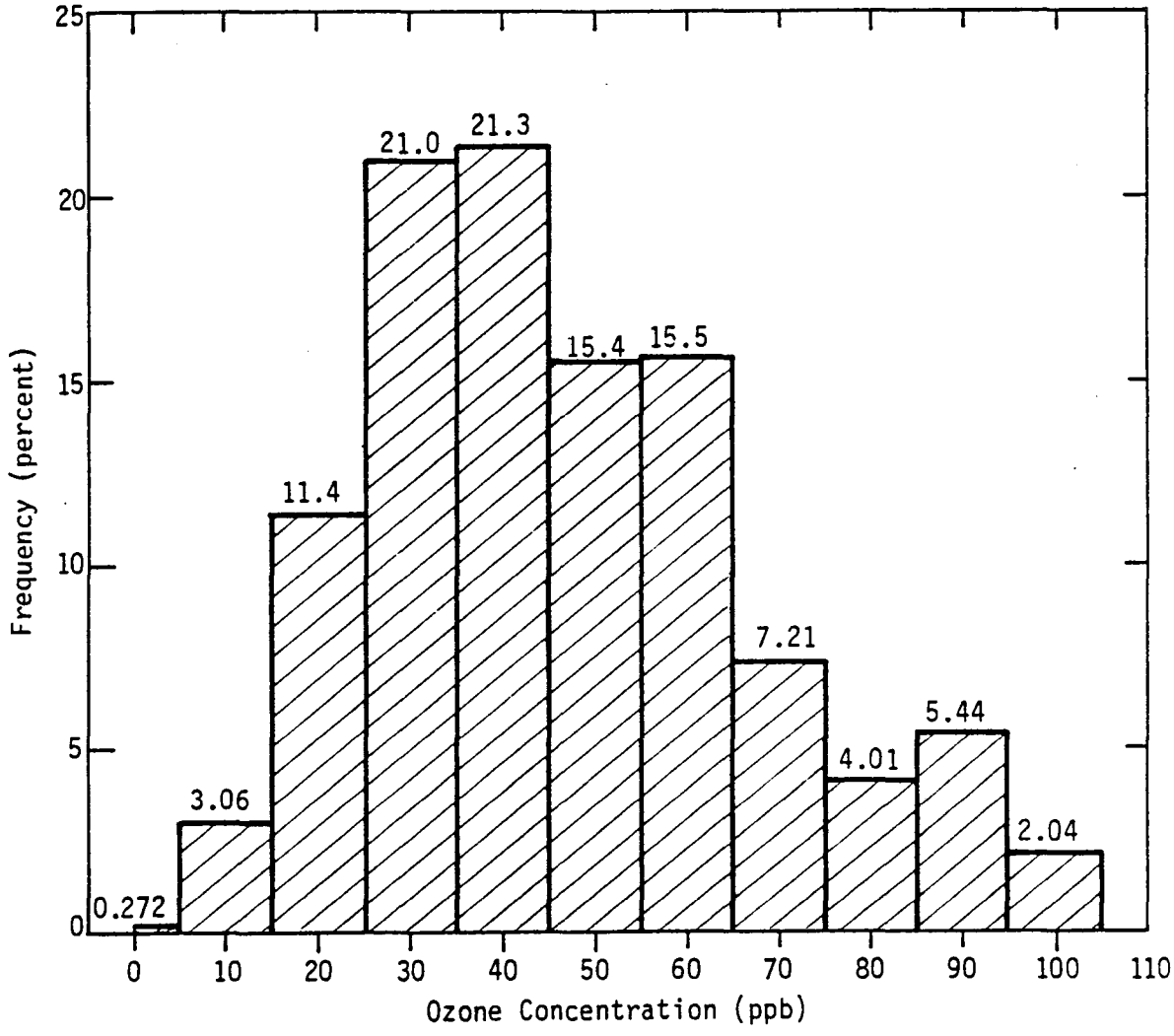

(a) February 1975 to January 1980

FIGURE 11. PEAK HOURLY VALUES FROM 12:00 A.M. to 11:00 A.M. AT CHINA LAKE

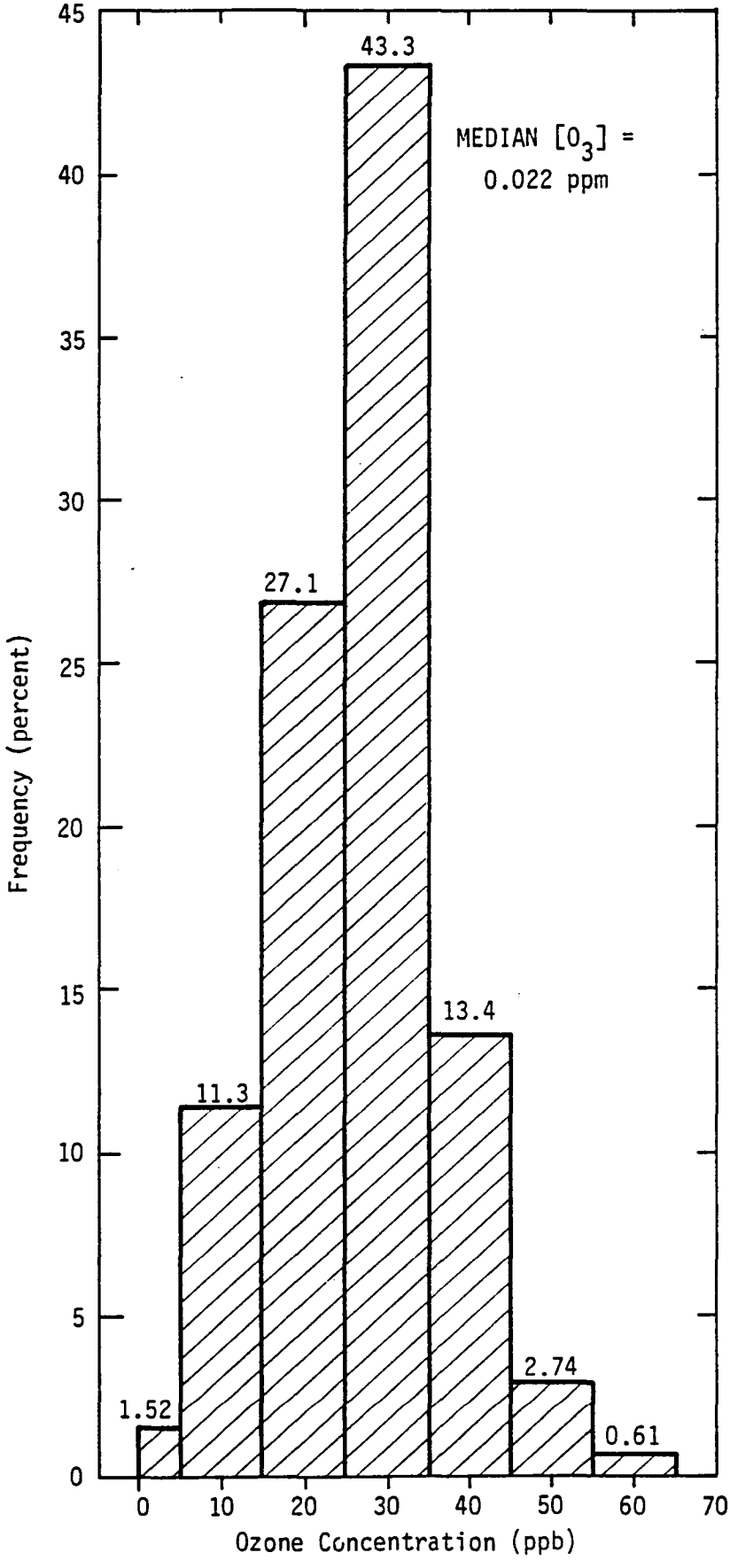

(b) December, January, and February

FIGURE 11 (Continued)

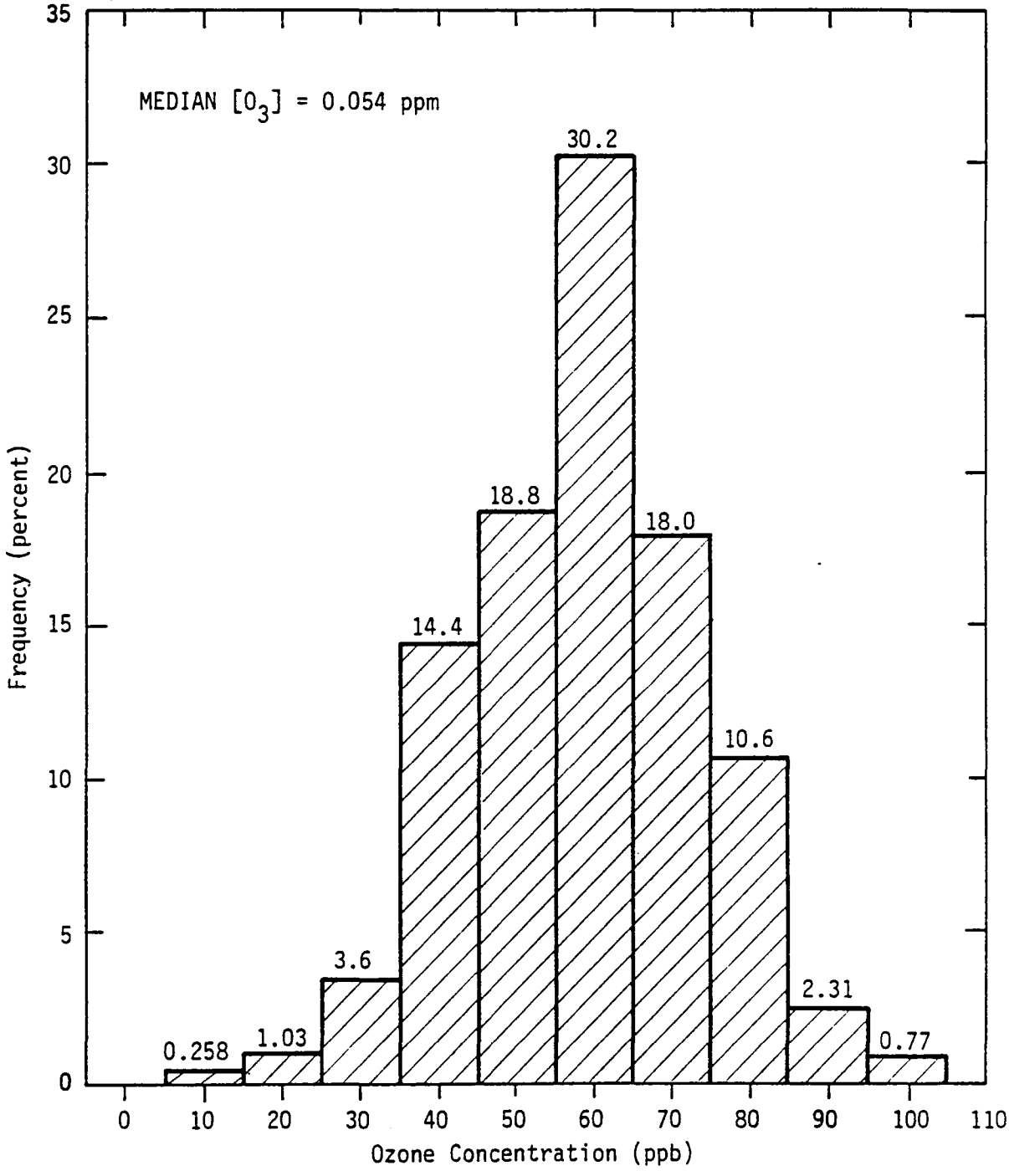

(c) June, July, and August

FIGURE 11 (Concluded)

range. For a homogeneous atmosphere without a plume, the following equation can be used to calculate visual range using scattering coefficient data.

$$\text{Background Visual Range} = \frac{3.912}{\text{Scattering Coefficient}} \quad (12)$$

Figure 12 shows the distribution of the China Lake scattering coefficient data for all data, winter data, and summer data collected during the period 1975 to 1980. Median visual ranges shown in these figures are 138 km for all year, 203 km for winter, and 132 km for summer. In this case, since China Lake is more remote, the visibility is probably higher than that at Edwards.

2.4 CHARACTERIZING THE POWER PLANT EMISSIONS

Pollutant emissions and stack data for the SCE electric generating facility proposed to be located at the Boron site are presented in the California Coal Project Notice of Intent (Bury et al., 1980). These emissions parameters are used in the visibility assessment as presented in table 2. According to the SCE Notice of Intent, these emissions are calculated assuming full-load operation (1500 MWe) and a 100 percent capacity utilization factor with all emissions controls operating at design efficiency. To evaluate the sensitivity of the results to the emissions loading estimates and also to provide some estimate of the visibility impairment that can potentially be caused by smaller-sized facilities (e.g., 500 MWe and 1000 MWe), different emissions were modeled with a reduction of the SO_2, NO_x, and particulate emissions by factors of 67 percent and 33 percent. The alternative emissions levels were evaluated as part of the generic impact analysis.

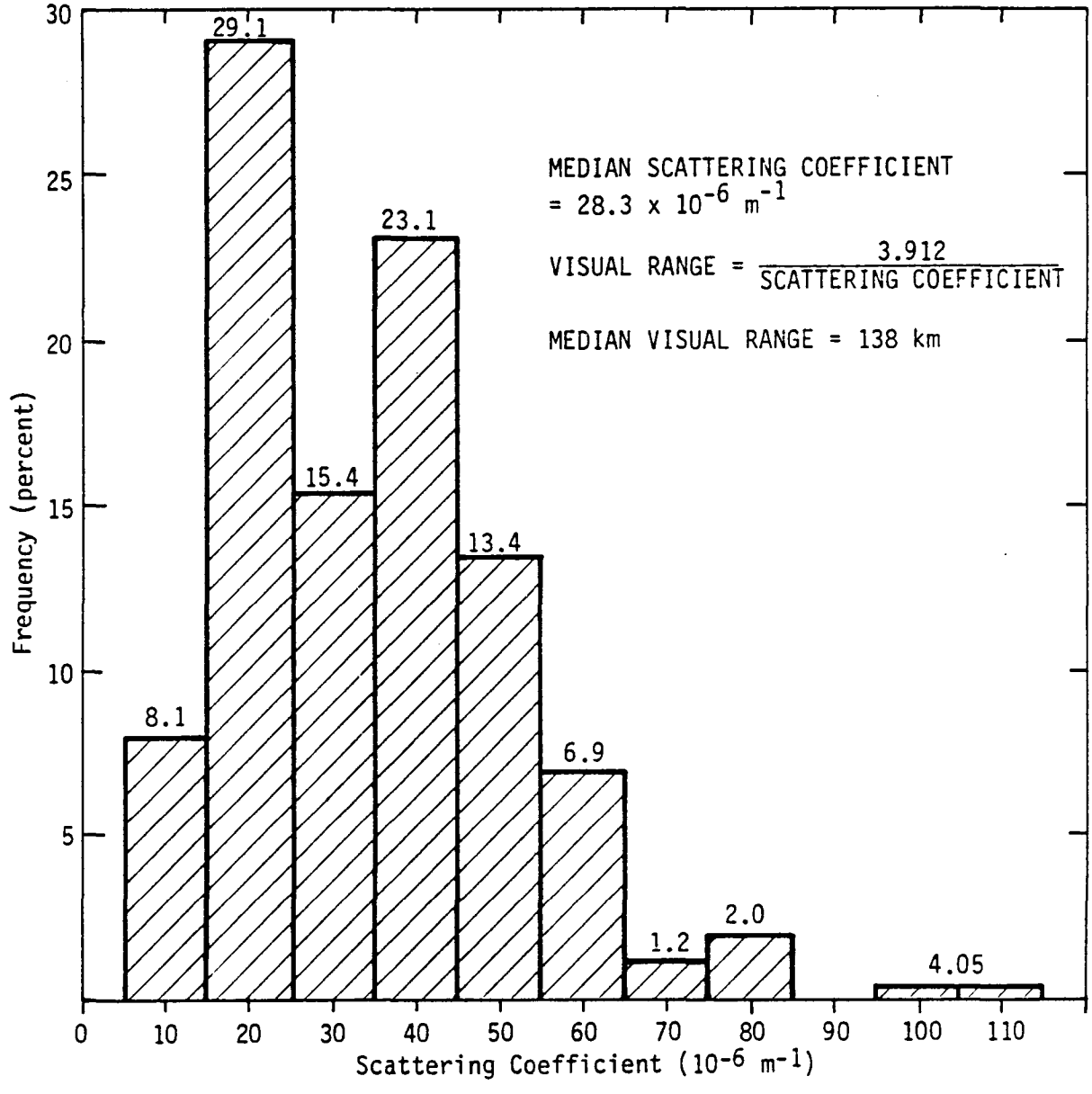

(a) August 1975 to January 1980

FIGURE 12. MONTHLY MEANS OF HOURLY VALUES FROM 7:00 A.M. to 11:00 A.M. AT CHINA LAKE

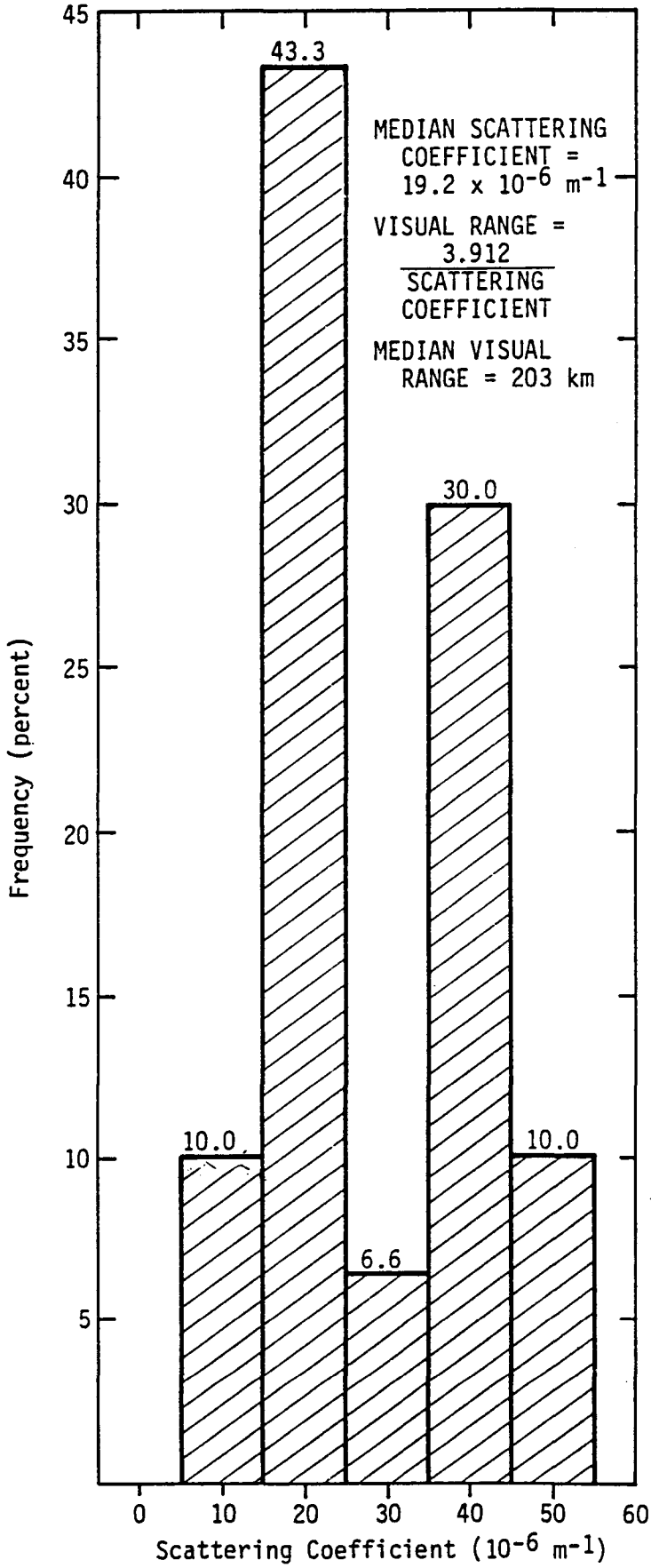

(b) December, January, and February

FIGURE 12 (Continued)

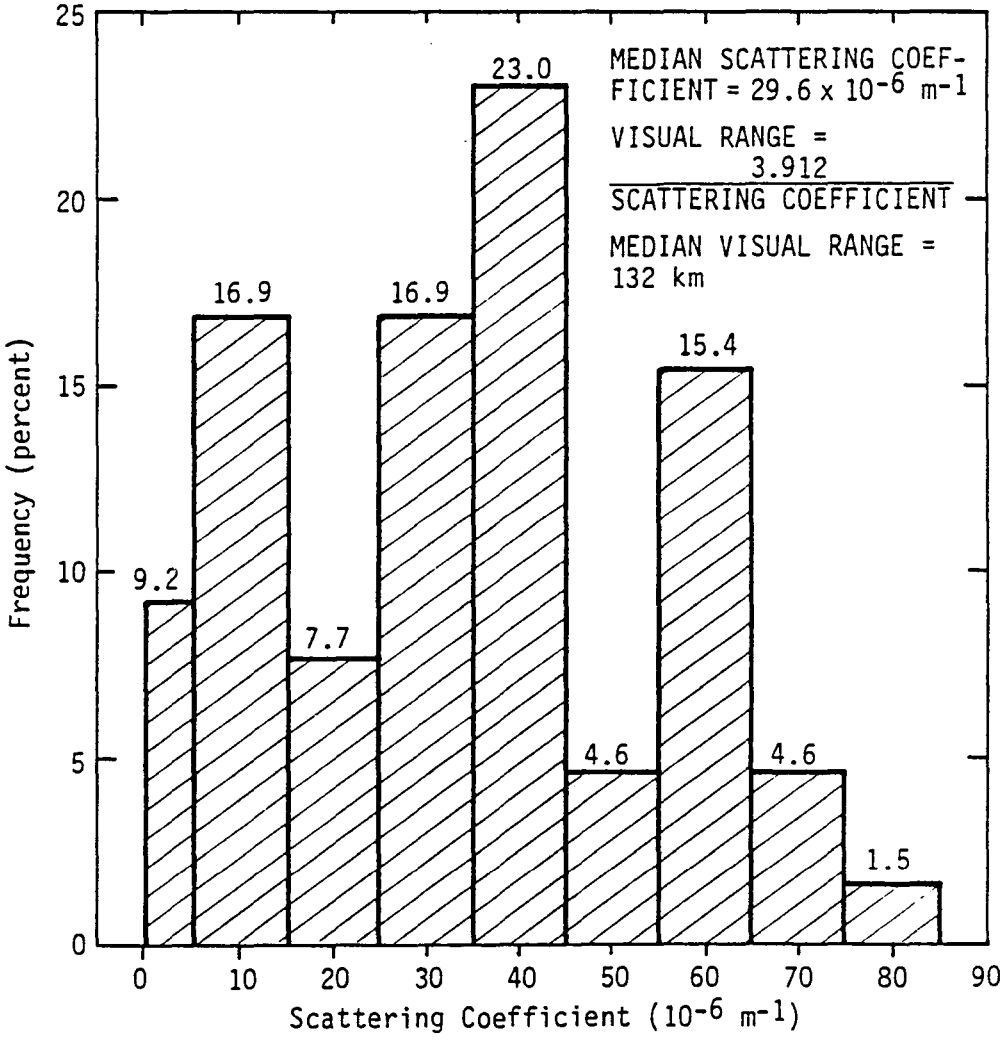

(c) June, July, and August

FIGURE 12 (Concluded)

TABLE 2. EMISSIONS AND STACK PARAMETERS FOR THE CALIFORNIA COAL PROJECT

Stack Parameter	
Elevation of Site	2500 ft MSL (762 m MSL)
Number of Units	3
Stack Height	500 ft (152 m)
Flue Gas Temperature	180°F (355°K)
Flue Gas Rate	2,352,000 ft^3/minute (1,109.86 m^3/minute)
Emissions	
Sulfur Dioxide	19.89 tons/day (208.8 g/s)
Nitrogen Oxides	85.03 tons/day (892.8 g/s)
Particulates	1.43 tons/day (15.01 g/s)

3 GENERIC EVALUATION OF VISIBILITY IMPAIRMENT

This analysis is intended to provide a generalized evaluation of the potential visibility impairment in the Upper Mojave resulting from a coal-fired electrical power plant such as that proposed for the California Coal Project. For this analysis the plume-based mode of the PLUVUE model was used to perform four different types of optics calculations at selected points along the power plant plume trajectory. In this section, the orientation of the observer to the plume and to background objects is not based on actual observer-object locations and plume trajectories. Instead, reasonably critical observer, plume, and background object orientations are assumed to provide a measure of the potential for visibility impairment and to provide relative comparisons of the extent of such impairment for different viewing situations. In order to represent different plume views, calculations are performed for these conditions:

- Horizontal views through the plume with a sky viewing background.
- Horizontal views through the plume with white, gray, and black viewing backgrounds.
- Nonhorizontal views through the plume with a sky viewing background.
- Horizontal views along the plume centerline with a sky viewing background.

As discussed in chapter 2, four measures of visibility impairment are calculated for this analysis: visual range reduction, contrast between the plume and background at the 0.55 μm wavelength, coloration or blue-red ratio of the plume to background, and plume perceptibility (i.e., color and brightness differences between the plume and background). To calculate these different measures of visibility impairment, the following parameters, which specify the observer, plume, background, and sun orientation, are given:

> Distance of observer to plume centerline (RP).

> Distance of observer to background to objects (RO) (for object views only).

> Horizontal azimuthal angle between the line of sight and the plume trajectory (α).

> Vertical elevation angle of the line of sight (β) (for nonhorizontal views only).

> Scattering angle (θ) between the incoming direct solar rays and the line of sight.

A more detailed explanation of the use of these parameters in calculations performed by the visibility model for the four viewing situations is presented in the appendix.

Care must be taken in the selection of those parameters that specify such conditions as the orientation of the plume to observer and the sun to the plume, because certain situations are physically impossible,* and because the degree of visibility impairment will vary for each of the measures (e.g., visual range reduction, contrast, etc.) depending on which parameters are selected. In selecting these parameters, calculations spanning a range of possible values were examined for each of the visibility impairment measures. The results of this evaluation are summarized in table 3. The values selected for these parameters were chosen to represent relatively realistic viewing relationships (i.e., not the highest or lowest impairment situation) and are as follows for each of the four viewing situations:

> Horizontal sky views

- RP = 7.2 km (10 percent of background visual range)
- α = 30°
- θ = 15°

---

* An example of a physically impossible situation for a horizontal view would be where the solar zenith angle is calculated as 65 degrees (i.e., 25 degrees off the horizontal) but the scattering angle is specified at less than 25 degrees. This situation would require that the observer be underground.

TABLE 3. EXAMINATION OF EFFECTS OF OBSERVER, PLUME, BACKGROUND, AND SUN GEOMETRY PARAMETERS ON MEASURES OF VISIBILITY IMPAIRMENT

	Visual Range Reduction	Plume/Background Contrast	Blue-Red Ratio	Plume Perceptibility
Horizontal sky views	> Not very sensitive to θ but generally highest at θ = 180° and 22° > Reduction greatest at α = 30° > Not sensitive to distance of observer from plume (RP)	> Contrast highest at θ = 135° and α = 30° > Contrast decreases as distance from observer to plume increases (i.e., plume becomes darker relative to background as observer-plume distance decreases)	> Sensitive to distance of observer from plume > Plume yellow-red coloration greatest at θ = 22°, α = 30°	> Sensitive to distance of observer from plume > Plume perceptibility greatest at θ = 22° and α = 30°
Horizontal object views	Not applicable	> Contrast varies considerably for white, gray, or background objects; white objects have greatest contrast with dark plume and black objects contrast most with white plumes > No distinguishable trend for values of O, RP, and RO	> Not highly sensitive to white, gray, or black background objects for a specified θ, RP, and RO > Maximum impact (coloration)	> Same as blue-red ratio > Perceptibility of plume increases with closeness of plume to observer and increased distance of object from observer
Nonhorizontal sky views	Not applicable	> Greatest impairment at θ = 22°, and α = 30° (lowest at θ = 90° and α = 90°) > Highest contrast at β = 15°	> Greatest impairment at θ = 22°, and α = 30° (lowest at θ = 90° and α = 90°) > Greatest coloration at β = 15°	> Greatest impairment at θ = 22° and α = 30° (lowest at θ = 90° and α = 90°) > Most perceptible at β = 30°
Sight along plume centerline	> Sensitive to length of plume being viewed > Greatest impact at θ = 180°	> Not very sensitive to length of plume being viewed > Greatest impact at θ = 22° > Decreasing impact with increasing observer-plume distance	> Not very sensitive to length of plume being viewed > Greatest impact at θ = 22° > Decreasing impact with increasing observer-plume distance	> Not very sensitive to length of plume being viewed > Greatest impact at θ = 22°

> Horizontal object views

  - RP = 7.2 km
  - RO = 14.4 km (20 percent of background visual range)
  - α = 30°
  - θ = 45°

> Nonhorizontal sky views

  - RP = 7.2 km
  - α = 30°
  - β = 45°
  - θ = 45°

> Sight along the plume centerline

  - RP = 7.2 km
  - θ = 45°.

3.1 THE BASE-CASE ASSUMPTIONS

For the generic evaluation of visibility impairment, a base case was defined by considering reasonably critical meteorological conditions in addition to the ambient air quality and background visual range assumptions used in the California Coal Project NOI. A summary of the base-case assumptions used in this study is presented in table 4. The major difference between conditions used as base-case model inputs for this study and those used in the NOI are the assumptions for atmospheric stability, wind speed, mixing height, and sulfate formation rate.

The visibility evaluation presented in the California Coal Project NOI assumed that unstable conditions (i.e., Pasquill-Gifford Class B) and moderate winds (i.e., 4 meters/second) would be of greatest interest in evaluating potential for adverse impacts. When combined with strong solar insolation during summer months and with high relative humidity, these conditions are most conducive to formation of secondary aerosols (e.g., sulfates and organics).

TABLE 4. GENERIC BASE CASE MODEL INPUT DATA AND ASSUMPTIONS

Atmospheric stability class	TVA-3
Wind speed	2.0 m/s
Ambient temperature	70°
Relative humidity	25 percent
Mixing depth	1000 m
$SO_4^=$ conversion rate	Base case OH• chemistry
Background visual range	72 kilometers
Background pollutant concentrations	
$[NO_x]_b$	0.01 ppm
$[NO_2]_b$	0.009 ppm
$[O_3]_b$	0.07 ppm
$[SO_2]_b$	0.01 ppm
$[SO_4]_b$	8.1 $\mu g/m^3$
$[NO_3^-]_b$	0.0 $\mu g/m^3$
$[\text{Coarse-mode particulates}]_b$	50 $\mu g/m^3$

However, for the distances (20 to 40 kilometers) and times of transport (1 to 6 hours) to viewing areas of concern for this project, light absorption (i.e., discoloration) by NO_2 formed in the plume, rather than light scattering by aerosols, will perhaps result in greater visibility impairment. The most intense plume discoloration will generally occur during light winds and stable atmospheric conditions. Estimates of the joint frequency of occurrence of stable atmospheric conditions with wind speeds of 2 meters/second or less indicate that such conditions occur in the area with sufficient frequency to be of interest.

Thus, for the visibility impairment base case, a stable, light-wind condition (TVA-3, 2 meters/second) is used for evaluating potential adverse impacts. However, the extent of visibility impairment has also been estimated for different dispersion assumptions in order to determine the sensitivity of the results to the assumed base-case conditions. Model input values for these sensitivity runs are presented later in this section.

The formation of sulfate was modeled for the base case by considering the reaction of SO_2 with the hydroxyl-free radical ($OH\bullet$), as mentioned in chapter 2 and as presented in greater detail in the appendix. No heterogeneous sulfate formation was assumed for the base case. As previously discussed, the heterogeneous mechanism for formation of sulfate in a plume from a rural area source is generally believed to be negligible. However, the upper Mojave Desert is subject to advection of more humid and polluted air from the Los Angeles air basin; therefore, during such episodes heterogeneous absorption of SO_2 on catalized water droplets entrained by the plume may also contribute to sulfate production. The visibility evaluation presented in the NOI assumed a 1 and 2 percent sulfate formation rate. Sensitivity evaluations performed for this study have also examined the effects of alternative assumptions on the rate of sulfate formation. The results of these sensitivity runs are presented later in this section, following the presentation of base-case evaluation results.

A mixing height* of 1000 meters was assumed for the base case. This height was selected somewhat arbitrarily but at a height sufficient to avoid greatly influencing model results. The meteorological case of interest (i.e., stable, light wind conditions) occurs most frequently in

---

* Turbulence in a "mixing layer" of air near the earth's surface accounts for most of the atmospheric dispersion of pollutants. This turbulent layer is often restricted by a layer of smooth, stable air flow which forms a "mixing lid" at the "mixing height."

the morning hours when, according to Holzworth (1972), mean mixing heights in this part of the county range from 400 to 600 meters. However, since effective plume height of the source may be nearly as large as these mixing heights, the model results could be greatly effected by the use of these values because of the assumed total reflection of the plume at the mixing lid (see the appendix--A.1.5 Limited Mixing). Therefore, it was considered more appropriate for this generic evaluation to use an assumption of a 1000-meter mixing height that would not result in plume reflection over the distances of interest.

According to the NOI, the California Coal Project fly ash emissions are likely to be in the range of less than 1 μm. For the base-case evaluation, it is assumed that the fly ash emitted from the generating station will have a mass media diameter of 1.7 μm, a geometric standard deviation of 1.5, and a density of $2g/cm^3$. This size distribution is within the range of size distribution measured in the outlets of electrostatic precipitations and baghouses at power plants throughout the country. The mass mean diameter was changed as part of the sensitivity runs to assess its effect.

The background pollutant concentrations, background visual range, and relative humidity used for the base-case evaluation were taken from the California Coal Project NOI. Additional model runs were performed for different assumed background visual ranges, relative humidities, and background ozone concentrations. These sensitivity tests are discussed in section 3.3. As shown in figure 11, the assumed background ozone concentration of 0.07 ppm or higher occurs in the morning hours at China Lake 20 percent of the time annually and 30 percent of the time during summer months. Using the information presented in figure 12, we can calculate that the base-case background visual range of 72 kilometers or greater occurs in the morning nearly 90 percent of the time year round and about 75 percent of the time during the summer. The frequency estimate of plume impact is presented in section 3.4.

3.2 RESULTS OF THE BASE-CASE VISIBILITY IMPAIRMENT EVALUATION

Results of the visibility impairment evaluation using the base-case modeling assumptions of emissions from a electrical generating station such as that proposed by the SCE for the Boron site are summarized in figure 13.* Figure 13(a) presents the results for horizontal views with background sky (i.e., lines labeled 1.0) and with white, gray, and black

* It may be useful for the reader to refer to figure 6 to interpret these results.

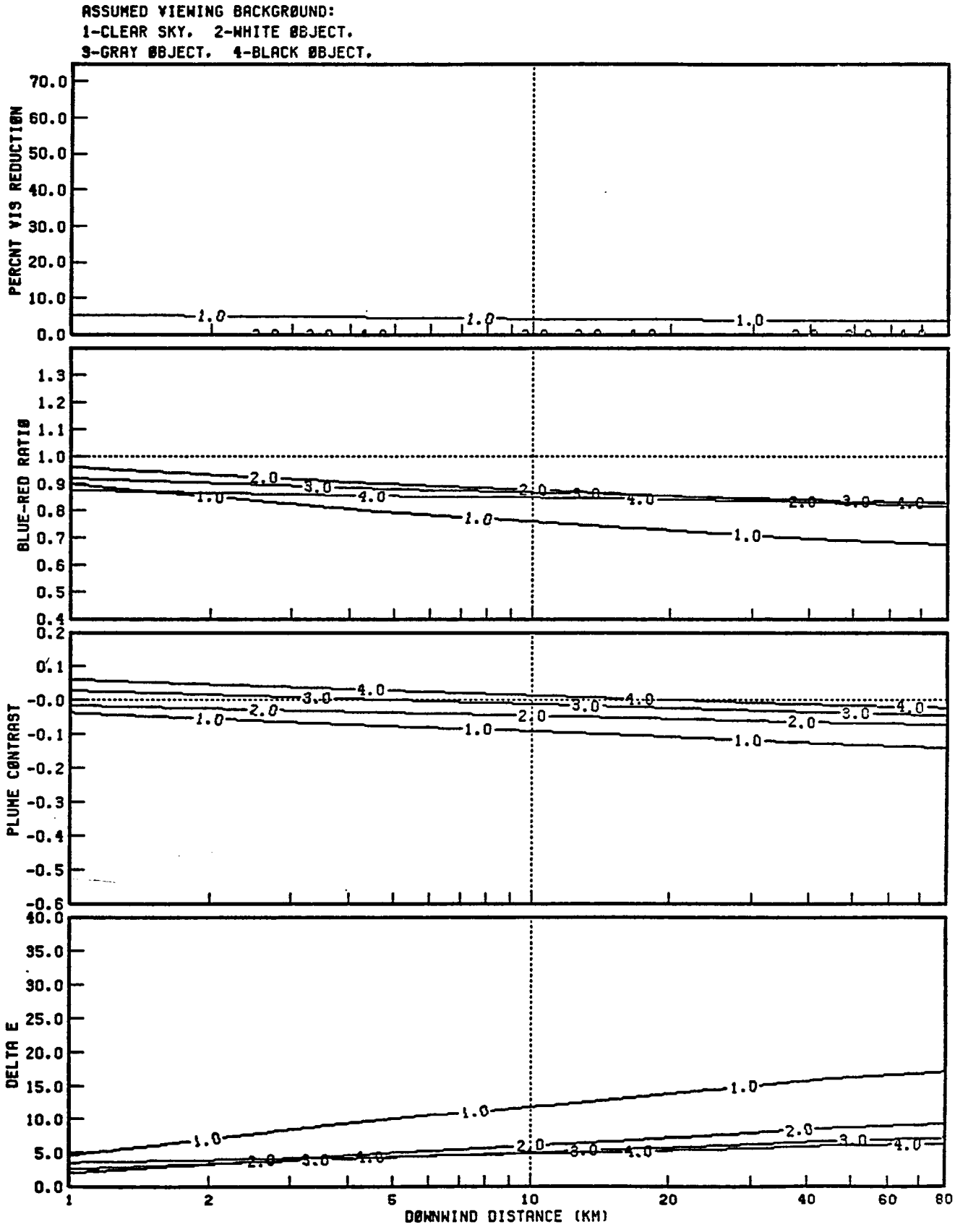

(a) Horizontal Views

FIGURE 13. GENERIC EVALUATION OF BASE CASE

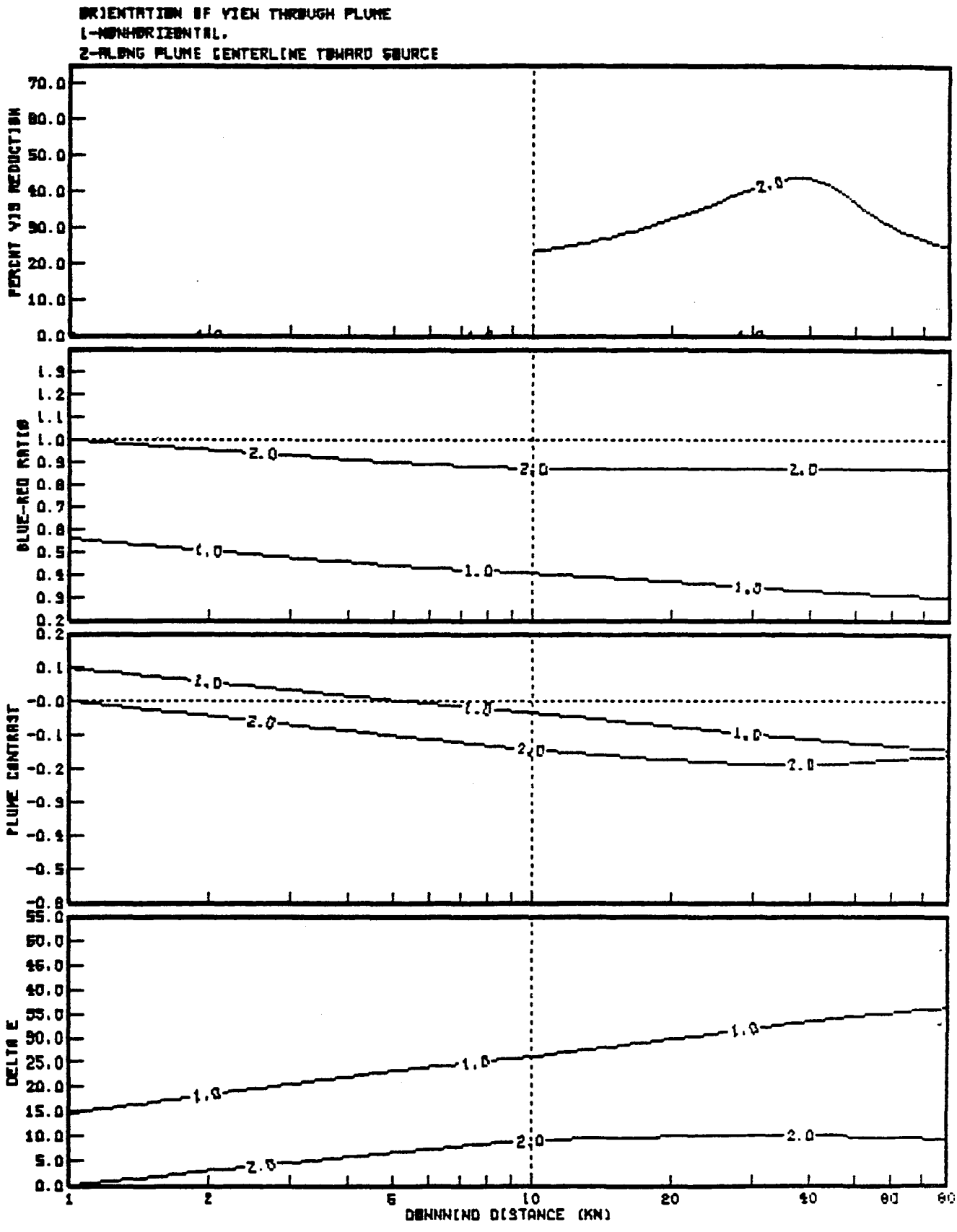

(b) Nonhorizontal and Axial Views

FIGURE 13 (Concluded)

background objects (i.e., lines labeled 2.0, 3.0, and 4.0, respectively). Figure 13(b) presents the results for a nonhorizontal view (i.e., labeled 1.0) and a view along the plume centerline (i.e., labeled 2.0).

In figure 13(b), the reduction in visual range for axial views (i.e., views along the plume centerline) is presented only for distances of 10 kilometers or more from the source. This has been done because the percent reduction in visual range is very sensitive to the length of the plume viewed and, at distances shorter than 10 kilometers, the length of the plume viewed is limited by the observer distance from the source.

At 10 kilometers, we assume that the line of sight of the observer intersects the plume centerline for a distance of 5 kilometers. Correspondingly, at 20 kilometers, we assume the length of the plume viewed is 10 kilometers, and at 40, 60, and 80 kilometers, the length of the viewed plume is 20 kilometers. As in all other calculations, the distance of the observer from the plume is taken at 10 percent of the visual range, or 7.2 kilometers. The plume-observer geometry for this viewing situation and for all other viewing situations is discussed in more detail in the appendix.

The results shown in figure 13(a) indicate that the plume, if viewed under the assumed conditions against the background sky, will be seen as brown in color (a blue-red ratio of 0.8 to 0.7), darker than the horizon sky (a contrast of -0.1), and will be perceptible ($\Delta E > 10$) at distances between 5 and 80 kilometers from the source. For horizontal views visual range may not be significantly impacted at a 5 percent or less reduction in background visual range. Also, the contrast, coloration, and perceptibility of the plume when viewed against background objects will not be as great as for horizontal sky views.

Figure 13(b) shows that, for views along the plume centerline, a very significant reduction in visual range of between 25 and 40 percent can be expected, with a peak at 40 kilometers from the source, assuming that the plume centerline is viewed by the observer from an upwind distance of 20 kilometers. This visual range reduction would put the visual range well below the limit necessary for optical system operation. Similarly, the visibility impairment, as represented by plume perceptibility for nonhorizontal and axial views of the plume, is greater than estimates for horizontal sky and object views.

These results suggest that under stable and light wind conditions, dispersion of the plume over an 80-kilometer distance is not sufficient to overcome effects on visual impairment caused by NO_2 formation in the plume. In fact, for these conditions, the maximum impact generally occurs at the farthest downwind distances examined by the model. This finding

does point out a limitation on the use and value of the results of the Gaussian plume formulation. For long-distance transport (> 50 km) of a plume, the dispersion of pollutants is probably not well represented by a Gaussian plume. However, there is presently no better theoretical and practical approach to the visibility impact analysis of a single source. Therefore, results obtained within a range of 5 to 50 kilometers from the source are considered more acceptable.

Recent results from the EPA-sponsored VISTTA program (Bergstrom et al., 1980) show that the plume model can predict the visual impairment from power plant emissions rather well. The major uncertainty appears to be in the specification of the dispersion (in particular, plume width). However, for the range of parameters of interest, the model results should be reasonable.

3.3 SENSITIVITY ANALYSIS

To evaluate the effect of changes in input assumptions on base-case results, we now present a series of results in which a single input assumption was altered from that of the base case. We first examine alternative meteorological conditions (i.e., stability and wind speed), followed by an examination of changes in model inputs for the sulfate formation rate, background ozone concentration, background visual range, relative humidity, size distribution of fly ash emissions, and, finally, reductions in power plant emissions. These parameters were selected for sensitivity analysis because, for a given viewing condition, they are most likely to affect the results, or because they are subject to some uncertainty, or for both these reasons.

3.3.1 Meteorological Conditions

For the base-case analysis, a TVA-3 stability class and a 2 m/s wind speed were used to represent reasonable worst-case conditions. Figures 14, 15, and 16 compare the base-case results with results obtained for different meteorological conditions that correspond to Pasquill-Gifford E stability class (2 m/s), TVA-4 stability class (2 m/s), and a wind speed of 4 m/s (TVA-3 stability class), respectively.

A comparison of base-case conditions with the results obtained using different stability classifications indicates few significant changes. In general, the degree of visibility impairment is greater for Pasquill-Gifford E and TVA-4 stability classes. Under Pasquill-Gifford E stability class (PG-E), the nonhorizontal views are characterized by increased coloration, contrast, and perceptibility of the plume over the base-case

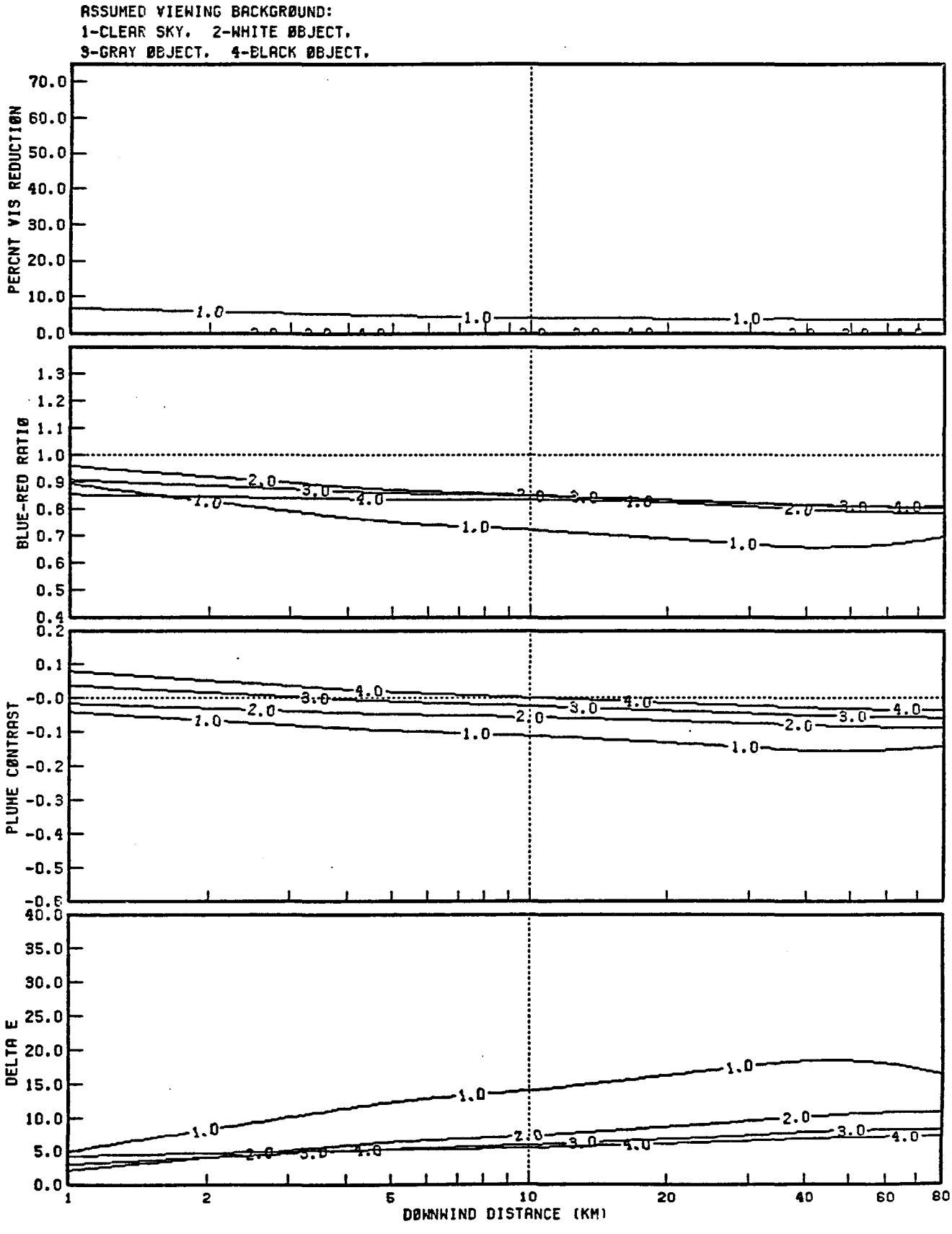

(a) Horizontal Views

FIGURE 14. SENSITIVITY EVALUATION--PASQUILL-GIFFORD STABILITY E

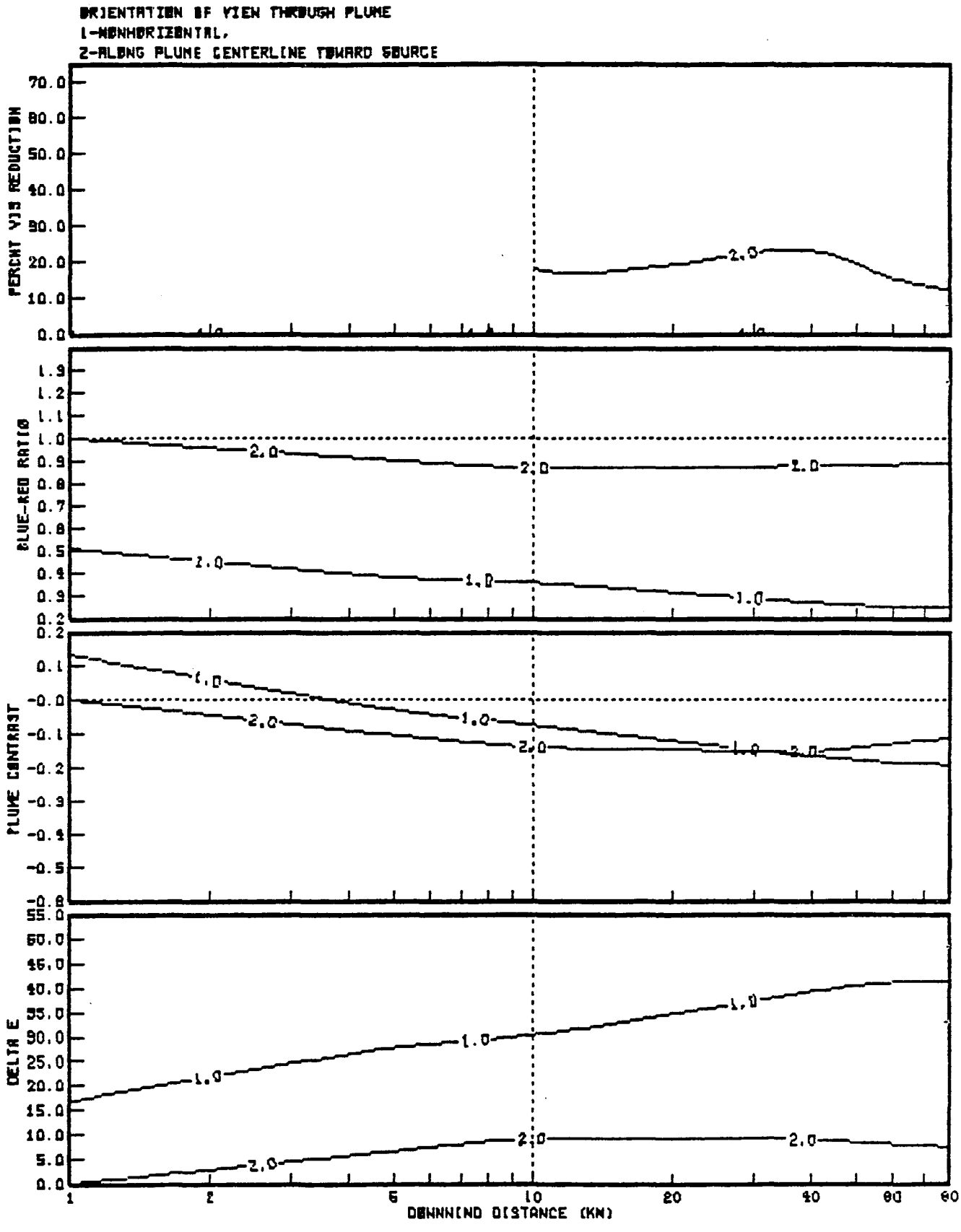

(b) Nonhorizontal and Axial Views

FIGURE 14 (Concluded)

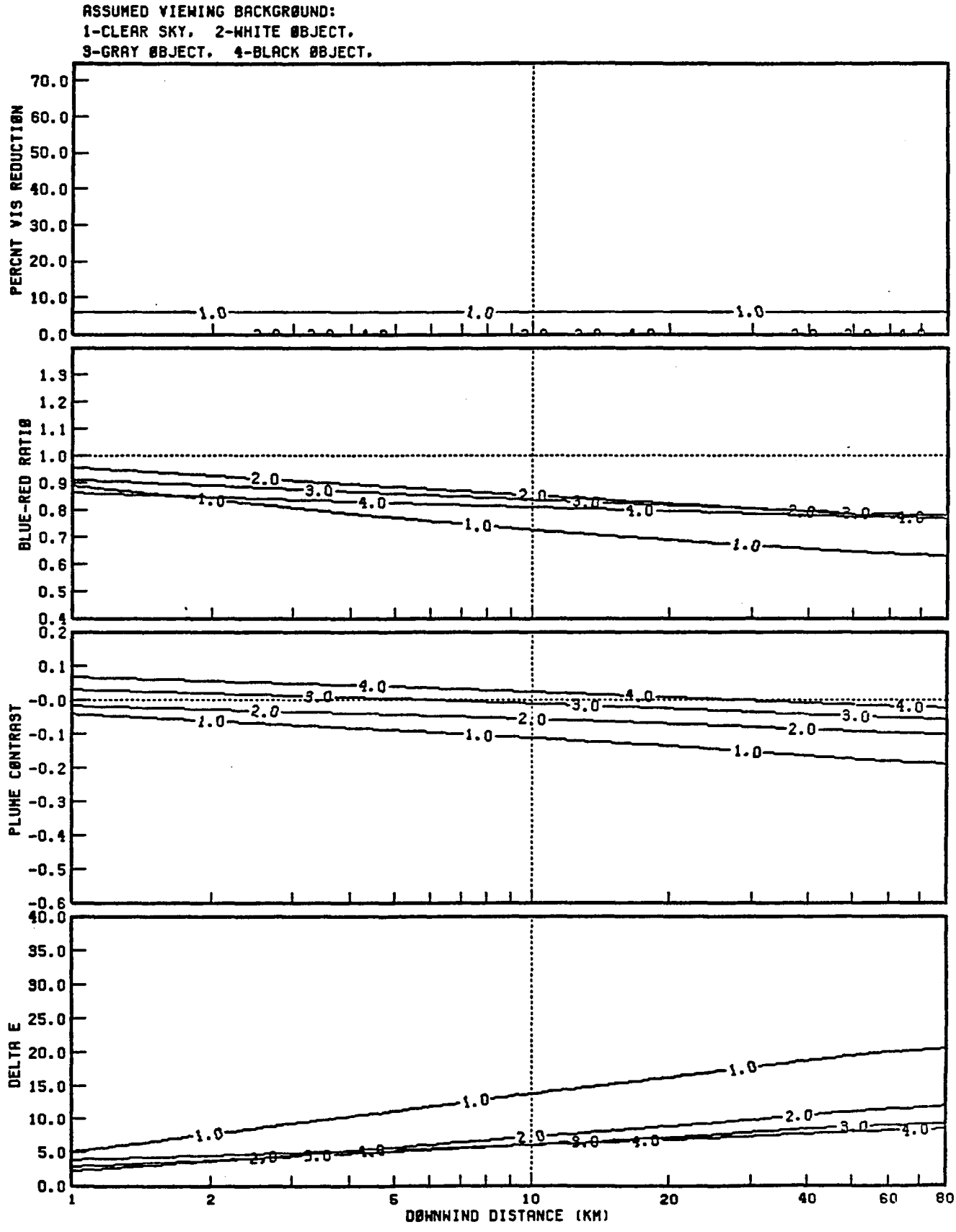

(a) Horizontal Views

FIGURE 15. SENSITIVITY EVALUATION--TVA-4

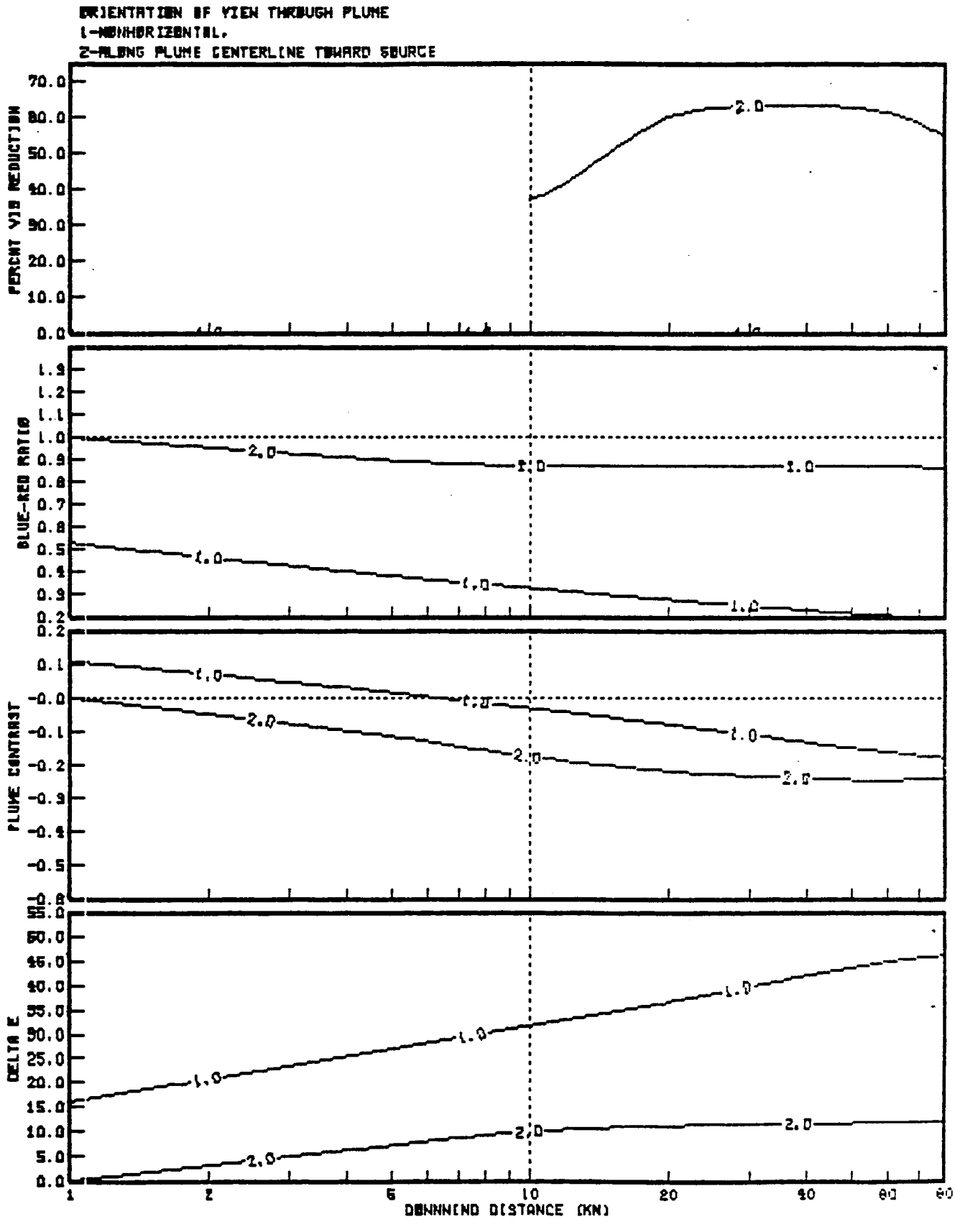

(b) Nonhorizontal and Axial Views

FIGURE 15 (Concluded)

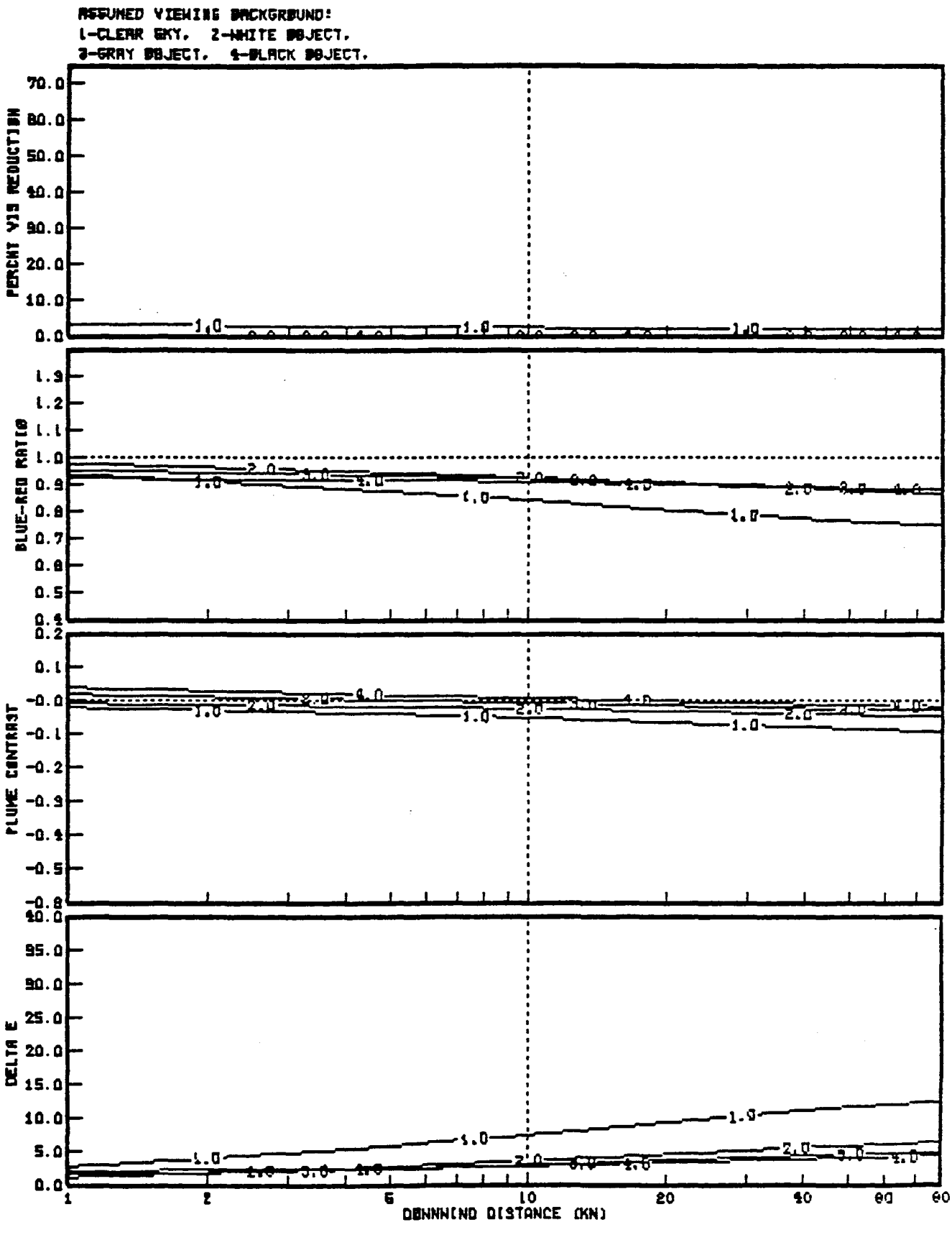

(a) Horizontal Views

FIGURE 16. SENSITIVITY EVALUATION--4 m/s WIND SPEED

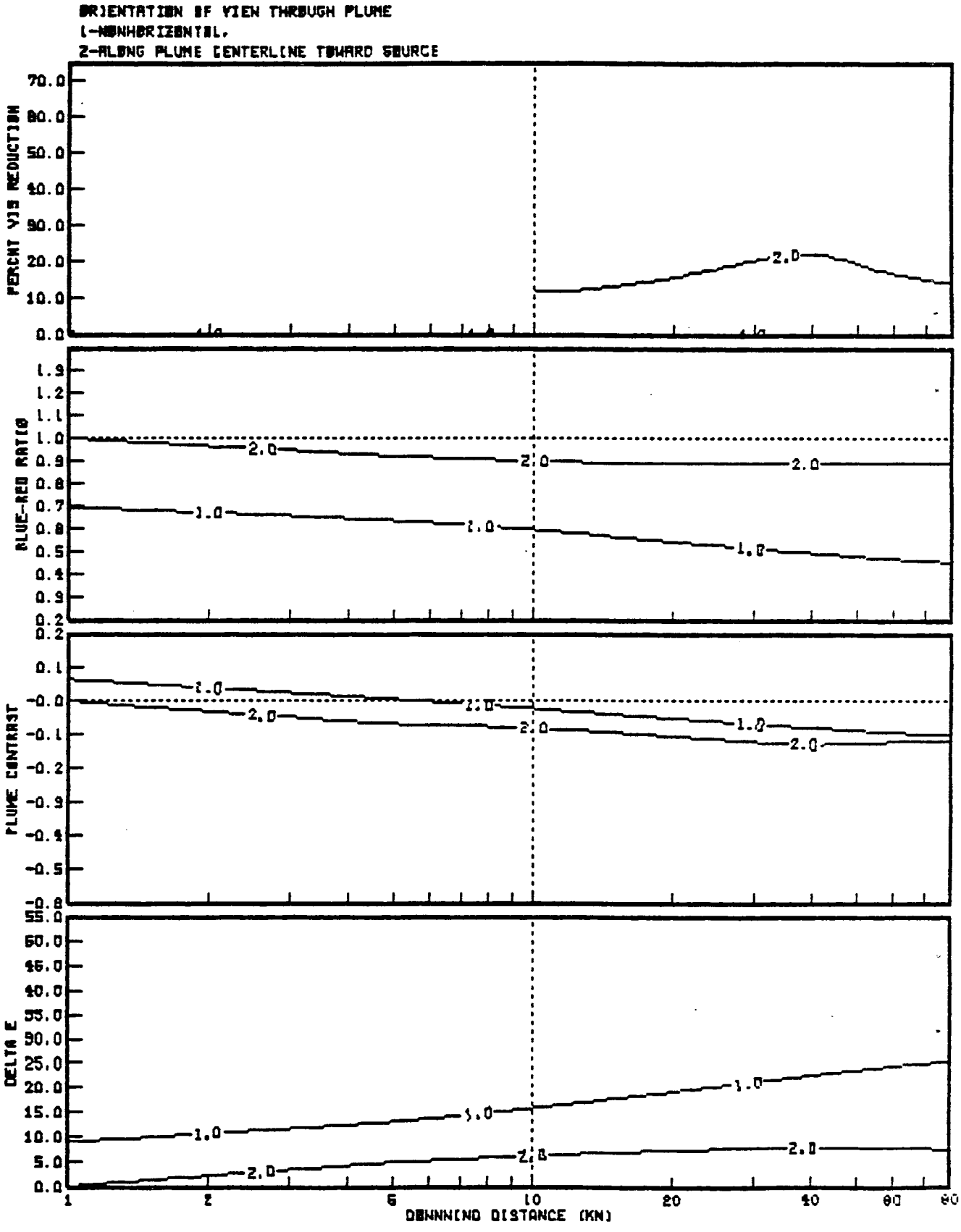

(b) Nonhorizontal and Axial Views

FIGURE 16 (Concluded)

condition. For PG-E, however, the reduction in visual range is notably less (20 percent) for views along the plume centerline.

These results are explained by the use of significantly greater values for horizontal dispersion (σ_y), which range from 400 m to 1500 m for distances of 10 to 50 km from the source for the PG-E stability class, compared to a range of 250 km to 750 km for the TVA-3 stability class. Although the value of σ_y has an effect on the estimate of visibility impairment for nonhorizontal views and for views along the plume centerline, it does not affect visibility impairment for horizonal views of the plume. The results obtained using a TVA-4 stability class (figure 15) indicate the potential for increased impairment of visibility under this condition as compared to the base case.

The results shown in figure 16 for a wind speed of 4 m/s, instead of 2 m/s as used in the base case, indicate a reduction in impact by a factor of one-third to one-half. Except for sky views of the plume, in which it will still appear brown and darker than the horizon sky, the visual impairment for horizontal views (e.g., object views) may not be significant. Impacts for nonhorizontal views and for views along the plume centerline, although reduced from those of the base case, may still cause significant visual impairment.

3.3.2 Sulfate Formation Rate

In addition to sulfate formation by reaction with the OH radical as considered in the base case, we have examined the effects of assuming a 1 percent and 2 percent heterogeneous sulfate formation rate.* Figures 17 and 18 show the results obtained using these increased sulfate formation rates. In general, higher sulfate concentrations will cause increased light scattering, resulting in visual range reduction and a brighter appearance of the plume because of the increased scattering of solar radiation.

For a 1 percent heterogeneous sulfate formation rate, the effects shown in figure 15 do not appear to be significantly different from the base case. The percentage of reduction in visual range is increased and the plume is brighter in contrast with black and gray background objects (i.e., horizontal view) and a background blue sky (i.e., nonhorizontal view). The plume coloration and perceptibility under all viewing conditions is unchanged or only slightly decreased from that of the base case.

---

* Sulfate conversion rates of 1 and 2 percent per hour were assumed by SCE in its NOI analysis.

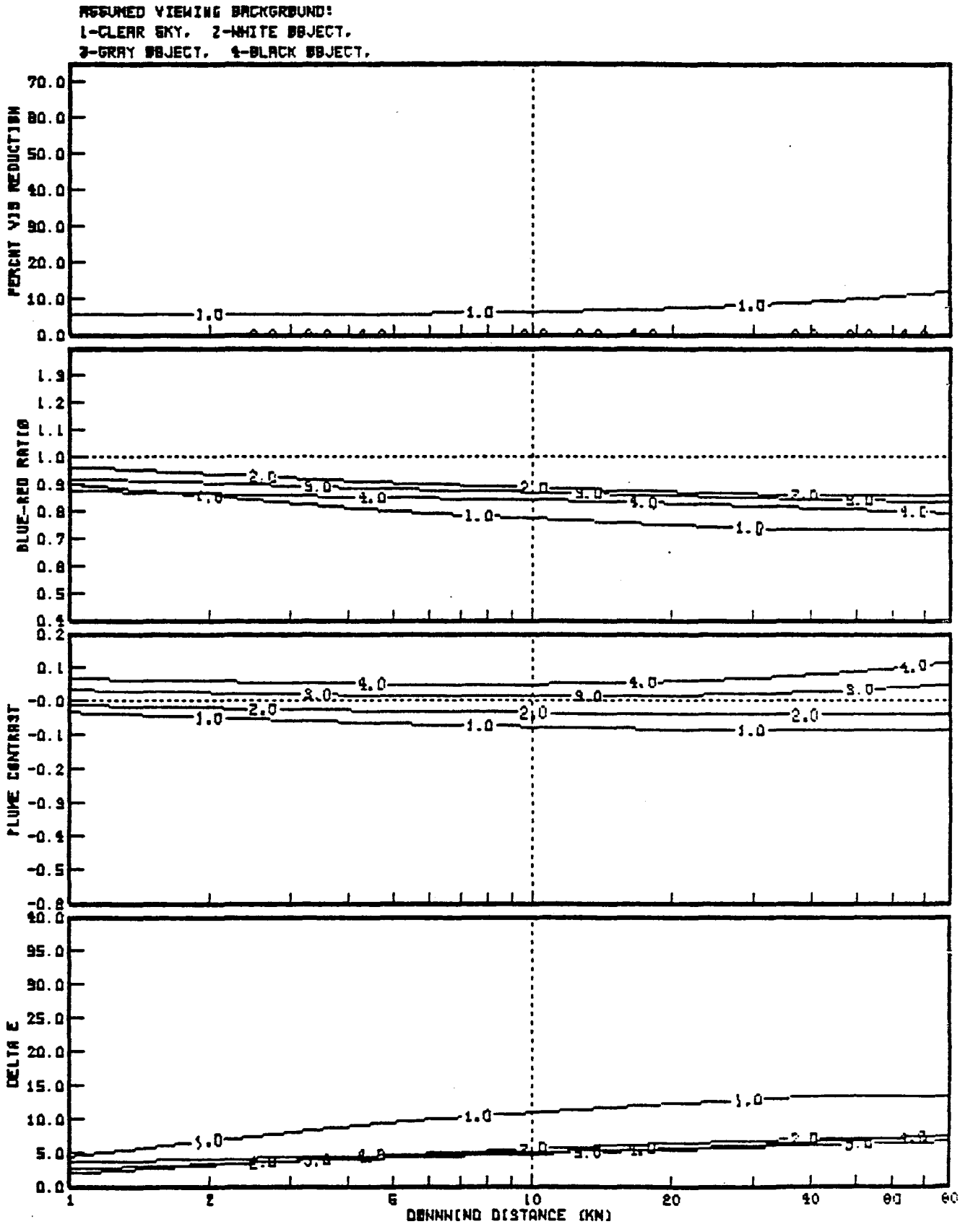

(a) Horizontal Views

FIGURE 17. SENSITIVITY EVALUATION--1 PERCENT SULFATE FORMATION RATE

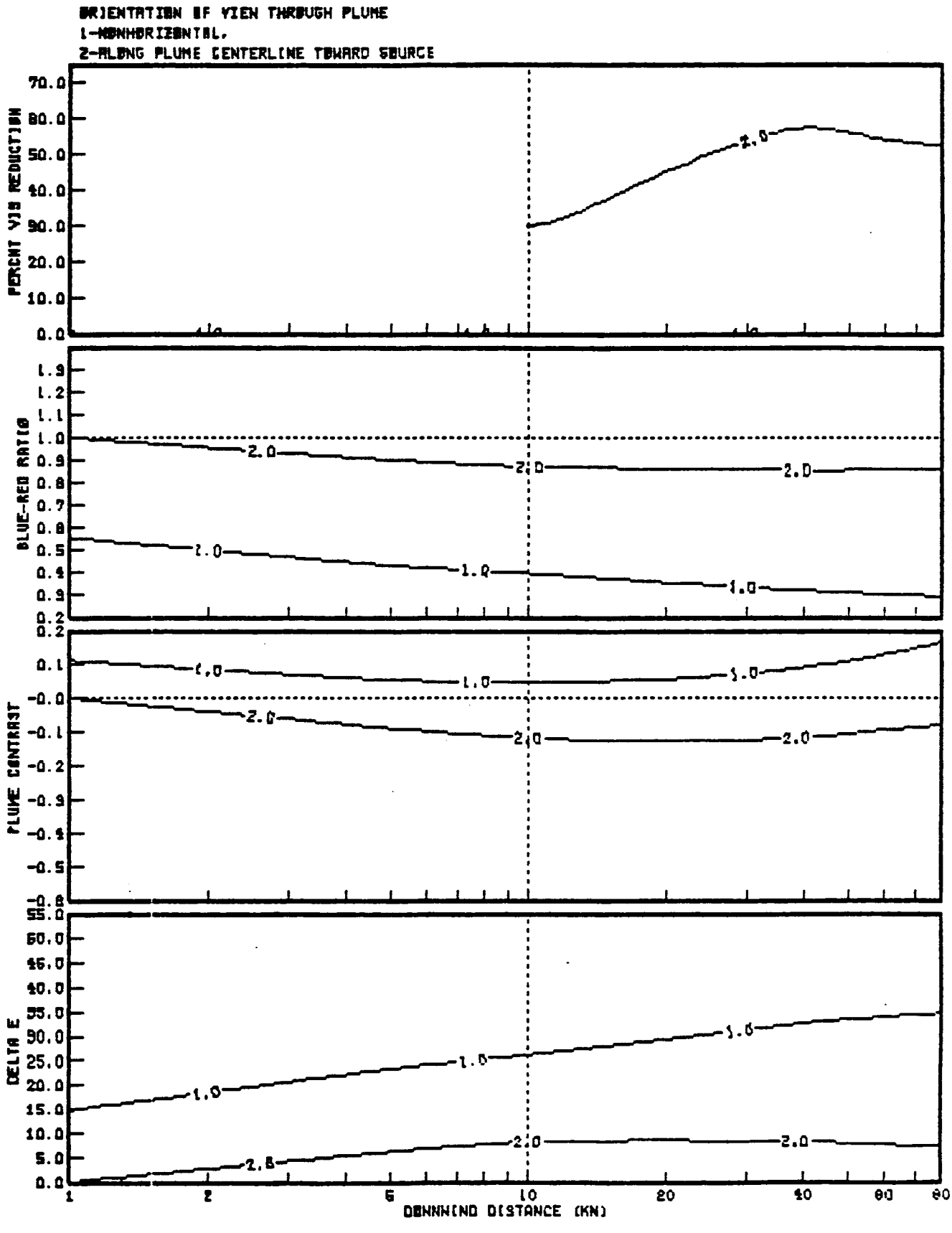

(b) Nonhorizontal and Axial Views

FIGURE 17 (Concluded)

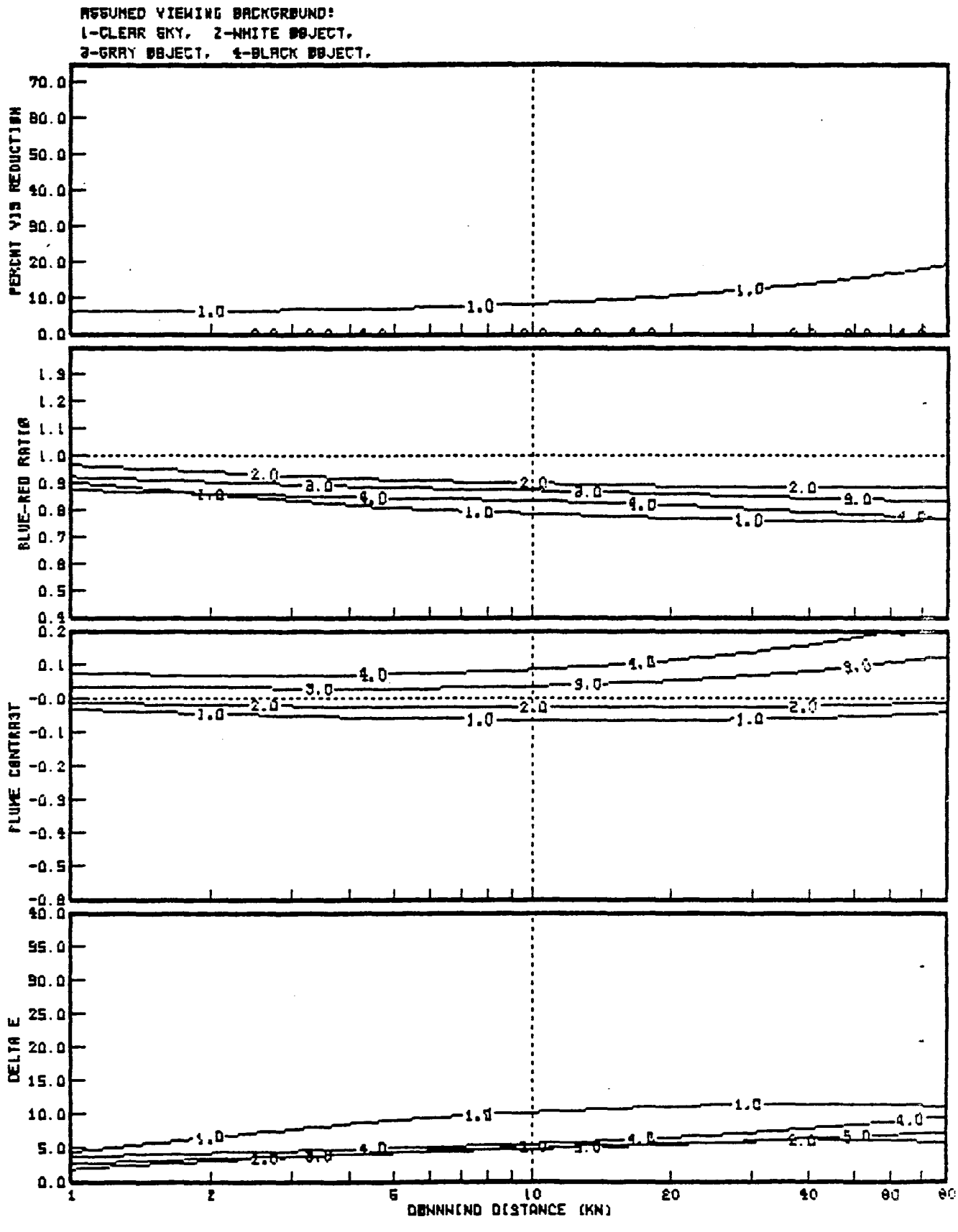

(a) Horizontal Views

FIGURE 18. SENSITIVITY EVALUATION--2 PERCENT SULFATE FORMATION RATE

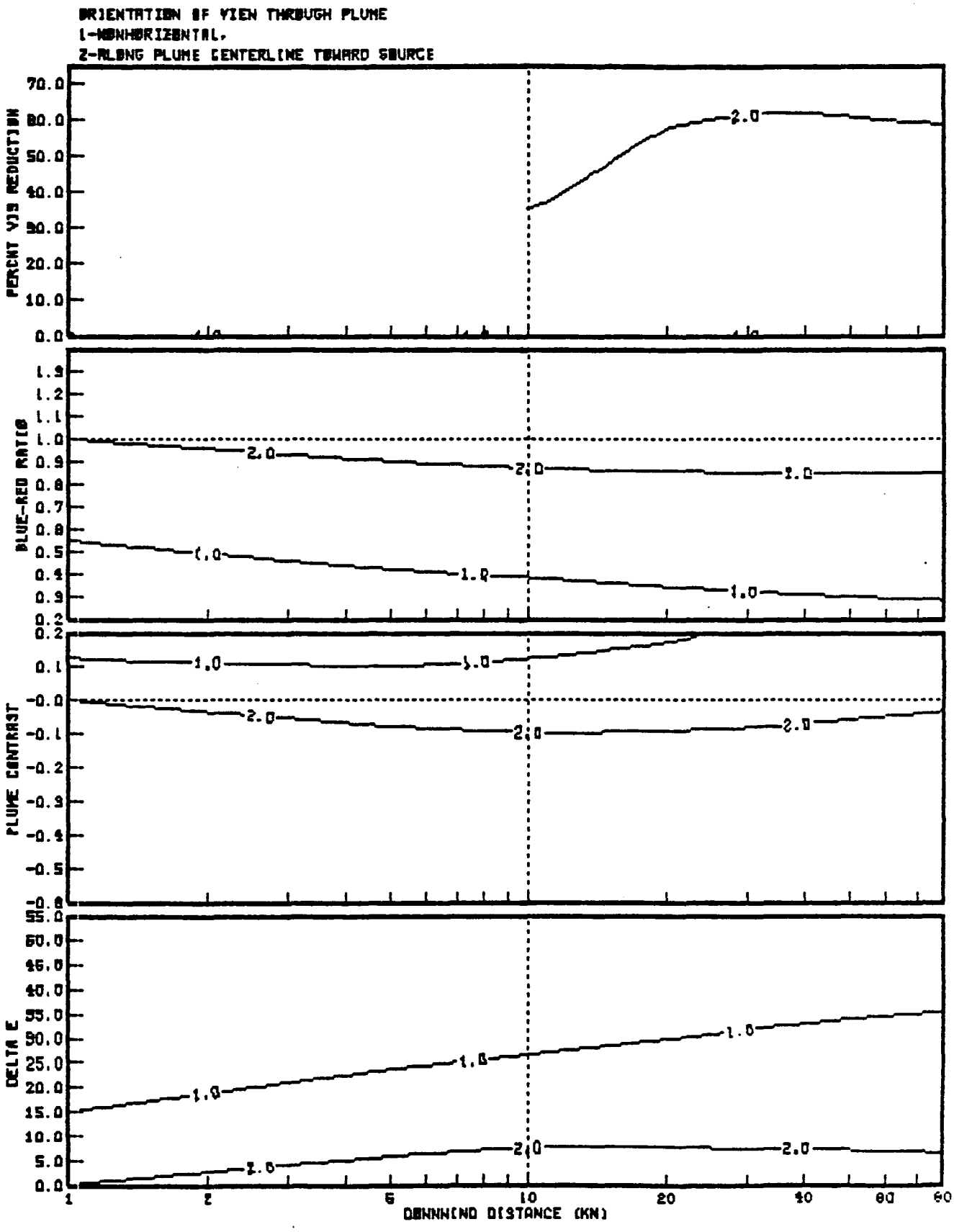

(b) Nonhorizontal and Axial Views

FIGURE 18 (Concluded)

With an assumed 2 percent heterogeneous sulfate formation rate, the effects described above are more evident. For horizontal sky views, the most significant effects are reduced perceptibility and coloration of the plume caused by the masking effect of sulfate-aerosol light scattering on NO_2 light absorption. For nonhorizontal views the plume will be much brighter than the blue sky, appearing as a haze layer. Similarly, for views along the plume centerline, this haze will cause a significant reduction in the background visual range (i.e., 40 to 60 percent).

3.3.3 Background Ozone Concentration

As mentioned in chapter 2, background ozone concentration affects the formation rate of NO_2 and $SO_4^=$. Since some uncertainty exists about selection of an appropriate background ozone concentration, three visibility model sensitivity runs were performed that assumed ozone concentrations of 0.03 ppm, 0.10 ppm, and 0.17 ppm. For the base case, a background ozone concentration of 0.07 ppm was assumed.

Figures 19, 20, and 21 show the results obtained using the alternative background ozone concentration values. Overall, these results indicate that visibility impairment is not highly sensitive to a range of between 0.03 and 0.1 ppm in background ozone values. For a 0.03 ppm ozone concentration, plume coloration and perceptibility is slightly decreased from that of the base case, but visual range is almost unaffected. For a concentration of 0.10 ppm, the perceptibility and coloration of the plume is slightly increased over that of the base case. At the highest background ozone concentration considered (0.17 ppm), the perceptibility and coloration of the plume is more significantly increased and the visual range is reduced from that of the base case for the view along the plume centerline. However, though the degree of impact is affected by very high ozone amounts, there is still significant perceptible impact at very low ozone levels.

3.3.4 Background Visual Range

Background visual range is an important input parameter because the magnitude of plume discoloration that is visible from a given location depends on the clarity of the intervening atmosphere. Plume discoloration is more noticeable during periods of extremely clear skies than on hazy days. In this sensitivity analysis we have examined the effect of increasing the background visual range on visibility. However, we have kept the ratios of observer-plume distance to background visual range and observer-object distance to background visual range the same as those used for the base case. Thus, though the background visual range is increased,

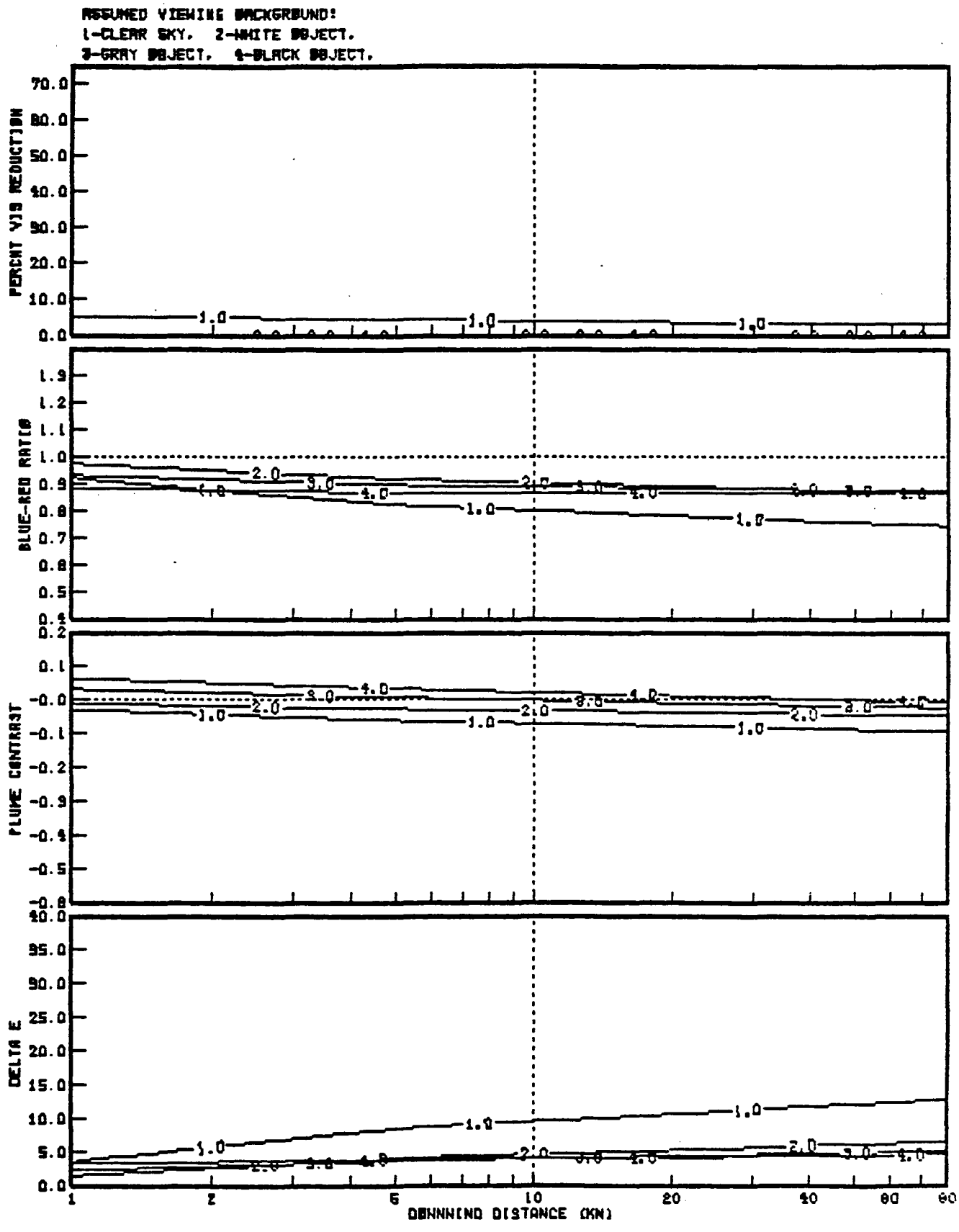

(a) Horizontal Views

FIGURE 19. SENSITIVITY EVALUATION--BACKGROUND
OZONE = 0.03 ppm

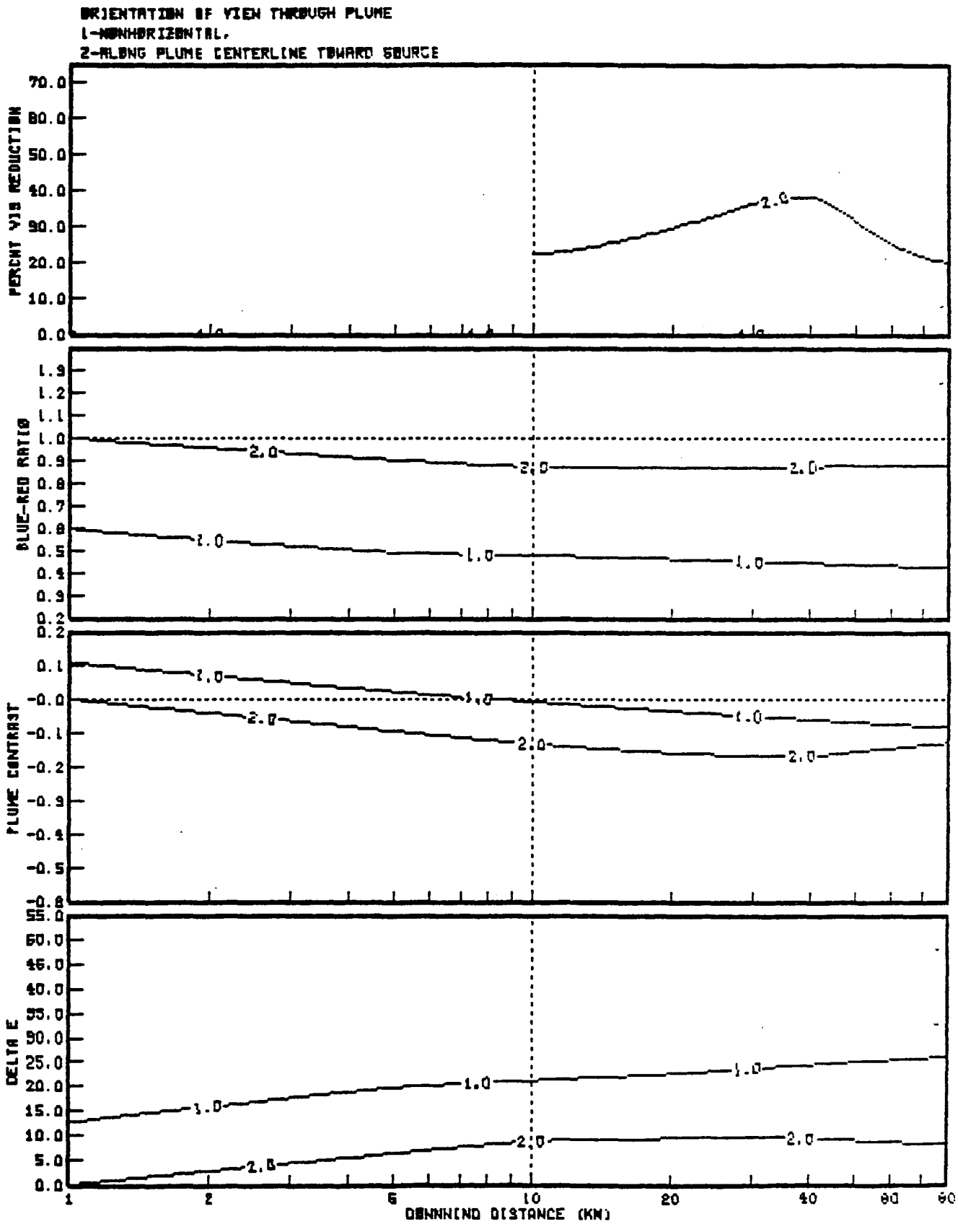

(b) Nonhorizontal and Axial Views

FIGURE 19 (Concluded)

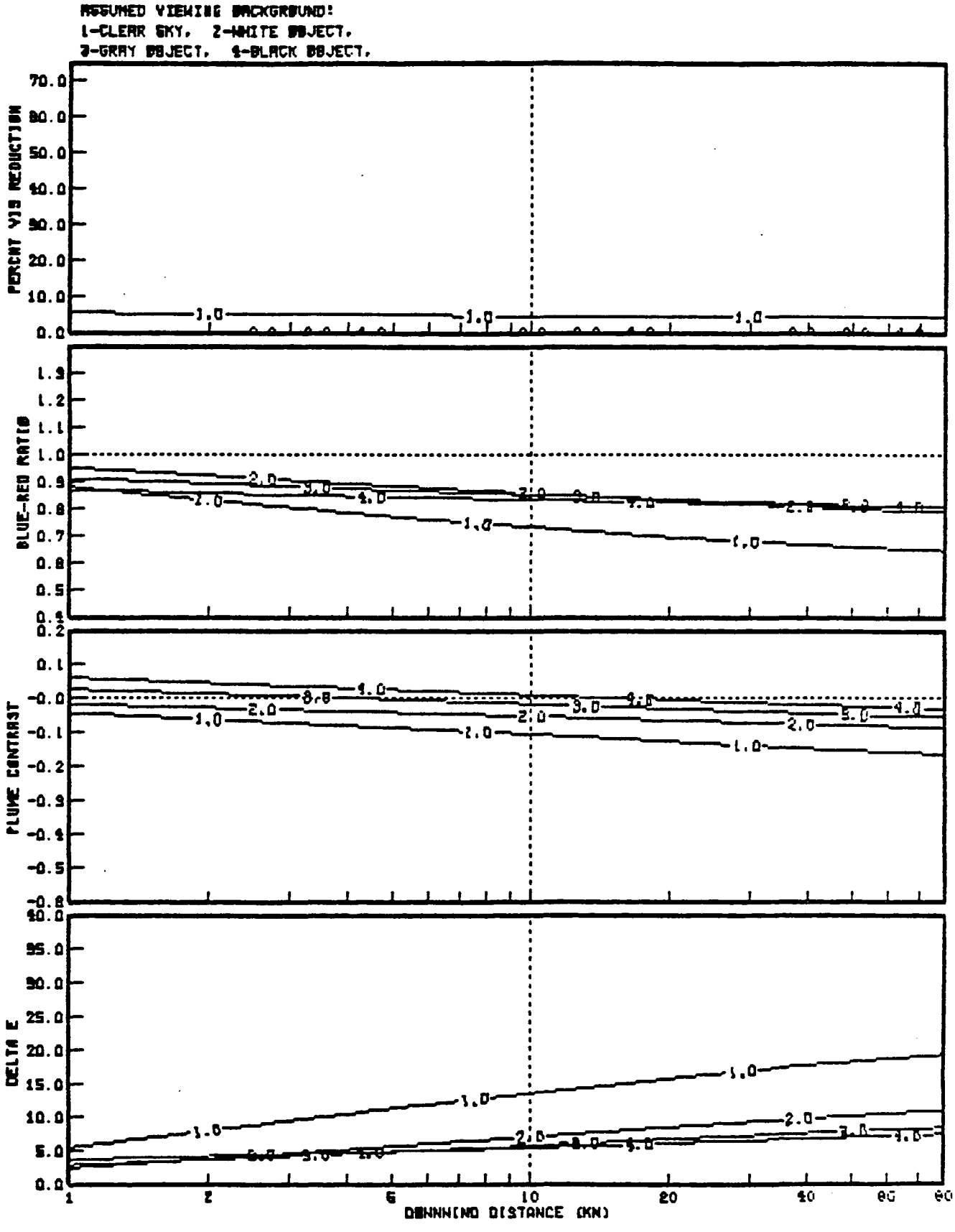

(a) Horizontal Views

FIGURE 20. SENSITIVITY EVALUATION--BACKGROUND
OZONE = 0.1 ppm

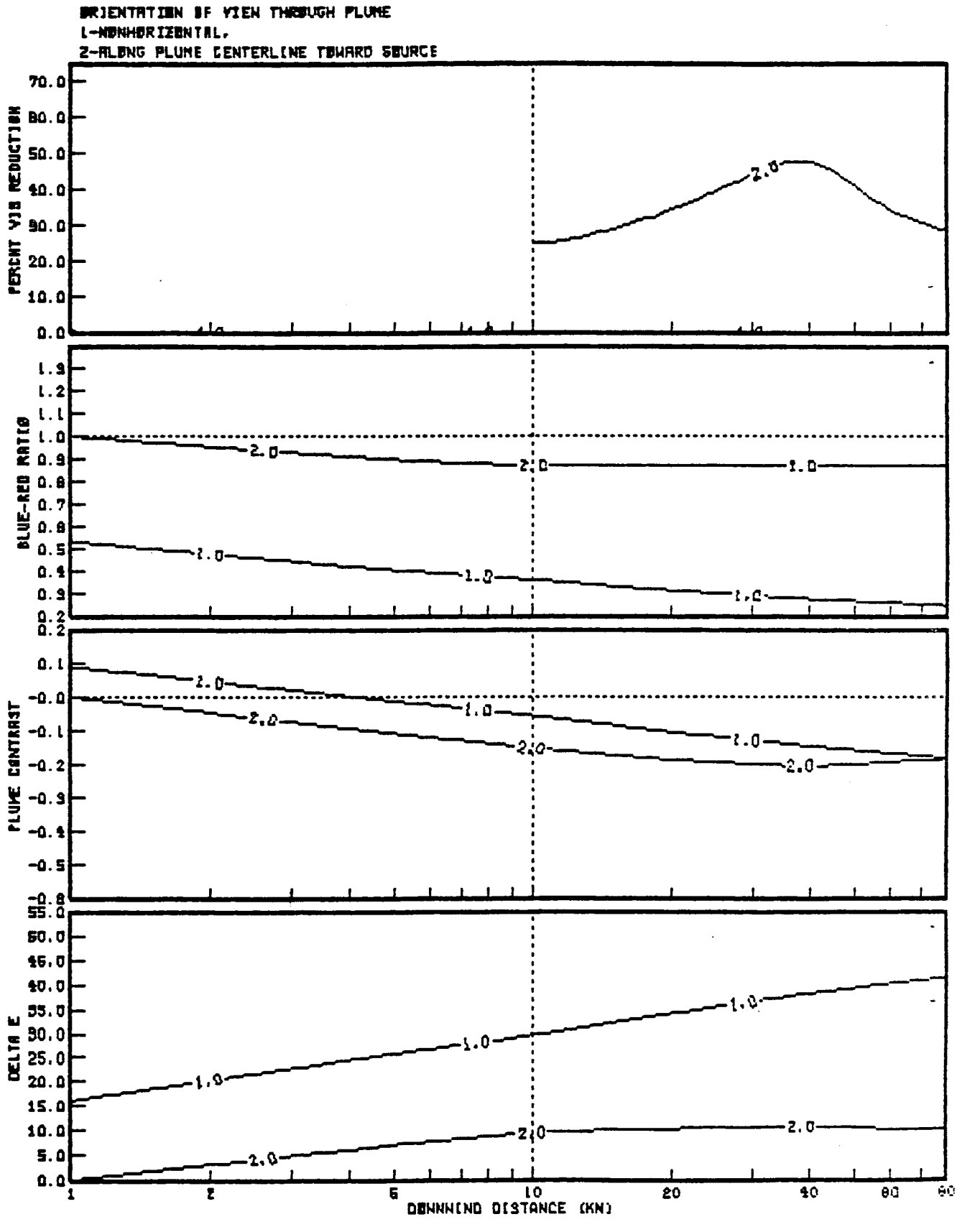

(b) Nonhorizontal and Axial Views

FIGURE 20 (Concluded)

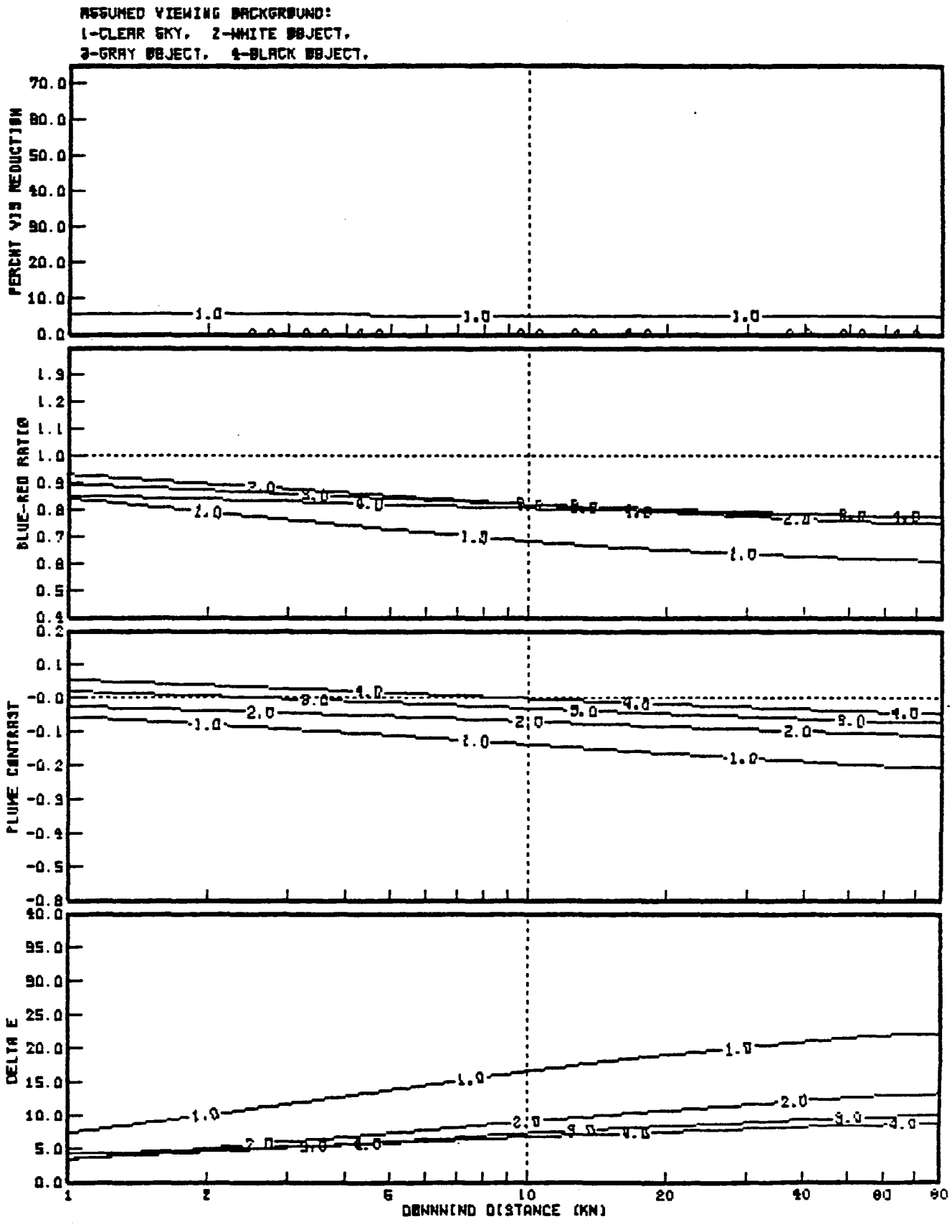

(a) Horizontal Views

FIGURE 21. SENSITIVITY EVALUATION--BACKGROUND
OZONE = 0.17 ppm

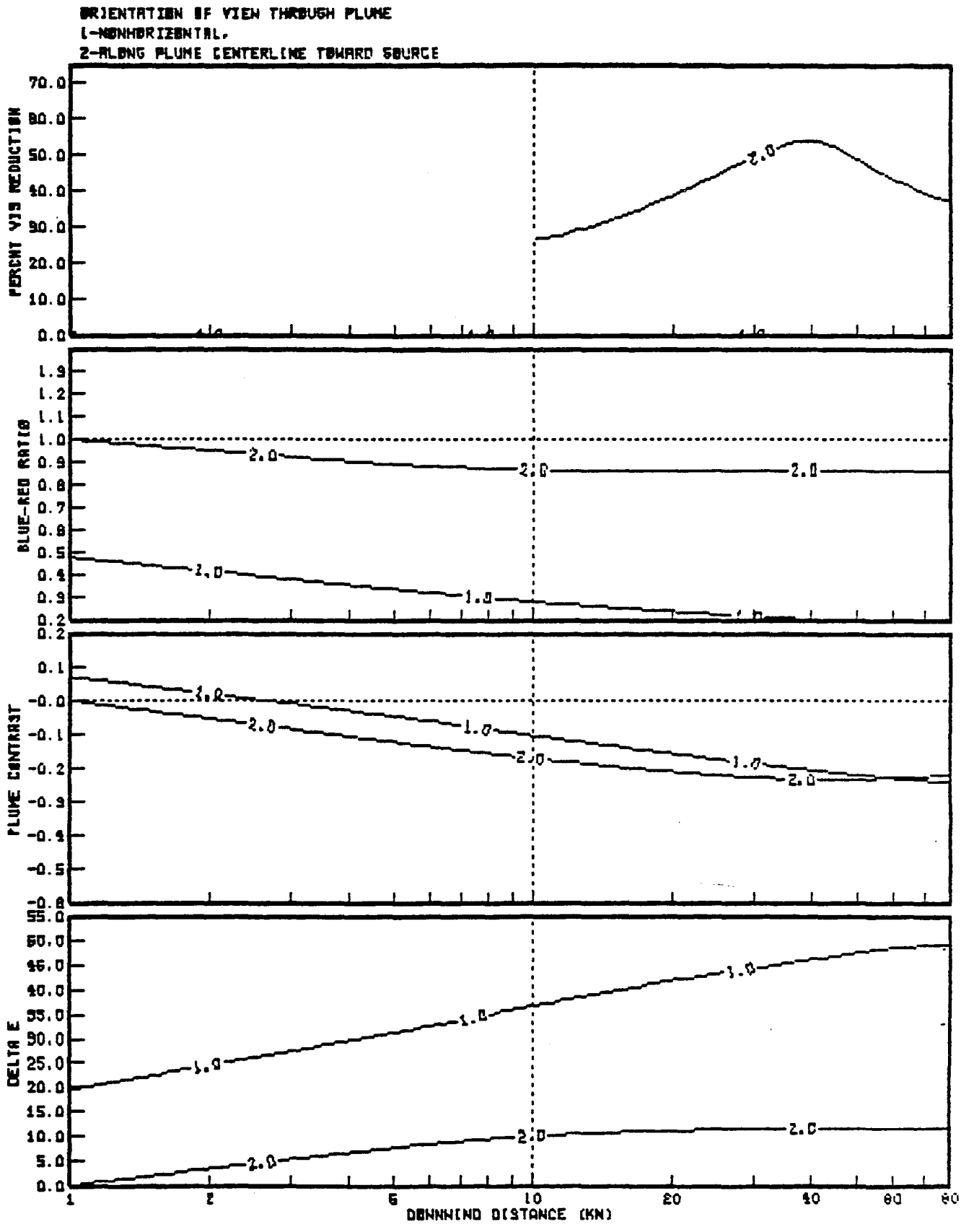

(b) Nonhorizontal and Axial Views

FIGURE 21 (Concluded)

the distances between the observer, plume, and background objects are also increased. This sensitivity analysis was performed to determine whether the results changed significantly from those of the base-case when background visual range and viewing distances were increased proportionally.

The results obtained assuming a background visual range of 100 km, an observer-plume distance of 10 km, and an observer-object distance of 20 km, are shown in figure 22. Similarly, figure 23 shows the effect on visibility when a background visual range of 200 km, and an observer-plume and background-object distance of 20 km and 40 km, respectively, are used.

A comparison of results for these cases indicates impairment almost equal to or greater than that of the base case. At a 100-km background visual range, and with proportional increases in the distances of the observer from the plume and background, the degree of visibility impairment is not significantly different from that of the base case. For a background visual range of 200 km, visibility impairment is increased over that of the base case even though the distances of the observer from the plume and background targets are greater. As shown in figure 12, a background visual range of between 100 and 200 km is a frequent occurrence in the vicinity of China Lake.

3.3.5 Relative Humidity

The amount of water vapor in the air has an effect on the rate of sulfate formation. Therefore, we have estimated visibility impairment using a higher relative humidity. Figure 24 shows the visibility impairment resulting from an assumption of 55 percent relative humidity as compared to 25 percent for the base case. The results indicate no discernible difference. Since relative humidity affects only the rate of sulfate formation and scattering coefficient, these results further indicate the importance of NO_2 light absorption. If more sulfate formation was present, the results would be more sensitive to relative humidity.

3.3.6 Mass Median Diameter of Fly Ash Emissions

Light scattering by particulates is most efficient for particles with a diameter of between 0.1 and 1.0 μm. Fly ash emitted from a coal-fired power plant, after removal of approximately 98 percent of the total mass generated, is largely made up of smaller particles that may be within the efficient light-scattering range. For the base case, we have assumed that the mass median diameter for fly ash emissions is 1.7 μm. For this sensitivity analysis, we examined the effect of assuming a mass median diameter of 0.3 μm, which should result in a near-maximum light-scattering

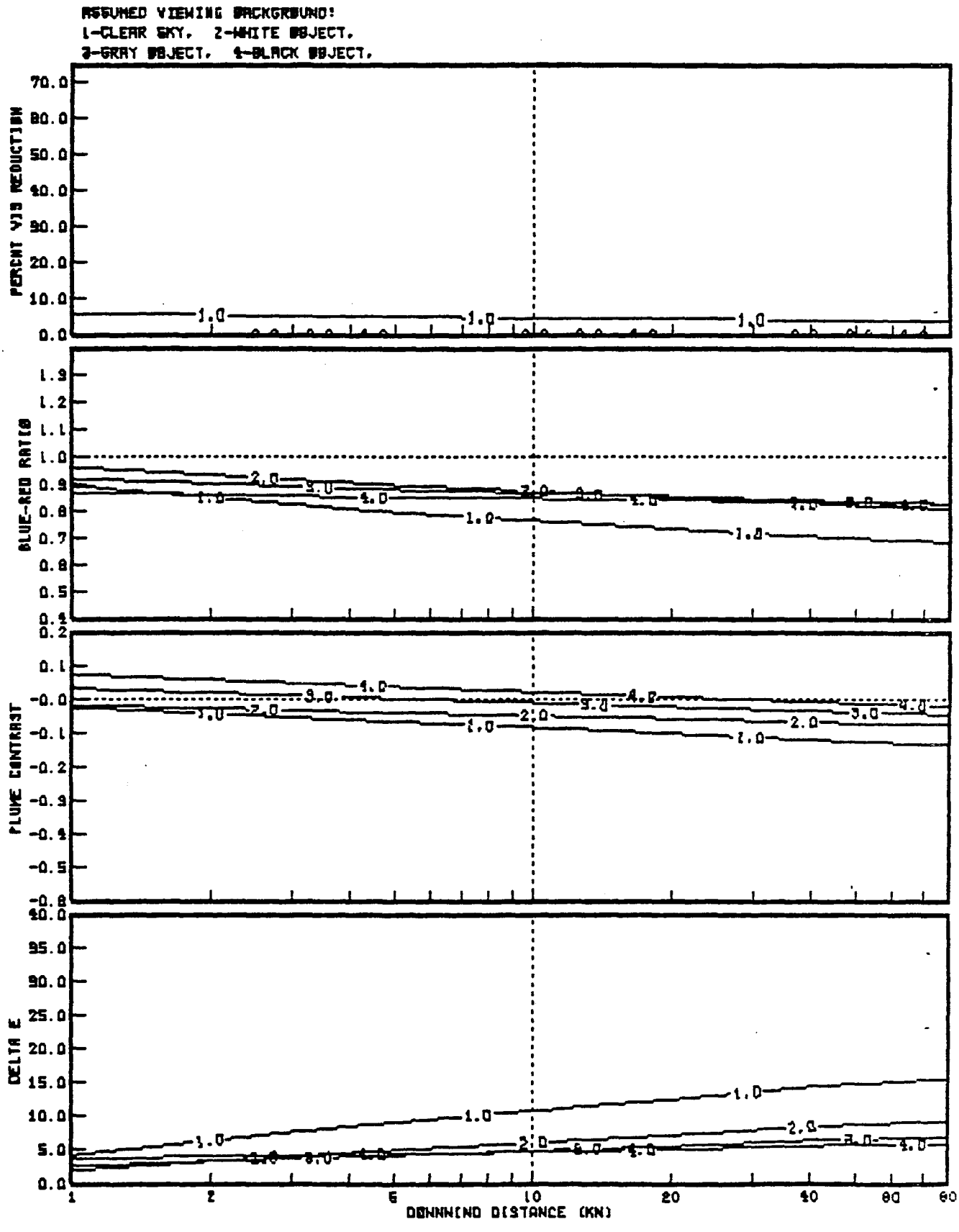

(a) Horizontal Views

FIGURE 22. SENSITIVITY EVALUATION--BACKGROUND
VISUAL RANGE = 100 km

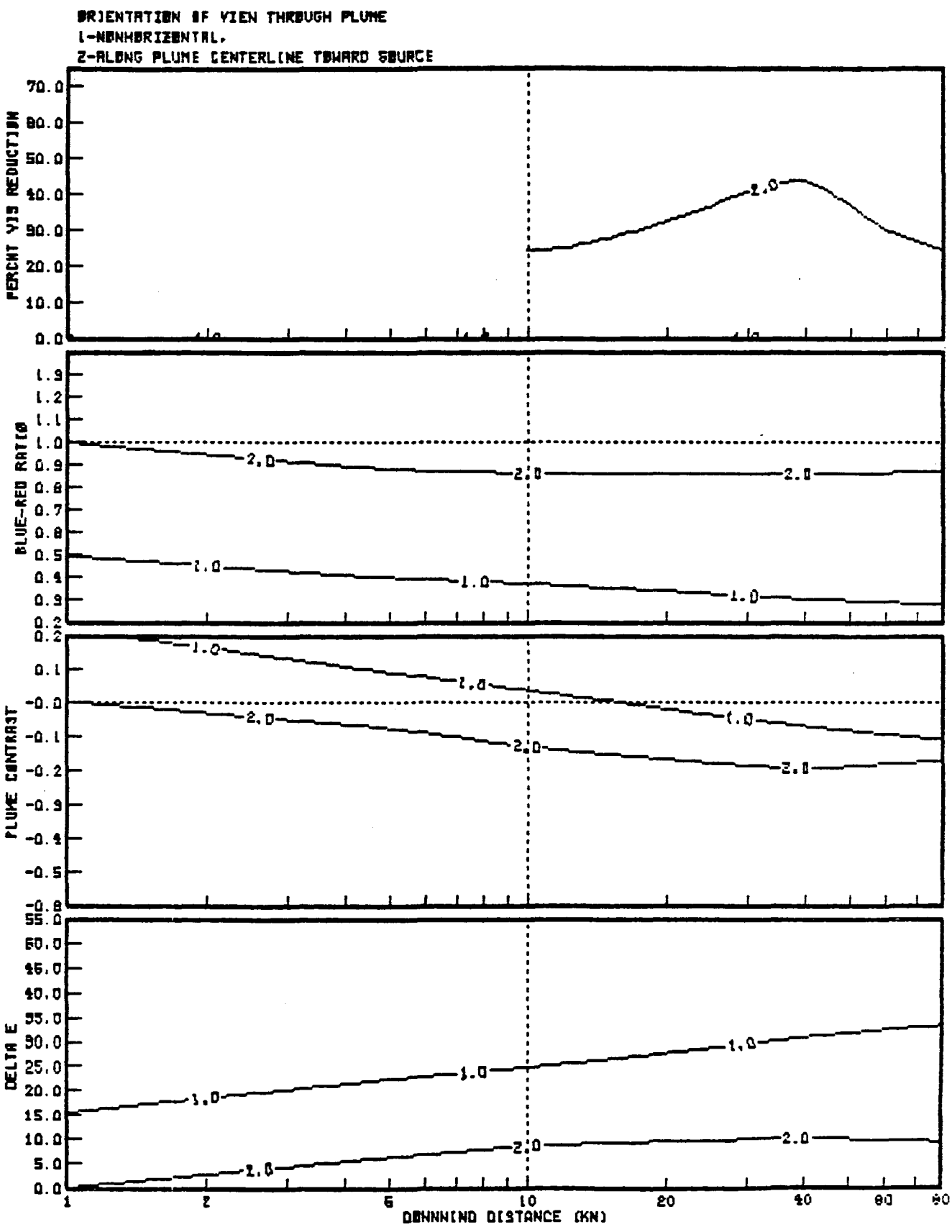

(b) Nonhorizontal and Axial Views

FIGURE 22 (Concluded)

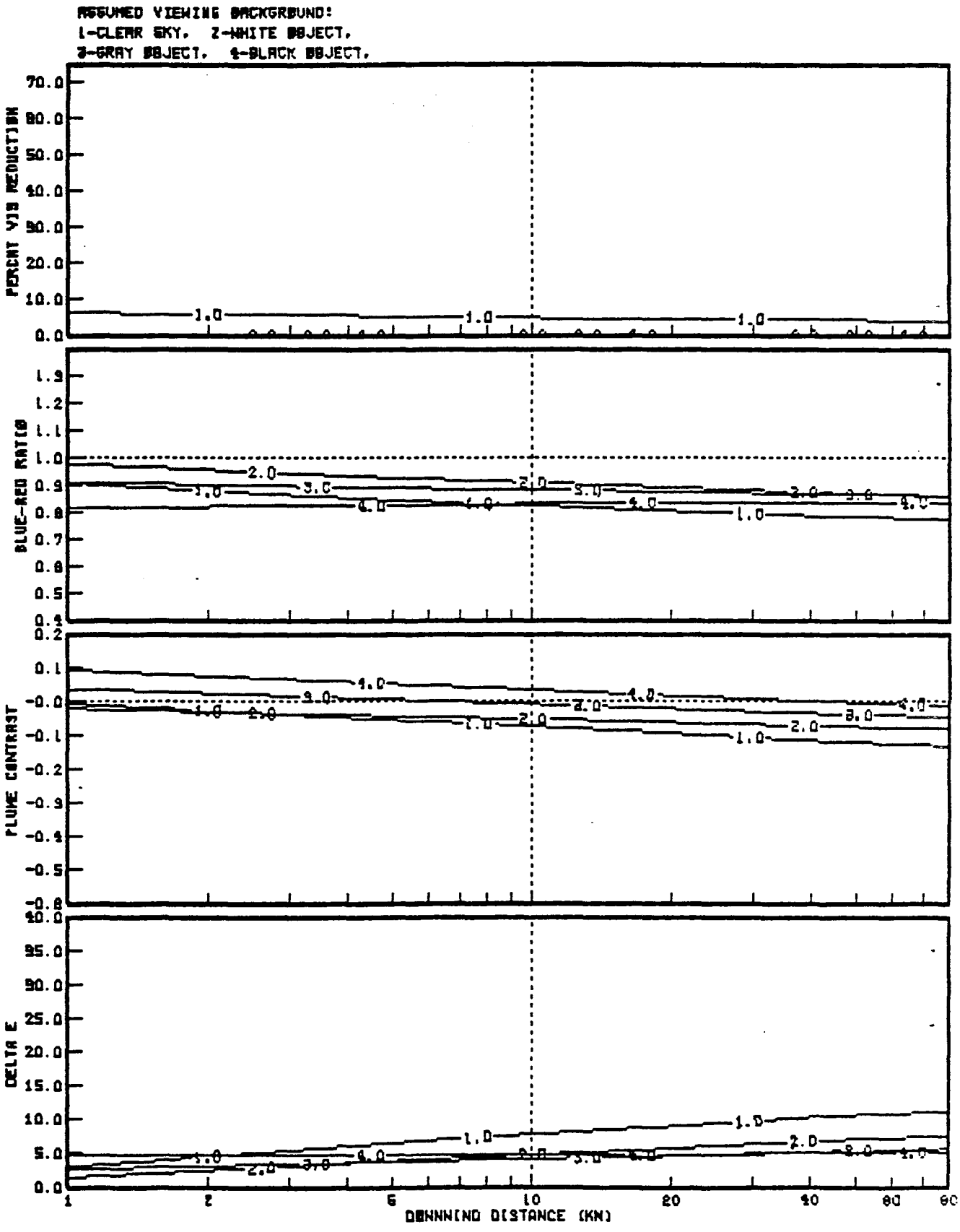

(a) Horizontal Views

FIGURE 23. SENSITIVITY EVALUATION--BACKGROUND
VISUAL RANGE = 200 km

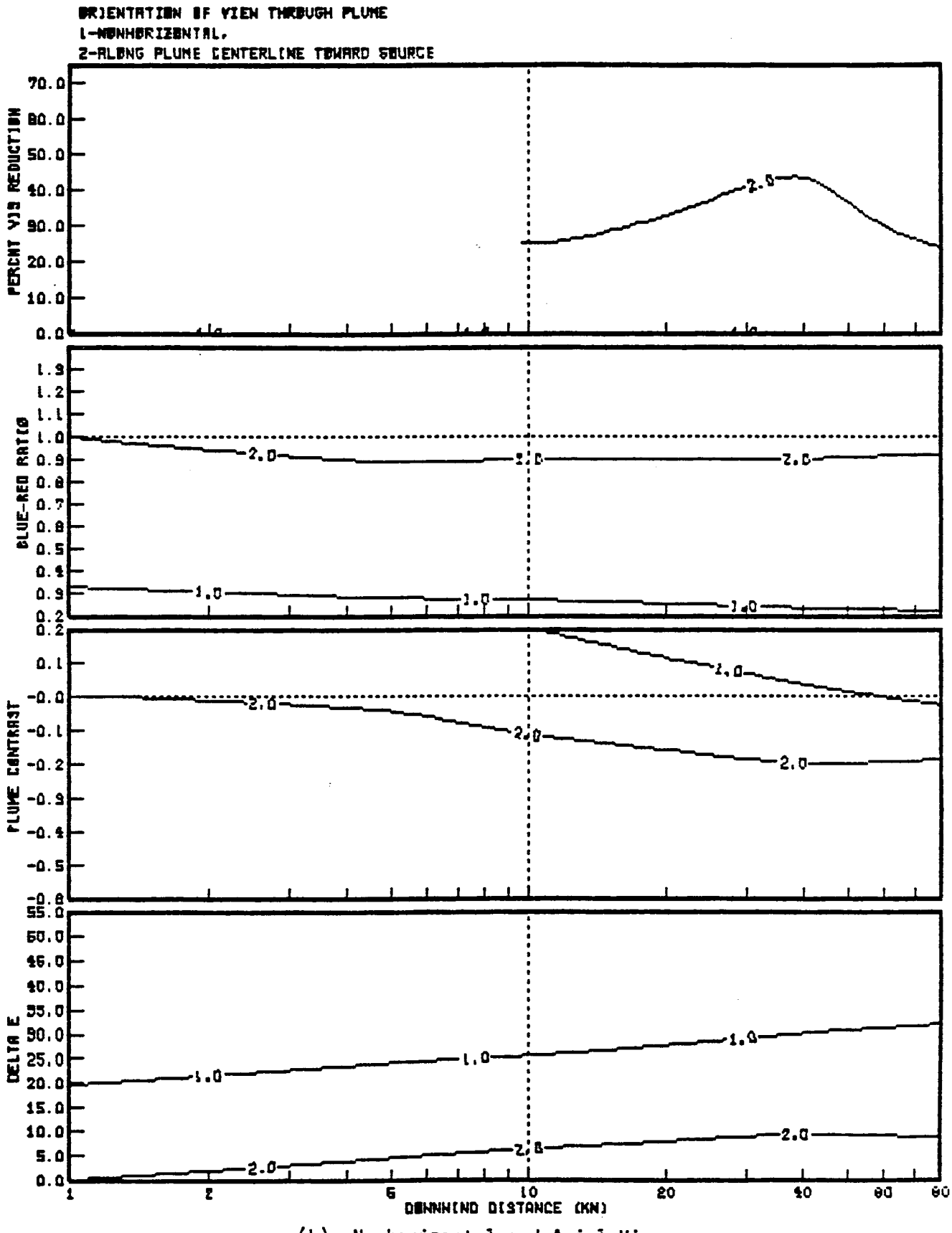

(b) Nonhorizontal and Axial Views

FIGURE 23 (Concluded)

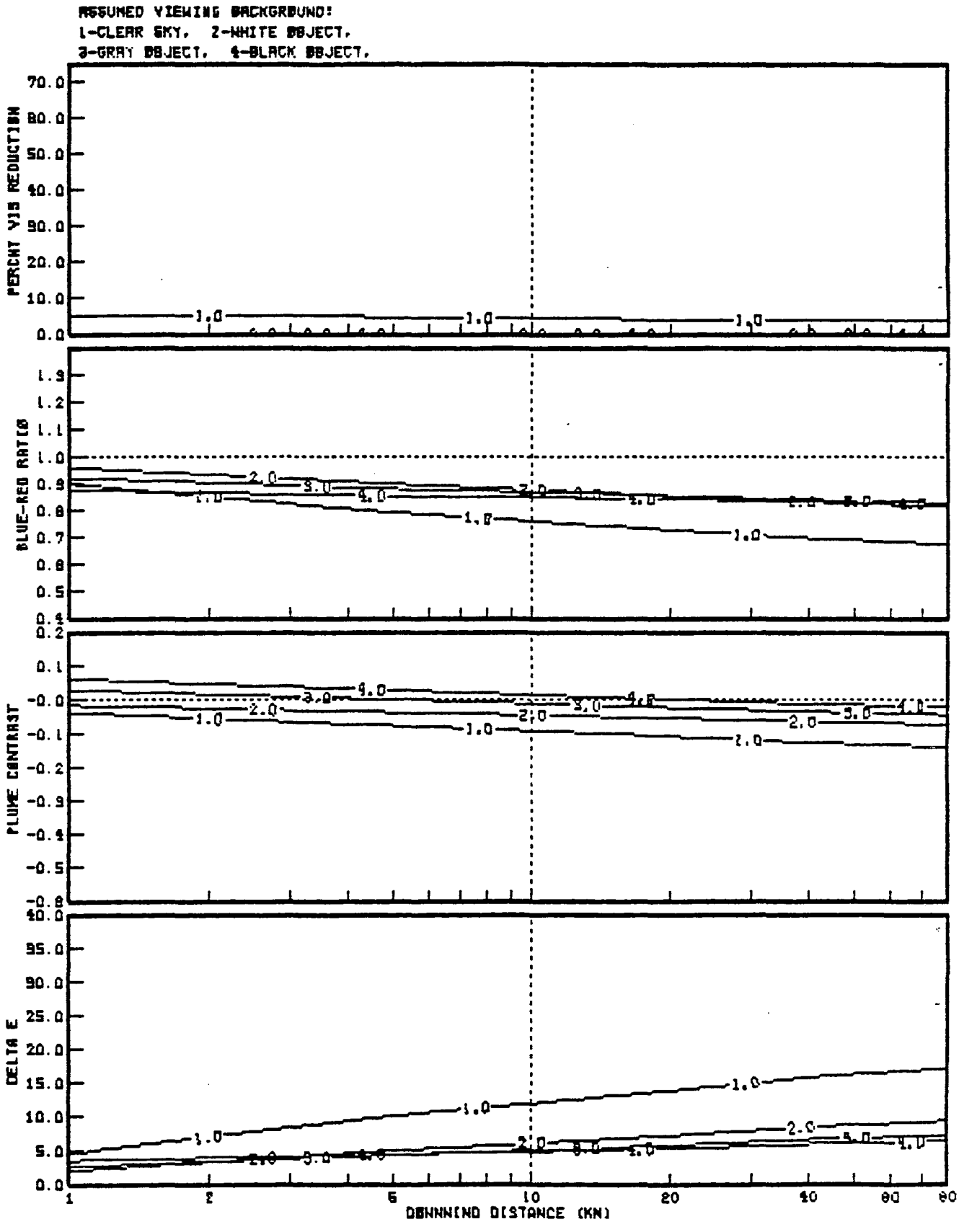

(a) Horizontal Views

FIGURE 24. SENSITIVITY EVALUATION--RELATIVE HUMIDITY = 55 PERCENT

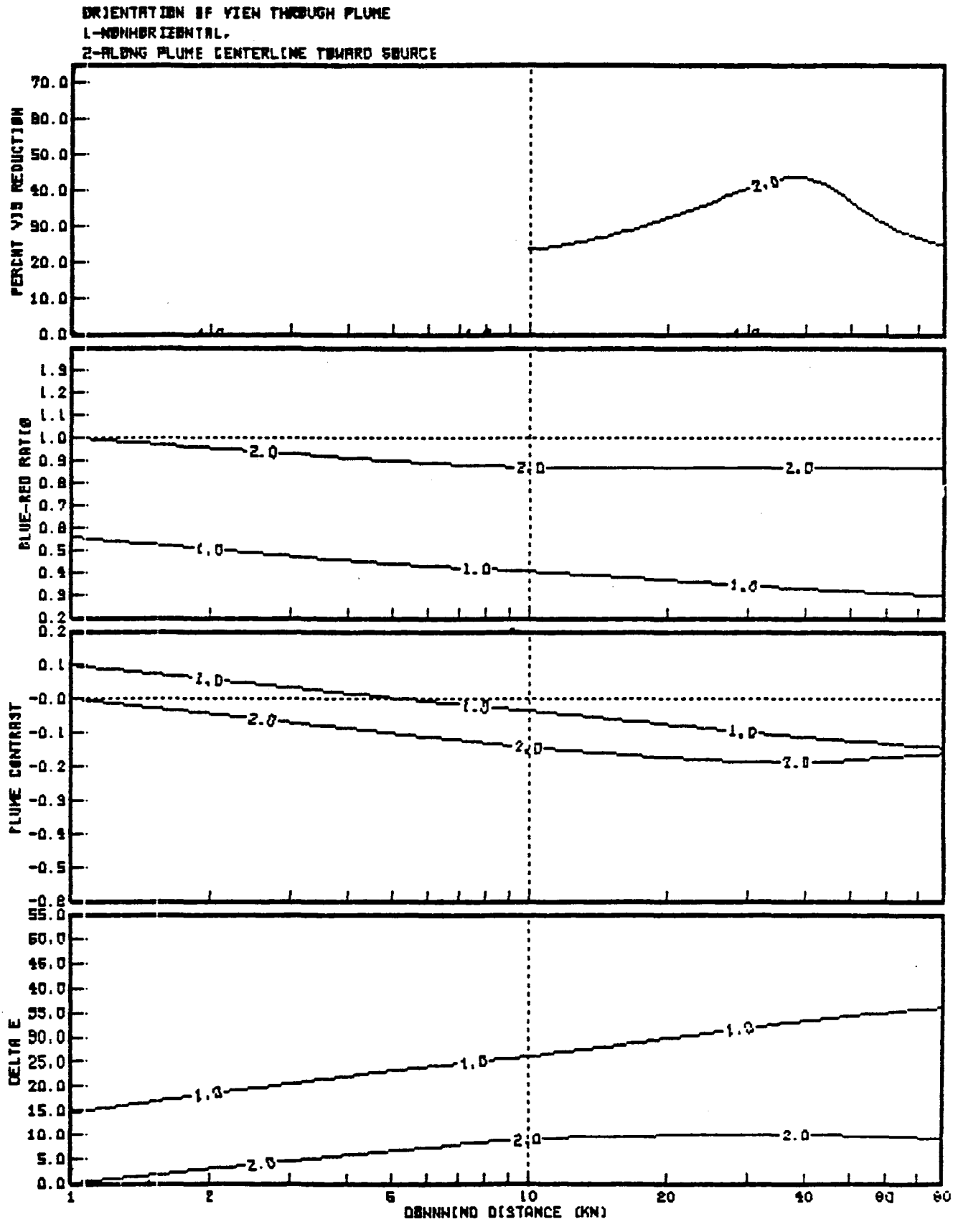

(b) Nonhorizontal and Axial Views

FIGURE 24 (Concluded)

effect from fly ash emissions. The results of this analysis are shown in figure 25.

The light-scattering effects of fly ash emissions, unlike those of secondary sulfate aerosols, are greatest near the source. As shown in figure 25(a), this light scattering causes a decrease in visual range and a brighter plume for the base case, especially at locations near the source. In nonhorizontal views [figure 25(b)], the plume is much brighter than the blue sky background. For the base case, the plume is generally dark when viewed against a blue sky background. Again, these effects are greater at short distances from the source but may not be negligible at longer distances of between 20 and 60 km.

3.3.7 Pollutant Emissions

In this sensitivity analysis we examine the effects of changes in emissions that might be achieved by reducing the capacity of the electrical generating facility or, for certain pollutants (e.g., NO_x), by increasing the control of emissions, or both. We have selected for analysis uniform reductions in all emissions (i.e., SO_x, NO_x and particulates) of 33 percent, 67 percent, and 90 percent. Figures 26, 27, and 28 show the estimated visibility impacts for each of these cases compared with the base-case results. These results indicate a reduction in visibility impairment that is nearly equal to the reduction in emissions.

With a one-third reduction in emissions, the plume is still perceptible against either the horizon sky or blue sky background. Also, if the plume is viewed along its centerline axis, reduction in visual range will still be significant (i.e., 20 percent) for this case.

With a two-thirds reduction in pollutant emissions, the plume may still be perceptible for horizontal and nonhorizontal views against a sky background. However, the coloration and darkness of the plume under these conditions is much reduced. With a 90 percent reduction in emissions, visibility does not appear to be significantly impaired for any of the observer viewing conditions.

3.4 LIMITED MIXING, STAGNANT CONDITIONS AT EDWARDS AIR FORCE BASE

As discussed in the appendix, concentration of pollutants under limited mixing in which the plume is uniformly dispersed throughout the mixed layer can be described by the following equation:

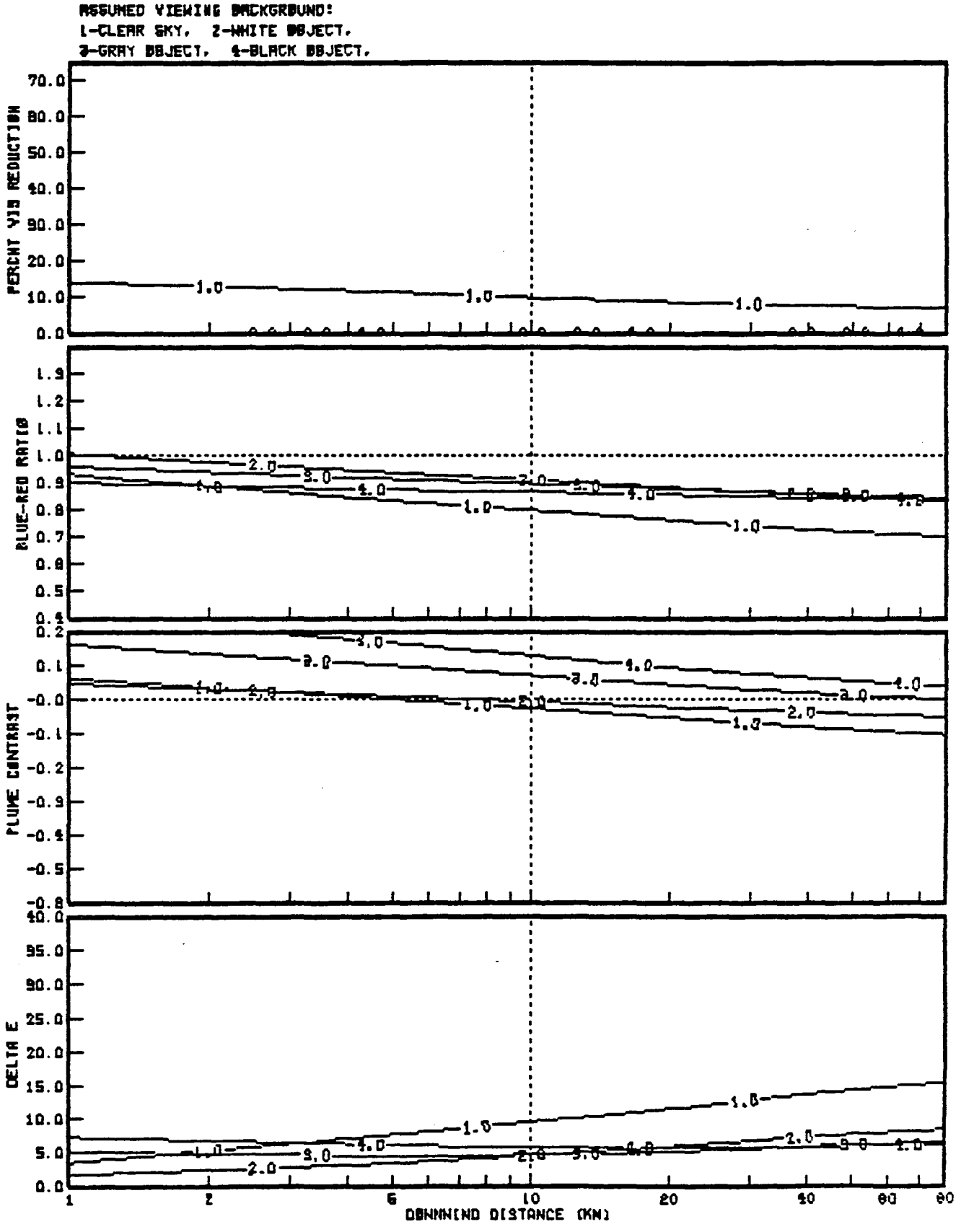

(a) Horizontal Views

FIGURE 25. SENSITIVITY EVALUATION--FLY ASH PARTICULATE MEAN DIAMETER = 0.3 μm

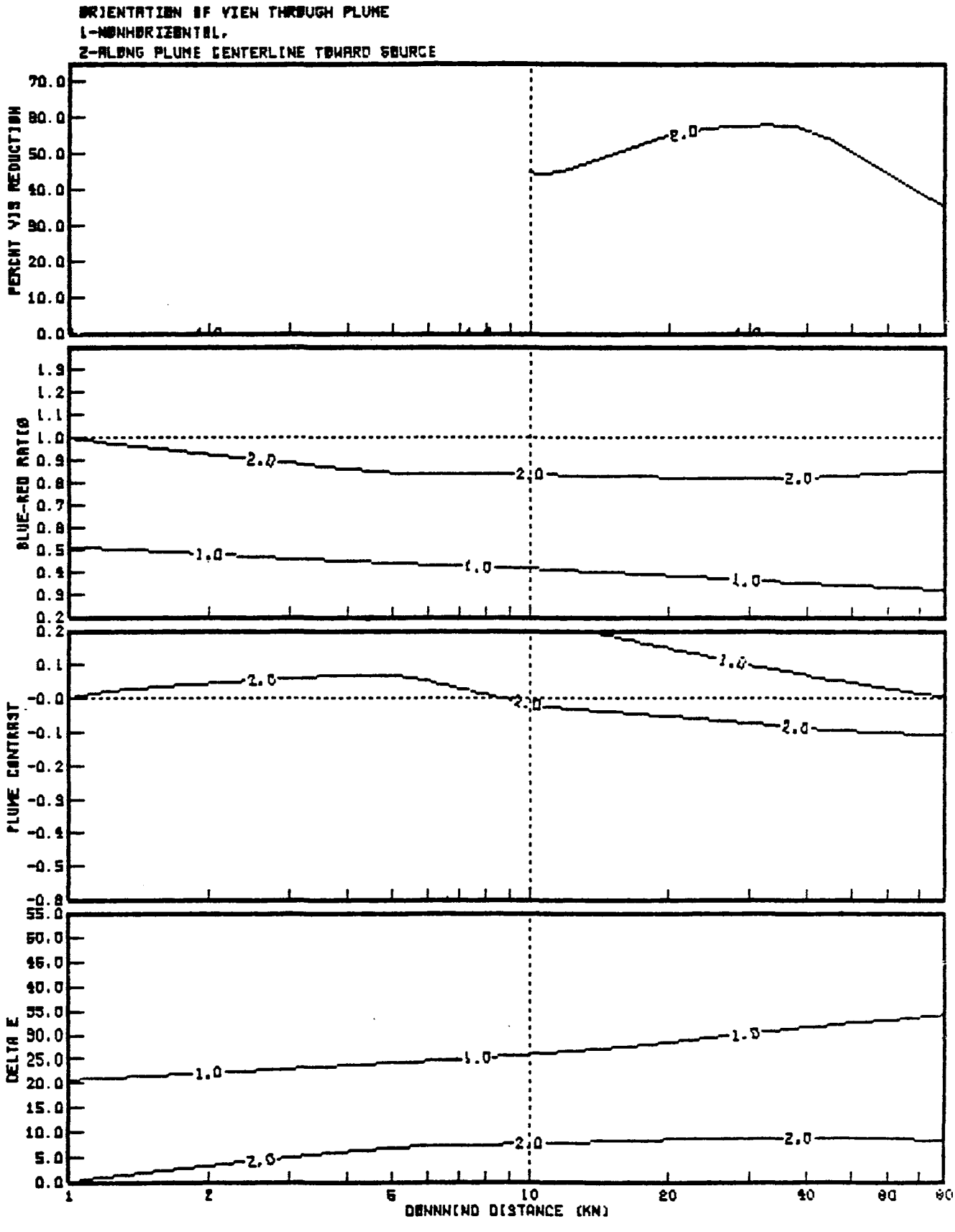

(b) Nonhorizontal and Axial Views

FIGURE 25 (Concluded)

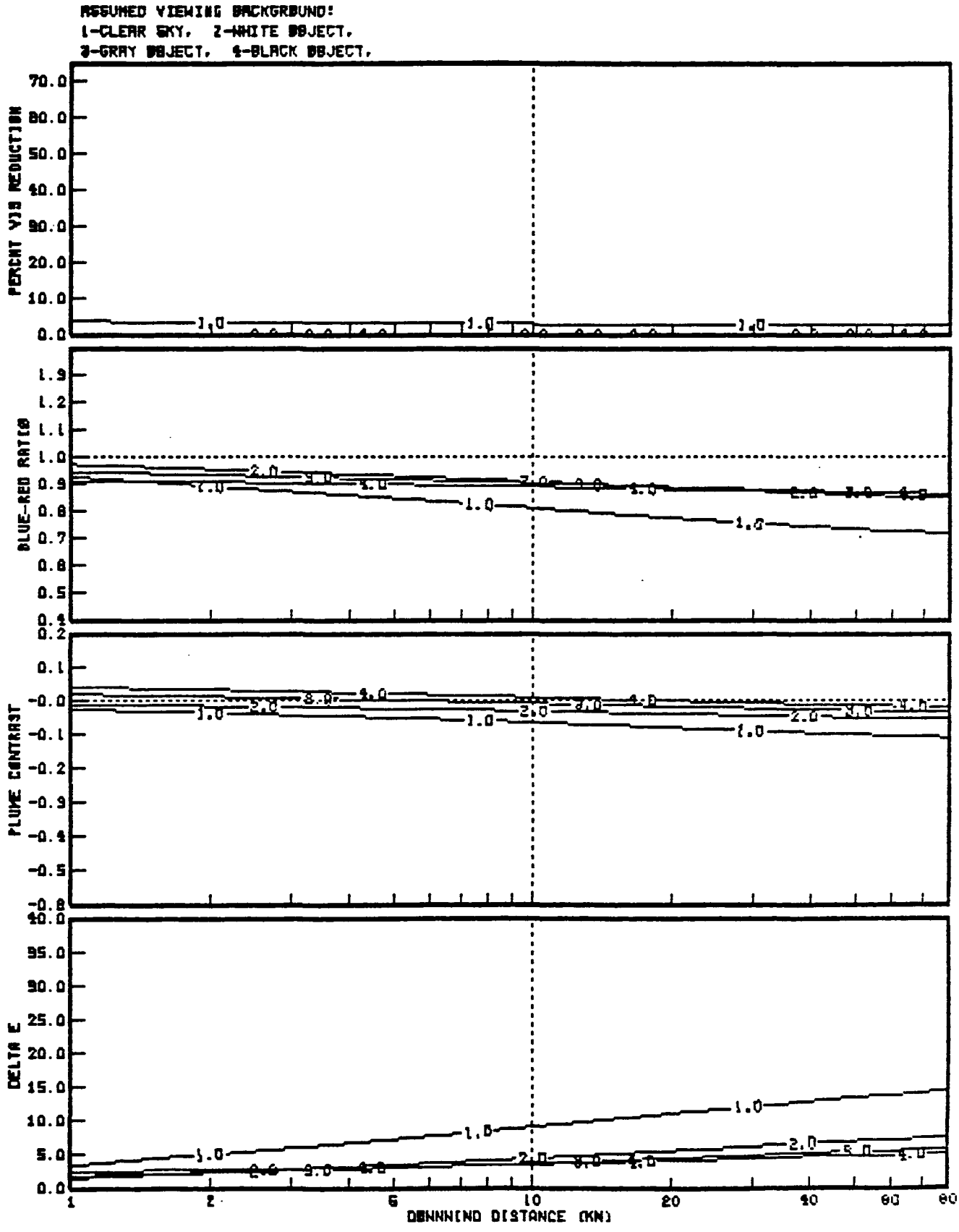

(a) Horizontal Views

FIGURE 26. SENSITIVITY EVALUATION--0.33 EMISSIONS REDUCTION

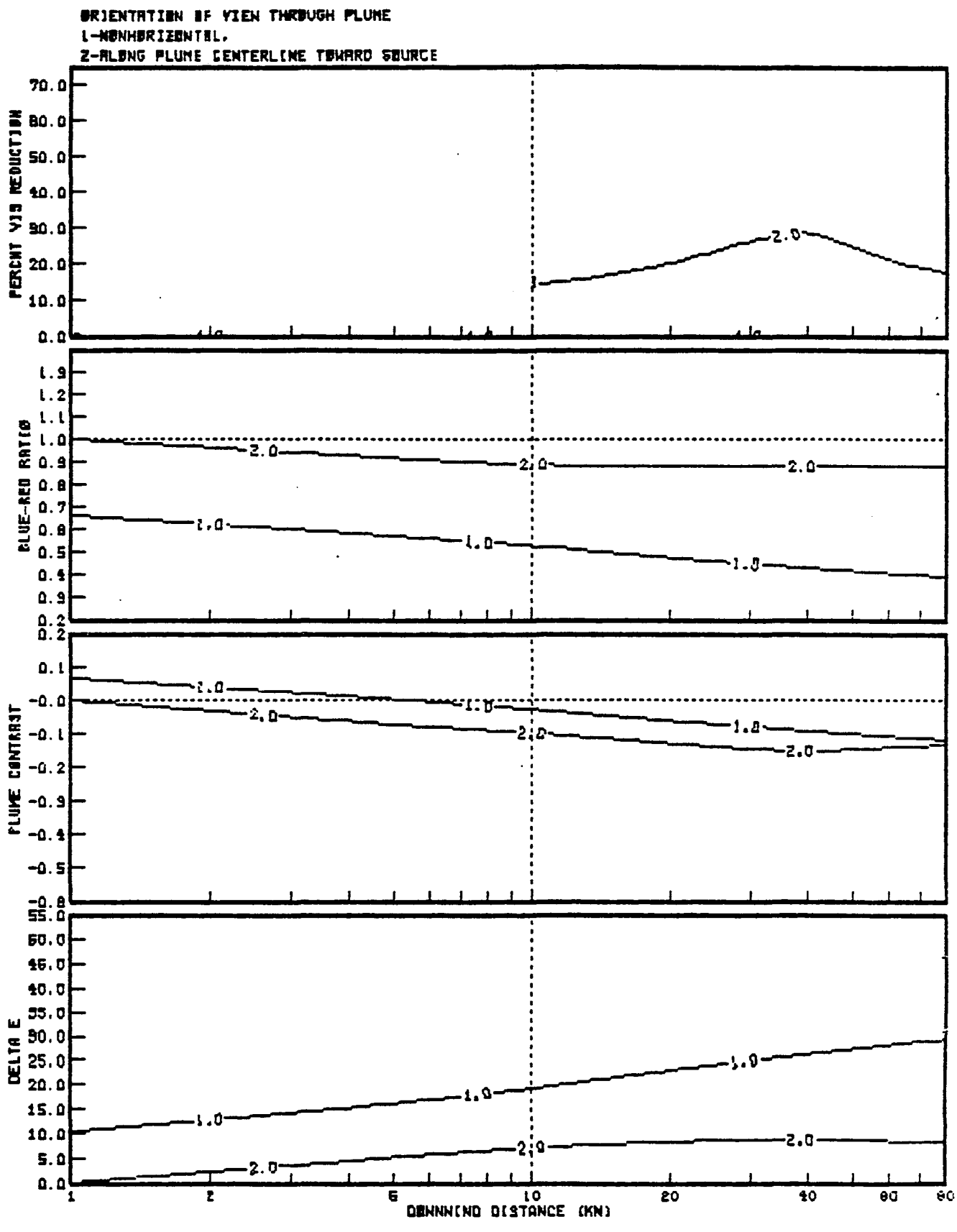

(b) Nonhorizontal and Axial Views

FIGURE 26 (Concluded)

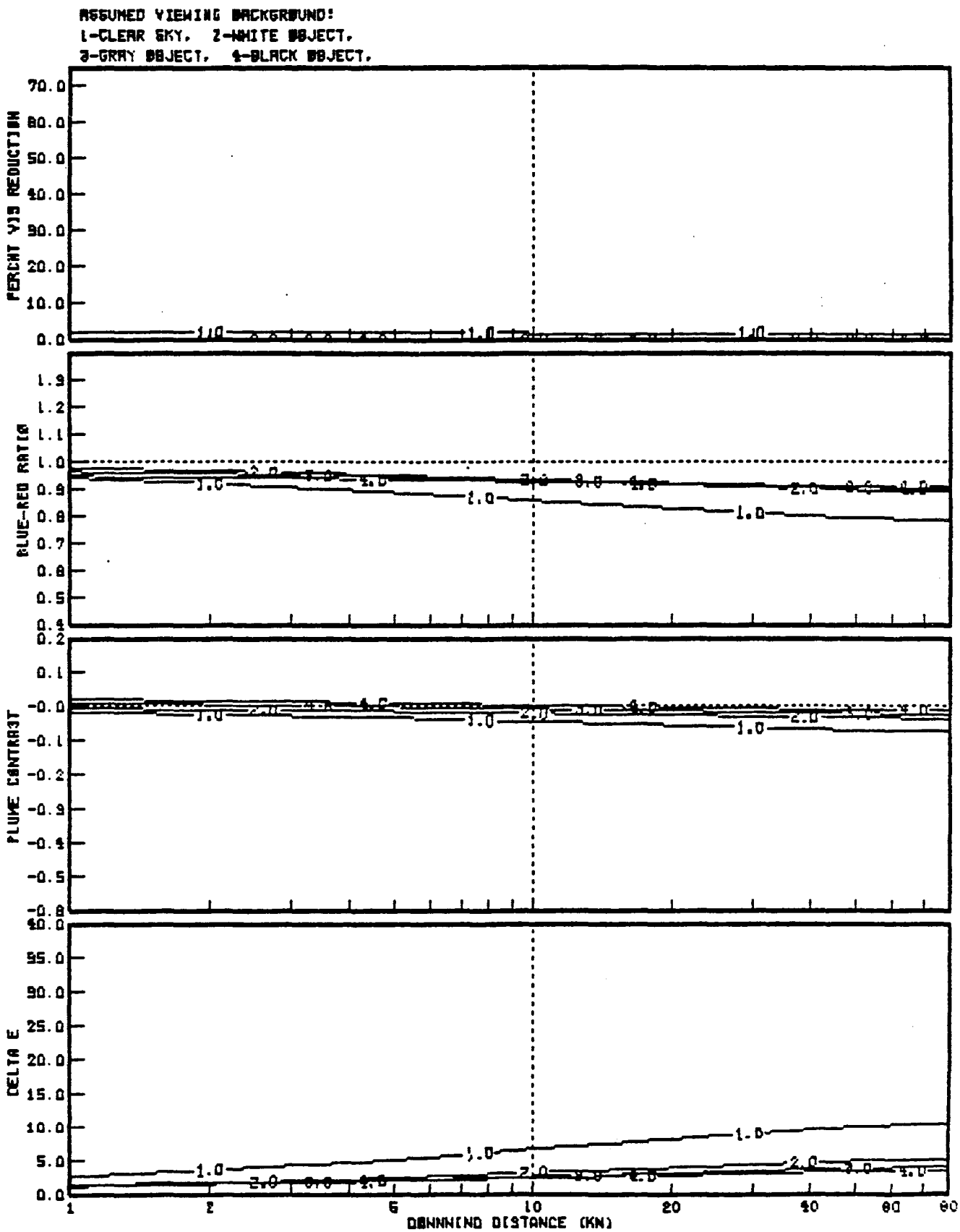

(a) Horizontal Views

FIGURE 27. SENSITIVITY EVALUATION--0.67 EMISSIONS REDUCTION

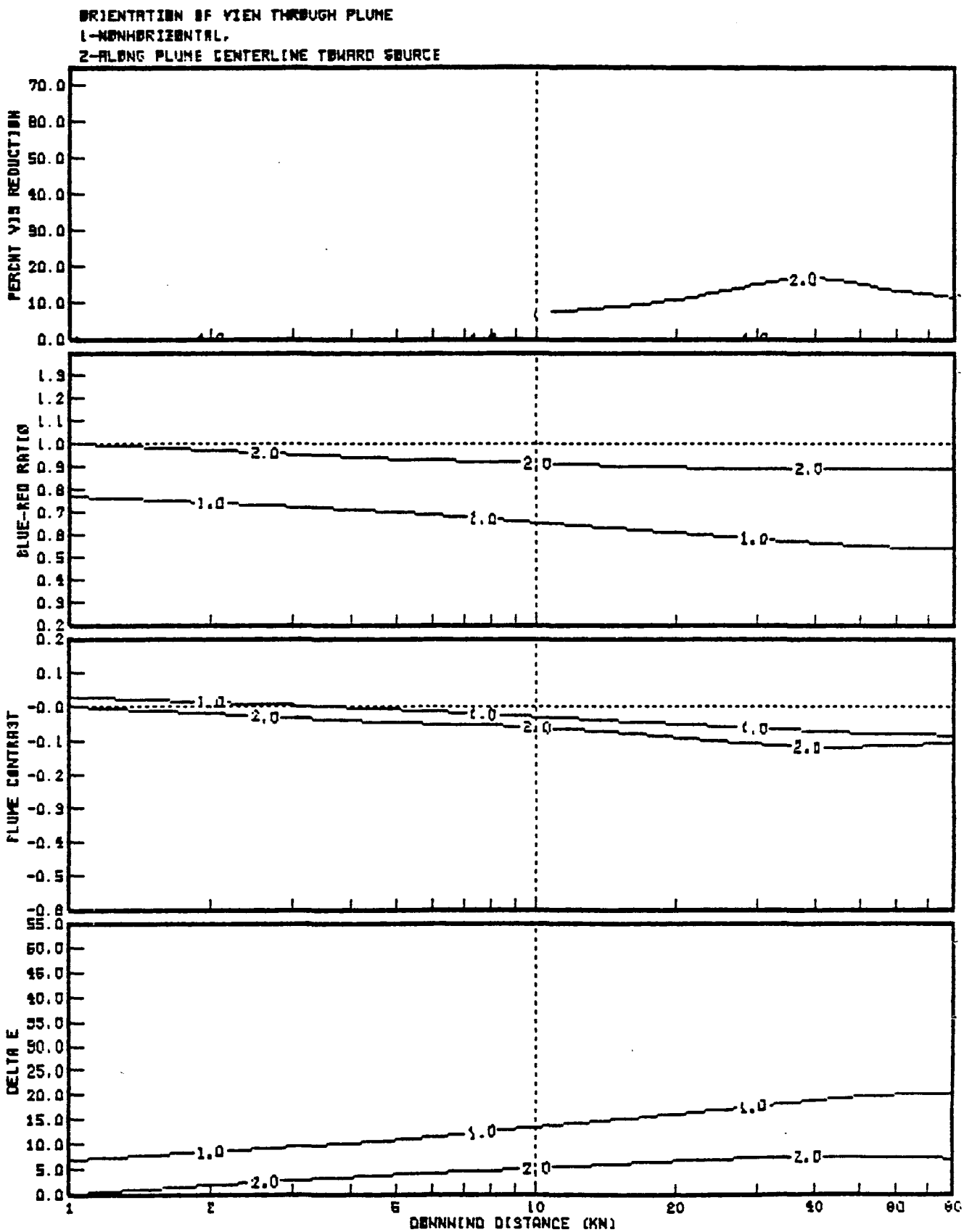

(b) Nonhorizontal and Axial Views

FIGURE 27 (Concluded)

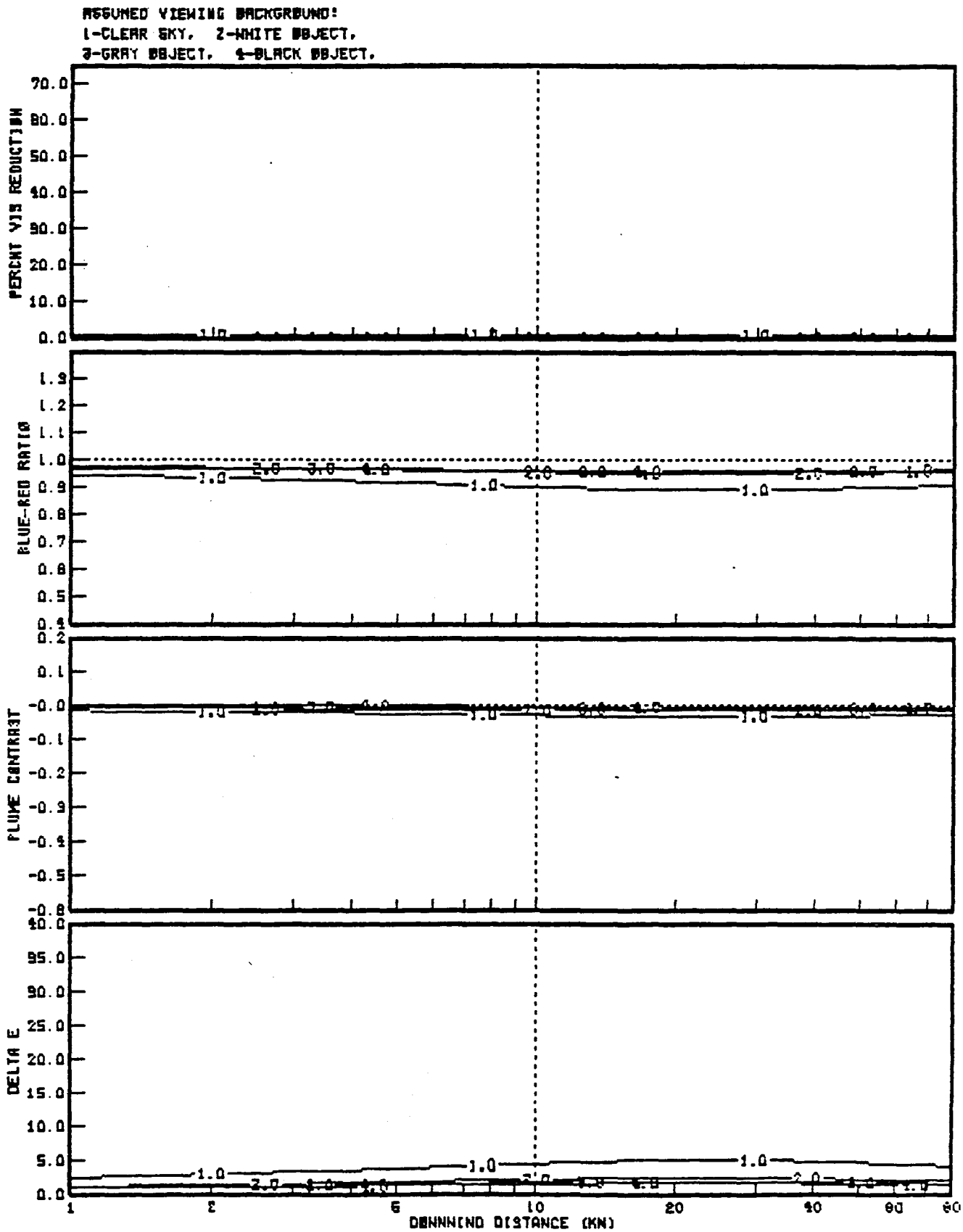

(a) Horizontal Views

FIGURE 28. SENSITIVITY EVALUATION--0.90 EMISSIONS REDUCTION

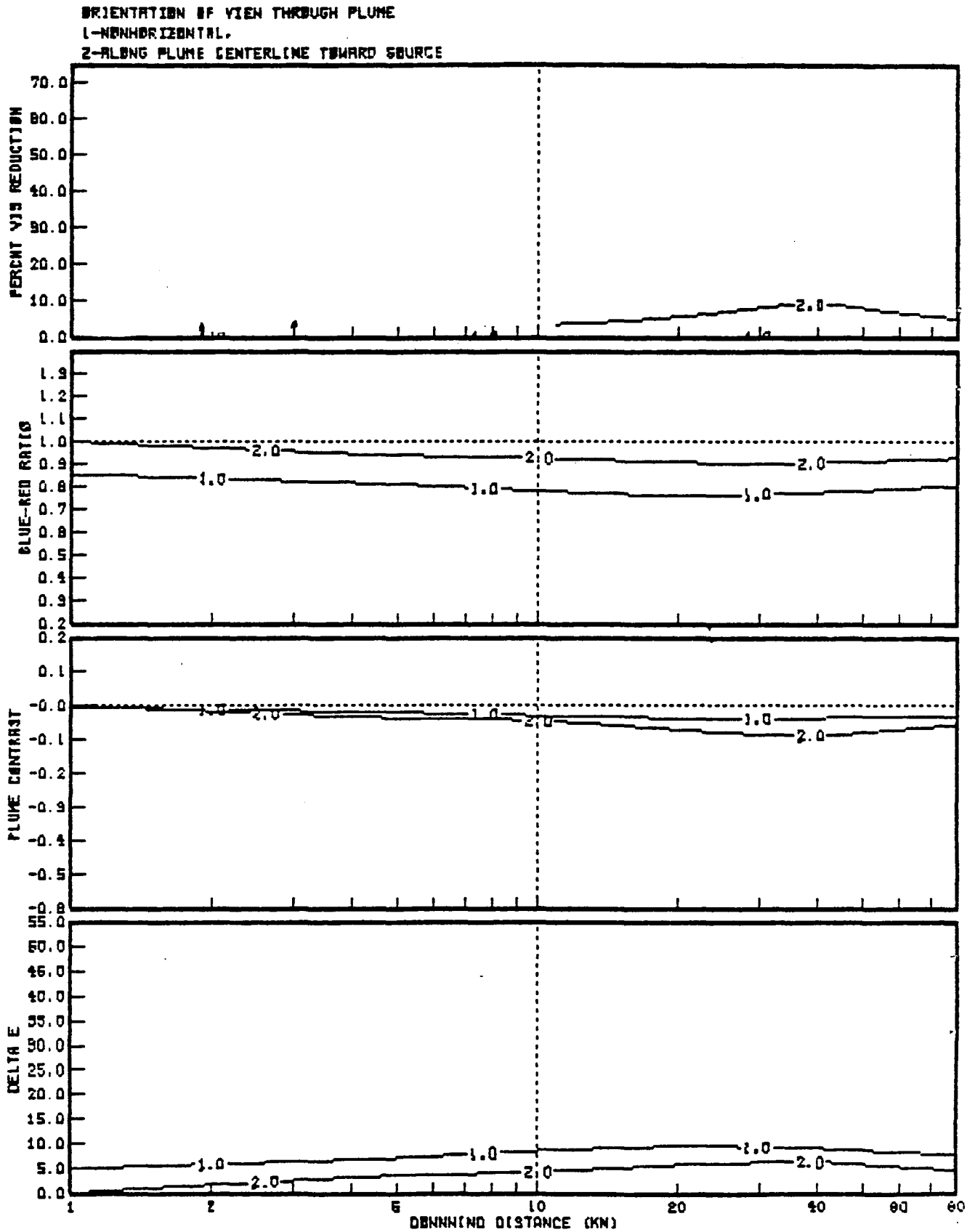

(b) Nonhorizontal and Axial Views

FIGURE 28 (Concluded)

$$X = \frac{Q}{(2\pi)^{1/2}\ \sigma_z\ u\ H_m}\left[\exp -\frac{1}{2}\ \frac{y}{\sigma_y}^2\right] \quad .$$

The expression for the concentration is then the same as for a Gaussian plume with H_m replacing $(2\pi)^{1/2}\ \sigma_z$. Thus, by comparing the product of the mean transport wind and mixing height for the limited mixing condition with the plume dispersion product $(2\pi)^{1/2}\ \sigma_z \cdot u$ discussed in section 2, we can relate the optical effects of a stagnant condition to the plume effects.

For typical perceptible plume impacts (discussed in section 3), the product of $\sqrt{2\pi}\ u \cdot \sigma_z$ is about 600 m^2/s. Thus for a mean mixing depth of 600 m, a transport wind of 1.0 m/s is required for comparable impact.

Available short-term data for the winter of 1979 suggest that such stagnant conditions occur at Edwards Air Force Base. If these conditions persist for several days, they have relatively high operational impact because of the possibility of several days of scheduling delays. The available hourly surface wind speed data base was surveyed to compute the frequency of occurrence of stagnant conditions.

The data show that for about 80 days per year (all in the fall- winter) the mean transport wind was less than 1.0 m/s for 24 hours. The mean transport wind was computed as the vector average wind for the time period specified. The results indicate that the frequency of occurrence of stagnant conditions at Edwards is rather high and that the impact is similar to the generic base case (ΔEs of 10). Also, if there is a significant secondary aerosol formation rate, the long residence time converts a larger fraction of the emitted SO_2 into sulfate, further increasing the visual impact. In addition, the angular extent of the visual impairment is greater. In the case of a plume, the impact is a relatively thin line across the sky, but in the case of stagnant conditions, the impact results in a general haze.

3.5 GENERAL ANALYSIS OF FREQUENCY OF OCCURRENCE

As shown, in the base case of TVA-3 with 4 m/s wind speed, the impact is perceptible at all downwind distances examined. This means that conditions with dispersion worse than TVA-3, 4 m/s wind speed will have a more adverse impact. Thus Edwards Air Force Base would receive impact at least 10.9 percent of the year (23.4 percent of the winter), and China Lake (Randsberg Wash) would receive impact 7.2 percent of the year.

For visibility frequency of occurrence calculations, Latimer and Ireson (1980) in the EPA guidance document for visibility recommend using

median ozone and visual range values. Since we have demonstrated that the results are relatively unaffected by ozone and visual range levels, we have used the values assumed by SCE in its NOI analysis. Thus we use only the joint frequency of stability and wind speed and direction.

For Edwards Air Force Base, this estimate is conservative. Specific stable wind directions that do not blow the plume directly to Edwards would still result in a perceptible plume (see next section). Moreover, stagnant conditions that occur at 80 days per year during the fall-winter will result in visual impact.

We conclude that the proposed power plant plume would be visible frequently from Edwards Air Force Base. It would be visible less frequently from Randsberg Wash. In the next section we discuss the significance of the typical impact with respect to target detectability.

4 RESULTS OF OBSERVER-BASED ANALYSES

In the previous section we discussed the overall visual impact of the proposed power plant in terms of plume perceptibility. In this section we discuss the impact of the plume on target detection for specific observer-plume-target geometries at the Naval Weapons Center and Edwards Air Force Base.

Since there are a multitude of possible geometries, we selected two important observer locations and several plume directions. We then computed the effect of the plume on targets of various reflectivities and locations behind the plume. The locations are shown in figure 29.

The input values for the observer-based cases are shown in table 5. These values represent conditions somewhat more "worst-case" than those in our base case discussed in section 3, but they are still highly probable. The major difference is the assumption of 2 percent per hour SO_2 to $SO_4^=$ conversion. This value represents the possible heterogeneous sulfate conversion rate and was used by Southern California Edison in its NOI. As shown in section 3, the plume effects are not highly sensitive to this assumption.

In this situation an attempt is made to simulate an observer tracking a plane that is flying at a fixed distance behind the plume. The geometry of the situation is shown in figure 30. Plume distance is θ_p, the downwind distance is x, the distance between the object and the plume is r_o, and the observer viewing direction is Az.

The results are presented for three different types of targets (white, grey, and black diffuse reflectors). Our objective is to discover the effect of the plume on the perceptibility of the target, and we accomplish this by comparing the color perceptibility (ΔE) of the target and the sky with the color perceptibility of the target against the sky with the plume in front. In this manner, the "masking" effect of the plume can be quantified.

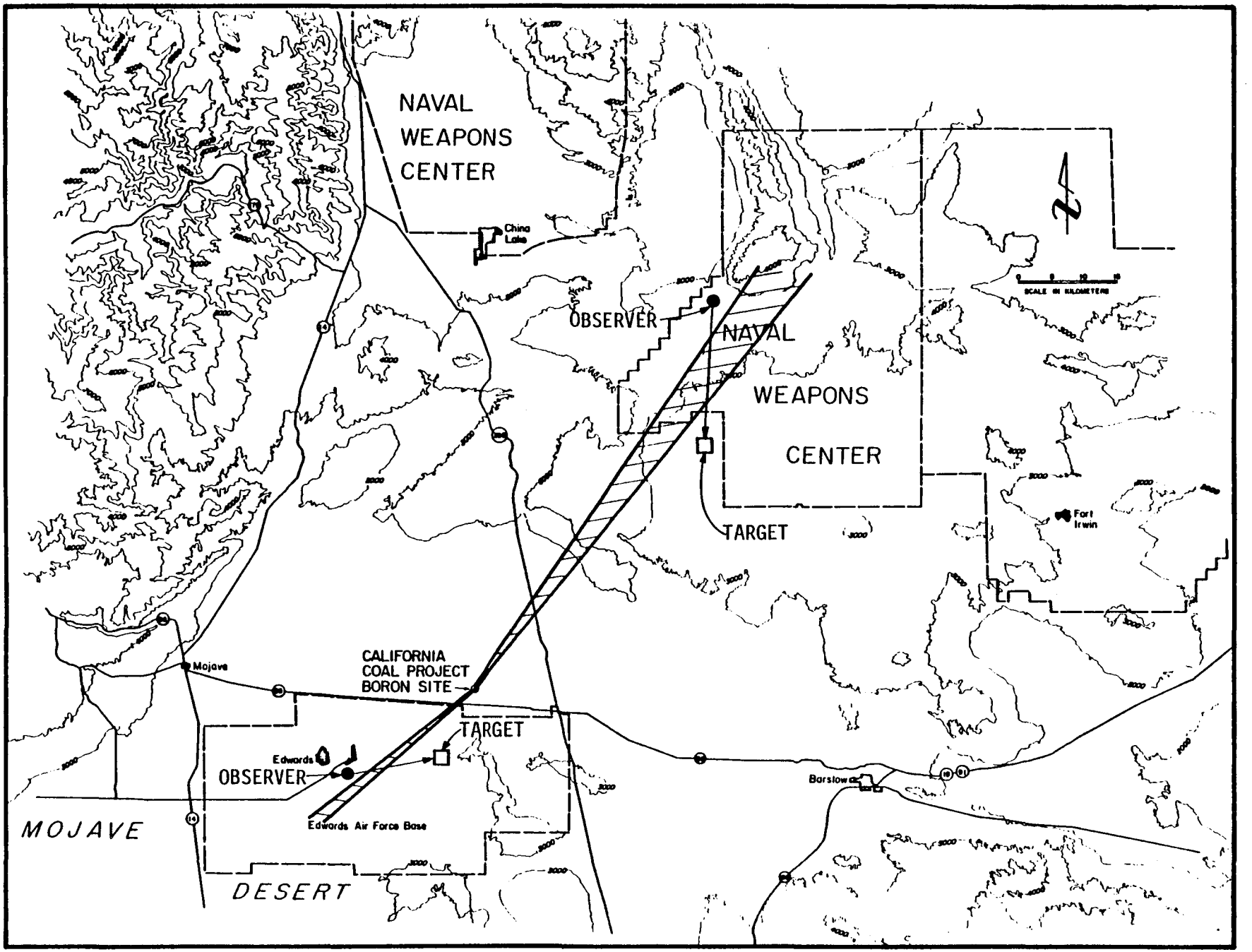

FIGURE 29. OBSERVER LOCATIONS USED IN CALCULATIONS OF PLUME EFFECTS ON TARGET VISIBILITY

TABLE 5. INPUT DATA COMMON TO ALL OBSERVER-BASED RUNS

A. Stability = TVA-4

B. $\partial T/\partial Z$ = -0.33°F/1000 feet

C. Wind speed input for plume height

D. No change in stability with distance

E. total emissions (in tons/day):

SO_2	NO_x	Primary Particulate
19.80	84.90	1.43

F. Flue gas flow rate = 2,352,000.0 cfm

G. Flue gas exit temperature = 180°F

H. Flue gas $[O_2]$ = 6. percent

I. Flue gas exit velocity = 22.8 m/s

J. Number of stacks = 3

K. Stack height = 500 feet

L. Mass median radius for background accumulation mode aerosol: 0.125 μm

M. Mass median radius for background coarse mode aerosol: 2.75 μm

N. Mass median radius for plume secondary aerosol = 0.125 μm

O. Mass median radius for plume primary particulate: 0.850 μm

TABLE 5 (Continued)

P. [Pollutant)$_{background}$:

$[NO_x]$	$[NO_2]$	$[O_3]$	$[SO_2]$
0.010	0.008	0.070	0.010

Q. Aerosol standard deviation of lognormal distribution:

Background Accumulation Mode	Background Coarse Mode	Plume Secondary Aerosol	Plume Primary Aerosol
2.2	2.2	1.5	1.5

R. Aerosol density (g/cm^{-3})

Background Accumulation Mode	Background Coarse Mode	Plume Secondary Aerosol	Plume Primary Aerosol
1.8	2.0	1.8	2.0

S. Deposition velocities (cm/sec^{-1})

SO_2	NO_x	Coarse Aerosol	Accumulation Mode Aerosol
1.0	1.0	0.10	0.10

TABLE 5 (Continued)

T. 2 percent SO_2 to $SO_4^=$ conversion in addition to OH• model calculation

U. Source Position	UTM Coordinates
x = 437.8 km y = 3875.3 km Elevation = 2450 feet	UTM Zone 11

V Flat terrain for transport and dispersion

W. Ambient temperature = 70°F

X. Time of day = 9 a.m.

TABLE 5 (Concluded)

Impact Area	Wind Speed (m/s)	Mixing Depth (m)	RH (percent)	W.D. (°)	Rv (km)	Date	Observer Position
Edwards AFB	2.	1000.	25.	55.5	100.	12/23/80	Edwards* Main RR
	plume travels directly over observer 22.25 km						
Edwards AFB	2.	1000.	25.	90.0	100.	12/23/80	Edwards* Main RR
	plume passes 12.6 km from observer 22.25 km						
Randsberg Wash	2.	1000.	35.	211.2	100.	12/23/80	NNE of † Source
	plume passes observer directly overhead 60 km						
Randsberg Wash	2.	1000.	35.	209.4	100.	12/23/80	†
	plume passes observer 2.17 σ_y to side 60 km						
Randsberg Wash	4.	100.	25.	211.2	70.	6/23/80	†
	plume passes directly over observer 60 km						
Randsberg Wash	4.	1000.	25.	209.4	70.	6/23/80	†
	plume passes 2.17 σ_y to side at 60 km						

* Edwards main runway
UTM coordinates:
x = 419.4 km, y = 3862.8 km, elevation = 2302 feet.

† UTM coordinates
x = 469.1 km, y = 3926.5 km, elevation = 2600 feet.

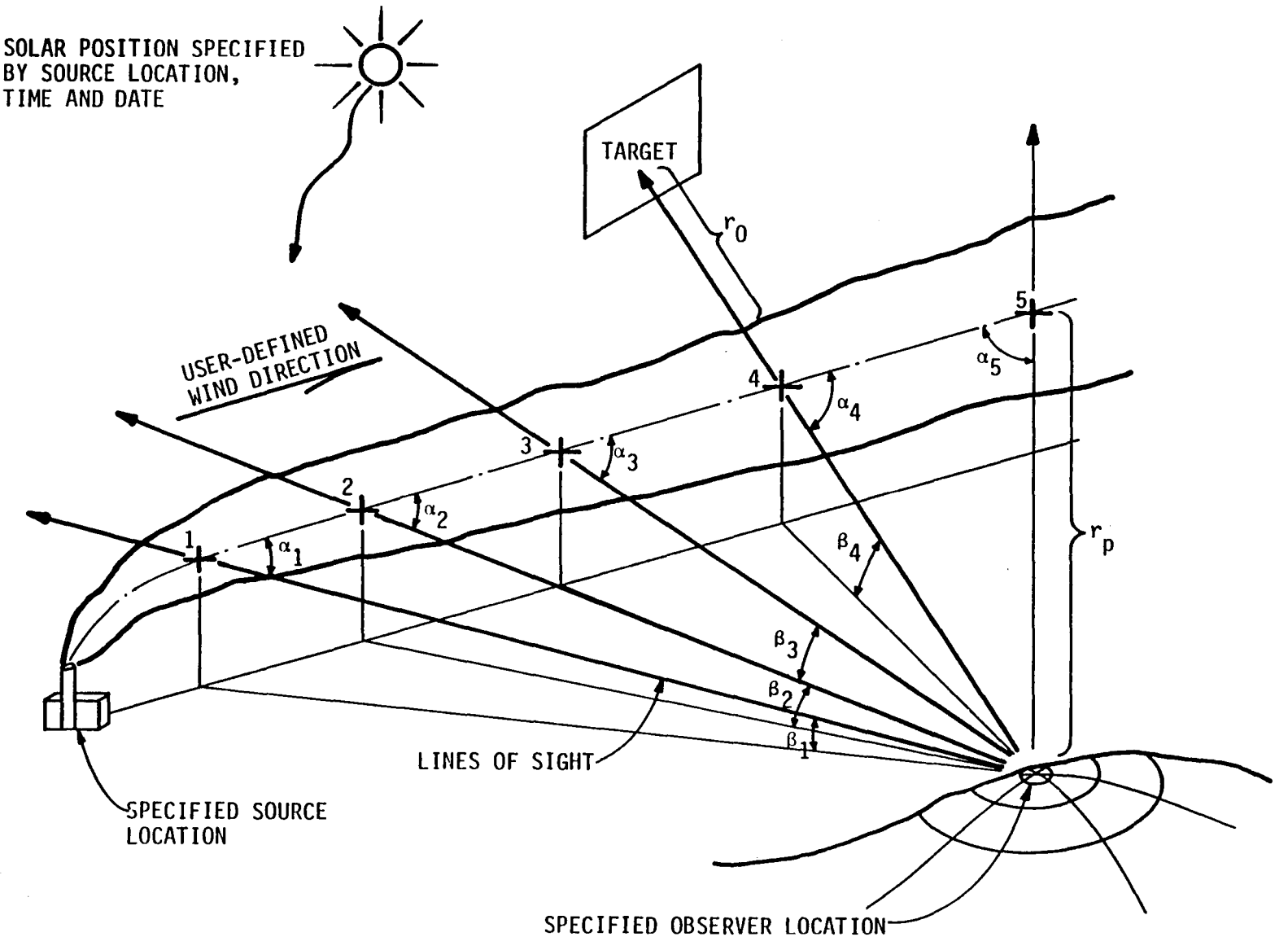

FIGURE 30. GEOMETRY USED FOR OBSERVER-BASED CALCULATIONS FOR NONHORIZONTAL VIEWS THROUGH THE PLUME FOR CLEAR-SKY BACKGROUNDS

4.1 RESULTS FOR OBSERVER LOCATED AT EDWARDS AIR FORCE BASE

The results for a situation in which the plume blows directly at an observer at Edwards Air Force Base are shown in table 6. As can be seen, the perceptibility (ΔE) of all three targets without the plume increases as the target passes overhead. For reference, a ΔE of 2 is just perceptible, and a ΔE of 10 is very apparent. With the plume in front, the target is completely masked at plume-observer distances that are less than 2.3 km. When the plume 1.3 km away from the observer, the white target is visible (ΔE of 9) but the gray and black targets are marginally visible with ΔEs of 2.32 and 1.28. When the plume is 0.5 km away, all three targets are visible but their perceptibility is greatly reduced.

The results for the case in which a plume is blown due west from the Boron site are presented in table 7. The plume does not actually cross over any part of Edwards Air Force Base, and it is slightly perceptible (ΔEs of 5). Its effect on the targets is relatively minor (10 percent reduction). The effect of the plume is shown for objects at a distance of 10 km and 50 km.

The effect of the plume on perceptibility is similar to its effect on visual range, which is defined as the distance at which an observer can distinguish a black object at 550 nm. For the plume in the case presented in table 7, the reduction in visual range was 5 percent at the closest downwind distance (20 km). The effect of the plume on color perceptibility appears to be slightly greater since the blue wavelengths are affected more by the NO_2 in the plume than are the green wavelengths (550 nm).

It should be stressed that computing the change in color perceptibility is a new application for the model. The results obtained are consistent with intuition, but more research needs to be done in this area. Two conclusions can be drawn from this study. One is that the plume will completely mask a target for the sight paths along it, and the other is that the plume will decrease the distance from which an object can be detected. As shown by the difference between table 6 and table 7, the amount of reduction is a function of the location of the plume relative to the observer and target.

4.2 RESULTS FOR OBSERVER LOCATED AT RANDSBERG WASH (CLNWC)

The results for the observer and the plume at Randsberg Wash are shown in table 8. Because of the higher wind speed and the greater distance of the observer at Edwards, the results are not as dramatic as those in the case in table 7. However, some effects of the plume can be seen;

TABLE 6. RESULTS FOR PLUME PASSING DIRECTLY OVERHEAD OBSERVER AT EDWARDS AIR FORCE BASE, OBSERVER AT X = 22.5 KM

r_o = 10 km

X (km)	Az °	r_p (km)	ΔE (Lab) Without	ΔE (Lab) With
1.0	55.8	21.2	10.26*	0.00
			6.44†	0.00
			15.33§	0.00
2.0	55.8	20.2	10.46	0.00
			6.73	0.00
			15.94	0.00
5.0	55.9	17.3	11.04	0.00
			7.70	0.00
			17.96	0.00
10.0	56.1	12.3	17.00	10^{-4}
			9.97	10^{-4}
			24.72	10^{-4}
15.0	56.5	7.3	17.70	0.0061
			11.65	0.0026
			24.63	0.0064
20.0	58.6	2.3	38.9	2.423
			20.70	0.2353
			20.52	0.8034
21.0	61.0	1.3	46.60	9.61
			24.59	2.32
			16.26	1.28
22.0	81.7	0.5	55.80	39.05
			30.72	18.20
			13.04	5.89
23.0	226.5	0.9	53.12	21.70
			27.60	7.18
			11.61	0.80

* White target.

† Grey (30 percent reflectivity) target.

§ Black target.

TABLE 7. RESULTS FOR A PLUME BLOWING DUE WEST FROM THE BORON SITE WITH THE OBSERVER AT EDWARDS AIR FORCE BASE

(a) r_o = 10 km

X (km)	Az	r_p (km)	ΔE (Lab) Without	ΔE (Lab) With
1.0	54.3	24.4	10.603*	9.062
			6.171†	5.236
			15.128§	12.532
2.0	52.7	20.6	11.158	9.668
			6.184	5.350
			15.493	13.060
5.0	47.0	18.3	12.348	10.955
			6.468	5.774
			16.769	14.545
10.0	33.9	15.1	14.153	12.809
			7.120	6.480
			18.947	16.837
15.0	15.2	13.0	14.363	13.079
			8.625	7.884
			21.187	19.079
20.0	352.7	12.6	12.609	11.310
			10.950	9.534
			22.756	20.431
21.0	348.3	12.8	11.951	10.652
			10.750	9.802
			22.889	20.492
22.0	343.9	13.0	11.221	9.953
			11.048	10.057
			22.951	20.471
23.0	339.8	13.3	10.236	9.000
			11.298	10.298
			22.952	20.393
24.0	335.9	13.7	9.313	8.109
			11.599	10.518
			22.892	20.216
25.0	332.2	14.1	8.318	7.189
			11.870	10.711
			22.728	19.973

TABLE 7 (Continued)

X (km)	Az	r_p (km)	ΔE (Lab) Without	ΔE (Lab) With
30.0	317.1	17.1	5.752	4.811
			11.621	10.059
			20.726	17.458
40.0	300.1	25.0	6.717	4.958
			7.463	5.514
			14.599	10.500
50.0	291.6	34.0	6.813	4.162
			4.583	2.729
			10.105	5.865

* White target.

† Gray target

§ Black target.

TABLE 7 (Continued)

(b) r_o = 50 km

X (km)	Az	r_p (km)	ΔE (Lab) Without	ΔE (Lab) With
1.0	54.3	21.4	2.168*	1.839
			3.163†	2.594
			5.434§	4.480
2.0	52.7	20.6	2.285	1.965
			3.267	2.703
			5.622	4.684
5.0	47.0	18.3	2.5611	2.235
			3.628	3.072
			6.209	5.292
10.0	33.9	15.1	3.100	2.703
			4.376	3.832
			7.265	6.379
15.0	15.2	13.0	3.448	2.945
			5.474	4.916
			6.452	7.591
20.0	352.7	12.6	3.407	2.838
			6.668	6.003
			9.537	8.576
21.0	348.3	12.8	3.310	2.746
			6.822	6.122
			9.646	8.644
22.0	343.9	13.0	3.207	2.652
			6.913	6.178
			9.685	8.641
23.0	339.8	13.3	3.017	2.484
			6.954	6.182
			9.659	8.569
24.0	335.9	13.7	2.858	2.347
			6.949	6.131
			9.573	8.430

TABLE 7 (Concluded)

X (km)	Az	r_p (km)	ΔE (Lab) Without	ΔE (Lab) With
25.0	332.2	14.1	2.685	2.197
			6.879	6.022
			9.419	8.230
30.0	317.1	17.1	4.860	4.417
			6.051	4.989
			8.258	6.819
40.0	300.1	25.0	0.890	0.635
			3.641	2.473
			5.479	3.779
50.0	291.6	34.0	1.325	0.851
			2.129	1.131
			3.584	1.985

* White target.

† Gray target.

§ Black target.

objects that were perceptible near the visual range ($\Delta E \sim 2$) are no longer visible until they are closer to the observer. As discussed previously, the plume reduces the distance at which the target is observable.

It should also be mentioned that since the targets (airplanes, etc.) probably would not be visible to the unaided eye because they would appear too small, the tracking of planes is done with high-power telescopic sights that magnify the image of the target. Such telescopic aids do not, however, improve the contrast of a target, and thus our analysis is still applicable. In other words, if the plume masks an object, no amount of magnification will make it visible.

TABLE 8. RESULTS FOR THE PLUME BLOWING TOWARD RANDSBERG WASH OBSERVER

(a) r_o = 10 km

X (km)	Az	r_p (km)	ΔE (Lab) Without	ΔE (Lab) With
1.0	211.5	59.0	0.722*	0.155
			1.142†	0.154
			1.88§	0.287
5.0	211.6	55.0	0.852	0.219
			1.257	0.208
			2.114	0.392
20.0	212.5	40.0	1.918	0.615
			2.143	0.537
			3.916	1.035
40.0	215.5	20.1	5.130	2.721
			4.806	2.442
			9.571	4.758
50.0	221.5	10.2	7.474	5.772
			7.909	6.408
			15.948	12.267
55.0	232.6	5.4	9.436	8.358
			10.339	9.697
			20.700	18.976
57.0	245.1	3.7	12.808	11.560
			10.531	9.471
			21.315	19.951
58.0	256.7	2.9	15.552	14.241
			10.349	8.747
			20.648	19.242
59.0	274.9	2.4	18.760	17.450
			10.151	8.050
			19.317	17.807
60.0	300.2	2.2	20.431	19.177
			9.866	7.662
			18.287	16.767

TABLE 8 (Continued)

X (km)	Az	r_p (km)	ΔE (Lab) Without	ΔE (Lab) With
61.0	325.1	2.4	18.885	17.666
			9.380	7.373
			18.690	17.221
62.0	342.9	3.0	15.534	14.299
			9.458	7.962
			19.915	18.477
63.0	354.2	3.7	12.163	10.985
			10.053	9.078
			20.807	19.317

* White target.

† Gray target.

§ Black target.

TABLE 8 (Continued)

(b) r_o = 50 km

X (km)	Az	r_p (km)	ΔE (Lab) Without	ΔE (Lab) With
1.0	211.5	59.0	0.351*	0.0080
			0.513†	0.033
			0.609§	0.050
5.0	211.6	55.0	0.340	0.020
			0.533	0.049
			0.646	0.078
20.0	212.5	40.0	0.320	0.076
			0.661	0.106
			0.908	0.184
40.0	215.5	20.1	0.582	0.365
			1.139	0.444
			1.810	0.794
50.0	221.5	10.2	0.653	0.480
			2.156	1.431
			3.230	2.236

TABLE 8 (Concluded)

X (km)	Az	r_p (km)	ΔE (Lab) Without	ΔE (Lab) With
55.0	232.6	5.4	1.903	1.454
			2.738	2.409
			3.916	3.501
57.0	245.1	3.7	4.305	3.533
			2.535	2.030
			2.878	5.745
58.0	256.7	2.9	6.680	5.745
			3.831	2.959
			3.012	2.232
59.0	274.9	2.4	9.413	8.446
			6.119	5.186
			4.777	3.836
60.0	300.2	2.2	10.740	9.833
			7.290	6.431
			5.818	4.961
61.0	325.1	2.4	9.375	8.519
			5.963	5.176
			4.529	3.751
62.0	342.9	3.0	6.664	5.875
			3.558	2.870
			2.492	1.853
63.0	354.2	3.7	4.280	3.618
			2.018	1.559
			2.153	1.899

* White target.

† Gray target.

§ Black target.

5 SUMMARY

Our study of the visibility impact of the proposed SCE power plant at the Boron site was divided into several sections. The first was an analysis of the meteorological data, which showed that the combination of stable conditions, low wind speed, and wind direction toward Edwards Air Force Base and China Lake Naval Weapons Center occurs rather frequently (10.9 percent and 7 percent respectively). Thus, at Edwards Air Force Base there will be visual impact on at least 40 days of the year.*

The next section of the study involved a generic evaluation of plume perceptibility for the range of meteorological conditions likely to be encountered. This analysis showed that the plume was perceptible most of the time, because of the NO_2 and particles, given stable, low wind speed conditions. Only a severe limitation in emissions (~ 90 percent) would cause the plume to become invisible.

The final section included an analysis of a specific situation for observers at Edwards Air Force Base and at Randsberg Wash (CLNWC). This simulation was an attempt to model the activity of detecting (or photographing) an airplane on the other side of the plume. The analysis showed that if the observer looks directly into the plume toward the source, the target is completely masked. For observation geometries in which the observer is viewing perpendicular to the plume, detectability is reduced but not eliminated for all distances. If targets are just perceptible without the plume, the plume makes them imperceptible. The effect is analogous to reducing the visual range. The actual reduction is a function of the meteorological conditions and observer-plume-target geometry. In the cases investigated, the perceptibility of a target was reduced by a minimum of 10 percent and a maximum of 100 percent.

---

* Analysis of the frequency of stagnant conditions revealed that at least 80 days per year the mean transport wind during a 24-hr period is low enough to cause visual impact.

Appendix

TECHNICAL OVERVIEW*

This section briefly outlines the technical details of the plume visibility model (PLUVUE). Those interested in more detail should consult Latimer et al. (1978).

As shown schematically in figure A-1, the modeling of visibility impairment requires mathematical descriptions for the following physical and chemical atmospheric processes in succession:

> Emissions.
> Atmospheric transport, diffusion, and removal.
> Chemical and physical reactions and transformations of precursors in the atmosphere.
> Light scattering and absorption characteristics of the resultant aerosol.
> Radiative transfer through the aerosol along different lines of sight.

Because the visibility model is based on atmospheric dispersion and chemistry models, the accuracy of the former depends on that of the latter. We recognize that future improvements in modeling dispersion--particularly on the regional scale and in complex terrain, as well as improvements in modeling secondary aerosol formation--will increase the accuracy of visibility models.

---

* Reproduced from Johnson et al. (1980), "User's Manual for the Plume Visibility Model (PLUVUE)," EPA Contract No. 68-02-3337, Research Triangle Park, North Carolina.

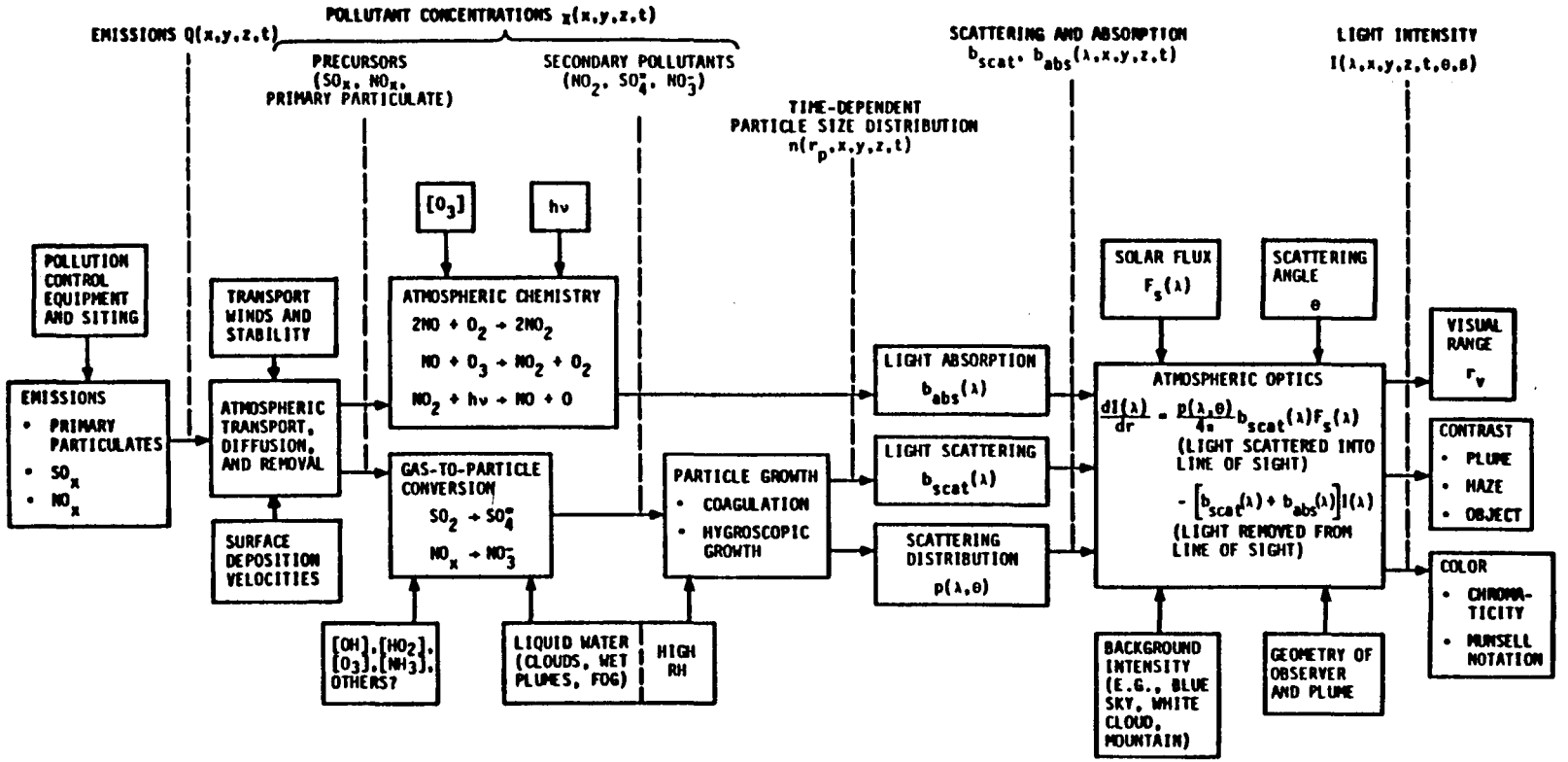

FIGURE A-1. SCHEMATIC LOGIC FLOW DIAGRAM OF THE PLUME VISIBILITY MODEL

A.1 POLLUTANT TRANSPORT, DIFFUSION, AND REMOVAL

There are two scales that are of interest in visibility impairment calculations. They require two different types of models:

- A near-source plume model designed to predict the incremental impact of one emissions source (such as a power plant or smelter).
- A regional model designed to predict, over time periods of several days, the impacts of several emissions sources within a region whose spatial scale is in the range of 1000 km.

Calculation of near-source visual impacts, which is the design objective of PLUVUE, requires a basic model that accurately predicts the spatial distribution of pollutants and the chemical conversion of NO to NO_2 and SO_x and NO_x to sulfates and nitrates. The plume model must be capable of handling the spatial scale from emissions at the source to at least 100 km downwind. Because the regional-scale problem may be caused by the long-range transport of pollutants over a spatial scale of 1000 km, an air quality model is needed that can account for multiple sources and for temporal variations in mixing heights, dispersion parameters, emission rates, reaction rates, and wind speed and direction. This second type of model, a regional visibility model, is beyond the scope of this user's manual. PLUVUE is a near-source plume visibility model.

In the following subsections, we discuss atmospheric dispersion modeling as it relates to the plume visibility model for the following spatial scales:

- Initial dilution in a buoyant plume
- Gaussian plume diffusion
- Limitations on mixing.

A.1.1 Initial Dilution in a Buoyant Plume

Modeling of the initial dilution of a plume from the top of the stack to the point of final plume rise is important when modeling the conversion of nitric oxide to nitrogen dioxide in a power plant plume because of the quick quenching of the thermal oxidation of NO. The rate of this reaction is second order with respect to NO concentrations; therefore, the rate is fastest in the initial stages of plume dilution. It is also important to account for the initial dilution of buoyant releases because the rate of dilution caused by the turbulent entrainment of ambient air by a rising plume parcel can be considerably greater than that indicated by diffusion coefficients based on measurements for nonbuoyant releases (e.g., Pasquill-Gifford σ_y, σ_z). Thus, initial plume dilution during plume rise should be taken into account to calculate accurately both plume dilution and atmospheric chemistry.

Briggs (1969) suggested that the characteristic plume radius increases linearly with the height of the plume above the stack and can be represented as follows:

$$R_p = 0.5\ (\Delta h) \quad . \tag{A-1}$$

Briggs described plume rise, as a function of downwind distance (the "2/3 power law"), as follows:

$$\Delta h = 1.6\ F^{1/3} x^{2/3} u^{-1} \quad . \tag{A-2}$$

For initial dilution, we can assume that the plume is circular in cross section and has a Gaussian profile. We can also assume that the radius of the plume is the distance from the plume centerline to the point at which the plume concentration is 10 percent of the centerline concentration. Thus, we have

$$R_p = y_p = z_p = 2.15\ \sigma_y = 2.15\ \sigma_z \quad . \tag{A-3}$$

The concentration of a given species at the centerline of the plume can be calculated by a modified Gaussian model that can be represented as

$$x = \frac{Q}{2\pi\sigma_y\sigma_z V} \quad , \tag{A-4}$$

where V is the velocity of the parcel, which has a horizontal component (the wind speed u) and a vertical component w, which can be calculated by differentiating equation (A-2). Thus

$$w = \frac{dz}{dt} = \frac{2}{3}\ 1.6\ F^{1/3}u^{-1/3}t^{-1/3} \quad . \tag{A-5}$$

With this formulation, time-dependent plume temperature and NO concentrations can be calculated for accurately predicting the thermal oxidation of NO during plume rise.

Combining equations (A-1), (A-3), and (A-4), we can calculate the initial dilution of plume material, after the plume has reached its final height, as follows:

$$x = \frac{2.94\ Q}{(\Delta h)^2 u} \quad . \tag{A-6}$$

Thus, plume material is assumed to be at least as dilute as that shown by equation (A-6). For emissions sources having more than one stack, it is assumed that there is an overlap of plumes from individual stacks. For cases in which the initial dilution during plume rise is greater than the standard Gaussian formula would predict at the downwind distance of final plume rise, a virtual point-source offset is introduced so that dilution at this distance is at least as much as that shown in equation (A-6).

A.1.2 Plume Rise

The final plume rise in PLUVUE is calculated using the modified plume rise formulas of Briggs (1969, 1971, 1972):

For unstable or neutral atmospheric conditions, the downwind distance of final plume rise is $x_f = 3.5\ x^*$, where

$$x^* = \begin{cases} 14\ F^{5/8}, & \text{if } F < 55\ m^4 s^{-3} \\ 34\ F^{2/5}, & \text{if } F \geq 55\ m^4 s^{-3} \end{cases} \quad . \tag{A-7}$$

The final plume rise under these conditions is

$$\Delta h = 1.6\ F^{1/3}(3.5\ x^*)^{2/3} u^{-1} \quad . \tag{A-8}$$

For stable atmospheric conditions, the downwind distance of final plume rise is $x_f = \pi\ u\ s^{-1/2}$, where the stability parameter s is defined as follows:

$$s = g\ \partial\theta/\partial z\ T^{-1} \quad . \tag{A-9}$$

The plume rise for stable atmospheric conditions is

$$\Delta h = \text{minimum of} \begin{cases} 2.6(F/(u\ s)]^{1/3} \\ 5\ F^{1/4} s^{-3/8} \end{cases} \quad . \tag{A-10}$$

The buoyancy flux (F) in the above equations is calculated on the basis of the flue gas volumetric flow rate per stack ($\dot{V}$), flue gas and ambient temperature in degrees Kelvin (T_{stack}, $T_{ambient}$), and gravitational acceleration (g), as follows:

$$F = \frac{g\dot{V}}{\pi}\left(1 - \frac{T_{ambient}}{T_{stack}}\right) \quad . \tag{A-11}$$

A.1.3 Gaussian Plume Diffusion

After the plume has achieved its final height (about 1 km downwind), plume concentrations for uniform wind fields can be adequately predicted using a Gaussian model if the wind speed u at plume height H ($h_s + \Delta h$) and the rate of diffusion are known for the particular situation so that diffusion coefficients (σ_y, σ_z) can be selected:

$$\chi = \frac{Q}{2\pi\sigma_y\sigma_z u} \exp\left[-\frac{1}{2}\left(\frac{y}{\sigma_y}\right)^2\right]\left\{\exp\left[-\frac{1}{2}\left(\frac{H+z}{\sigma_z}\right)^2\right] + \exp\left[-\frac{1}{2}\left(\frac{H-z}{\sigma_z}\right)^2\right]\right\}. \quad \text{(A-12)}$$

Equation (A-12) is appropriate for a conservative species and can be modified to be appropriate for a nonconservative species by changing the source term Q.

It is necessary for calculating plume visual impact to integrate, along the line of sight, the plume extinction coefficient, the magnitude of which depends on primary and secondary particulate and nitrogen dioxide concentrations. Equation (A-12) can be integrated [Ensor, Sparks, and Pilat (1973)] in the cross-wind direction y, from $y = -\infty$ to $y = +\infty$, to obtain the optical thickness of the plume:

$$\tau_{py} = \int_{-\infty}^{+\infty} b_{ext}\, dy = \frac{Q'(x)}{(2\pi)^{1/2}\sigma_z u}\left\{\exp'\left[-\frac{1}{2}\left(\frac{H+z}{\sigma_z}\right)^2\right] + \exp\left[-\frac{1}{2}\left(\frac{H-z}{\sigma_z}\right)^2\right]\right\}, \quad \text{(A-13)}$$

where b_{ext} is the incremental increase in extinction coefficient in the plume and Q' is the flux of the plume extinction coefficient over the entire plume cross section at downwind distance x. In the vertical direction z, from z = 0 to z = $+\infty$, the plume optical thickness is

$$\tau_{pz} = \int_0^{\infty} b_{ext}\, dz = \frac{Q'(x)}{(2\pi)^{1/2}\, \sigma_y u} \exp\left[-\frac{1}{2}\left(\frac{y}{\sigma_y}\right)^2\right] \quad . \qquad \text{(A-14)}$$

A.1.4 Observer-Plume Orientation

The magnitude of the visual impact of a plume depends on the orientation of the observer with respect to the plume because the plume optical thickness will vary depending on this orientation. Figure A-2 shows plan and elevation views of an observer and a plume and indicates that the sight path distance through the constituents of the plume is a function of angles α and β. The optical thickness for most combinations of angles α and β can be approximated as follows:

$$\tau_p(\alpha,\beta) = \frac{1}{\sin\alpha}\left[\left(\tau_{py}\cos\beta\right)^2 + \left(\tau_{pz}\sin\beta\right)^2\right]^{1/2} \quad . \qquad \text{(A-15)}$$

Figure A-2 suggests that plume optical thickness is greater for horizontal sight paths than vertical ones, particularly during stable conditions when the plume cross section is flattened.

A.1.5 Limited Mixing

When vertical diffusion is limited by a stable capping layer, equation (A-12) is no longer valid, and a Gaussian formulation, with terms for reflection from the top of the mixed layer (at altitude H_m), is used. Let H' be the height of the virtual source positioned above the top of the mixed layer:

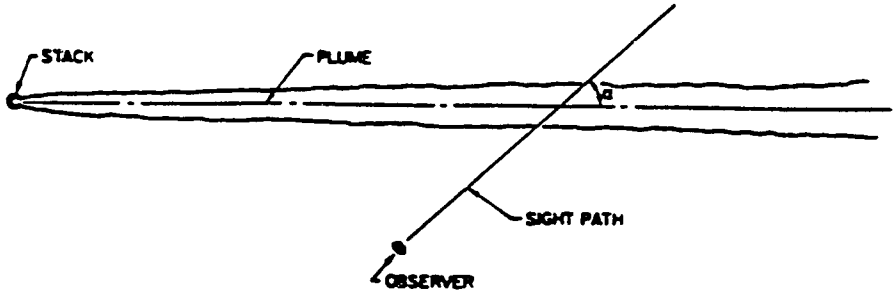

(a) Plan View

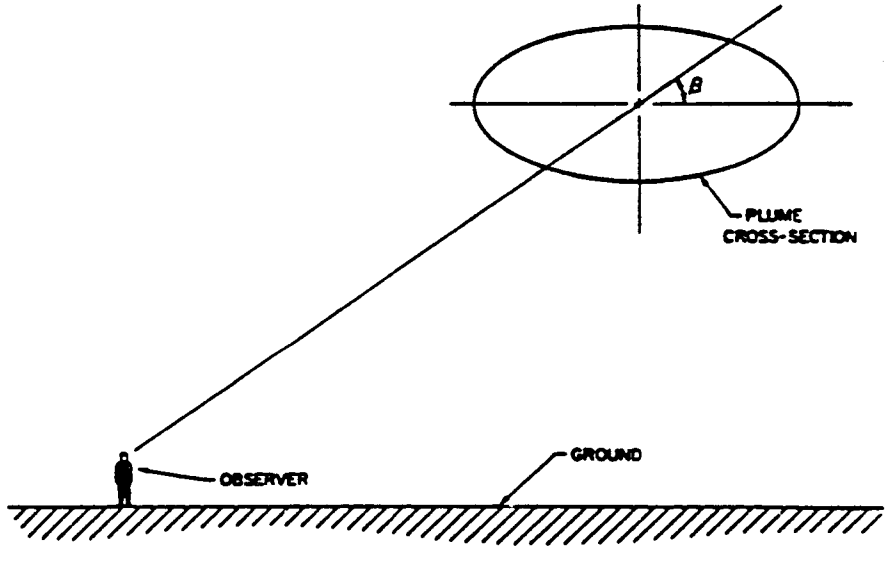

(b) Elevation View

Source: Latimer and Samuelsen (1978).

FIGURE A-2. GAUSSIAN PLUME VISUAL IMPACT MODEL: OBSERVER-PLUME GEOMETRY

$$H' = 2\,H_m - H \quad .$$

The Gaussian formulation for limited mixing is

$$\chi = \frac{Q}{2\pi\,\sigma_y\sigma_z\,u}\exp\left[-\frac{1}{2}\left(\frac{y}{\sigma_y}\right)^2\right]\left\{\exp\left[-\frac{1}{2}\left(\frac{H+z}{\sigma_z}\right)^2\right]+\exp\left[-\frac{1}{2}\left(\frac{H-z}{\sigma_z}\right)^2\right]\right.$$

$$\left.+\exp\left[-\frac{1}{2}\left(\frac{H'-z}{\sigma_z}\right)^2\right]+\exp\left[-\frac{1}{2}\left(\frac{H'+z}{\sigma_z}\right)\right]\right\} \quad . \qquad \text{(A-16)}$$

In this instance of limited mixing, the plume material eventually becomes uniformly mixed in the vertical direction for $0 \leq z \leq H_m$. In the limit, the concentration is expressed as follows:

$$\chi = \frac{Q}{(2\pi)^{1/2}\,\sigma_y u H_m}\exp\left[-\frac{1}{2}\left(\frac{y}{\sigma_y}\right)^2\right] \quad . \qquad \text{(A-17)}$$

The calculation of plume optical thickness in the y-direction becomes simply

$$\tau_{py} = \frac{Q'(x)}{uH_m} \quad . \qquad \text{(A-18)}$$

A.1.6 Surface Deposition

Surface deposition is calculated by integrating the plume concentrations at the ground and multiplying by a deposition velocity, V_d, that characterizes gas and particulate surface depletion:

$$-\frac{dQ}{dx} = V_d \int \chi\, dy \qquad \text{(A-19)}$$

Since nocturnal ground-based stable layers shield a plume from the ground at night, surface deposition is effectively zero at night. This is handled in the model using a flag keyed to the time of day at which the plume parcel is at a given downwind distance.

A.1.7 Power Law Wind Profile Extrapolation of Surface Winds

PLUVUE is designed to use either wind speed aloft or surface wind speed (commonly measured at 7 m above the surface). The power law extrapolation presented in "User's Manual for a Single-Source (CRSTER) Model" (EPA, 1977) is used. The surface wind speed is extrapolated to stack height for the plume rise calculation, and the surface wind speed is extrapolated to the final plume height for Gaussian concentration calculations. The power law extrapolation is as follows:

$$u = u_0 \, (z/7)^p \quad , \tag{A-20}$$

where

u = wind speed at altitude z (ms^{-1}),
u_0 = surface wind speed (ms^{-1}).

The profile exponent p is a function of stability and has the following values:

Pasquill Stability Class		Wind Speed Profile Exponent (p)
A	Extremely unstable	0.10
B	Moderately unstable	0.15
C	Slightly unstable	0.20
D	Neutral	0.25
E	Slightly stable	0.30
F	Moderately stable	0.30

A.2 ATMOSPHERIC CHEMISTRY

As shown in figure A-1, the conversion of emissions of nitric oxide (NO) and sulfur dioxide (SO_2) to nitrogen dioxide (NO_2) gas and sulfate ($SO_4^=$) aerosol--species responsible for visual effects--must be calculated in the visibility model.

The rate of chemical conversion of these primary emissions to secondary species responsible for visual impact is dependent on the concentration of the reacting species and ultraviolet (UV) solar flux. Thus, conversion rates are dependent on both plume dilution and time of day. A plume parcel at a given downwind distance has a specific age, time of emission, and history of UV irradiation, which can affect the amount of NO_2 and $SO_4^=$ in the plume at a given time. Thus, the chemical conversion in each plume parcel must be treated separately, taking into account these factors.

PLUVUE is structured to take a "snapshot" of a plume at a given time. In PLUVUE, the chemical conversion is calculated for each plume parcel, observed at a given distance, in a Lagrangian manner; i.e., the reaction rates are calculated at each of several discrete downwind distances and times from the point of emission to the downwind distance at which the plume parcel is observed. Thus, the age of a plume parcel observed at downwind distance x_{obs} is x_{obs}/u, where u is the wind speed. The time at which a plume parcel is at a given downwind distance relates to the time of observation as follows:

$$t = t_{obs} - \frac{x_{obs} - x}{u} \quad . \tag{A-21}$$

The UV flux is calculated as a function of time that a plume parcel is at a given downwind distance x from the solar zenith angle (i.e., the angle between direct solar rays and the normal to the earth's surface). The zenith angle is calculated on the basis of the latitude, longitude, date, and time using a subroutine developed by Schere and Demerjian (1977).

The rate of chemical conversion is also dependent on the location of the plume parcel within the plume. PLUVUE makes calculations at the following altitudes within the plume (y = 0): at the plume centerline (z = H) and at $z = H \pm n\ \sigma_z$, where n = 1 and 2.

A.2.1 Conversion of NO to NO_2

Nitrogen dioxide gas can cause a yellow-brown discoloration of the atmosphere. Although some discoloration is a result of wavelength-dependent light scattering caused by submicron aerosol, as discussed in the workbook of this regulatory guidance series, the dominant colorant of power plant plumes is NO_2, which causes a yellow-brown discoloration that may be apparent at significant distances downwind of large coal-fired power plants, particularly in areas where the background visual range is excellent.

Very little NO_2 is emitted directly from combustion sources. However, colorless nitric oxide is formed by the thermal oxidation of atmospheric nitrogen at the high temperatures experienced in the combustion zone (the boiler in a power plant) and the oxidation of nitrogen that may be present in the fuel. Chemical reactions in the atmosphere can form sufficient NO_2 from NO to cause atmospheric discoloration. Available measurements of NO and NO_2 concentrations in power plant plumes in non-urban areas suggest that the conversion of NO to NO_2 can be calculated from a simple set of three reactions.*

The first of these is the thermal oxidation of NO to NO_2:

$$2NO + O_2 \rightarrow 2NO_2 \qquad \text{(A-22)}$$

---

* In urban areas, a complete photochemical mechanism should be applied to calculate NO_2 concentrations. Also, it should be noted that NO_2 is destroyed by reaction with the hydroxyl radical (OH•), as discussed in the next subsection.

The reaction is termolecular, but bimolecular with respect to NO; it is therefore very fast at high concentrations of NO but slow at the lower concentrations that exist in the atmosphere or in a plume. The reaction rate for equation (A-22), based on Baulch, Drysdale, and Horne (1973) is

$$\frac{d[NO_2]}{dt} = \left[4.015 \times 10^{-12} \exp\left(\frac{1046}{RT}\right)\right][NO]^2[O_2] \text{ ppm/s} \quad . \quad \text{(A-23)}$$

where R is the universal gas constant and T is the absolute temperature.

The reaction with ozone also affects the conversion of NO to NO_2:

$$NO + O_3 \rightarrow NO_2 + O_2 \quad . \quad \text{(A-24)}$$

The reaction is fast, with a rate (Leighton, 1961; Davis, Smith, and Klauber, 1974; Niki, 1974) at 25°C of

$$\frac{d[NO_2]}{dt} = 0.44\ [NO][O_3] \text{ ppm/s} \quad . \quad \text{(A-25)}$$

This reaction accounts for the ozone depletion measured within power plant plumes and is important because ozone concentrations can be high even in nonurban regions. Measured ozone concentrations in nonurban areas of the western United States range from 0.02 to 0.08 ppm.

Whereas the thermal oxidation rate in reaction (A-23) decreases as the plume mixes (because the NO concentration decreases), the formation of nitrogen dioxide via equation (A-24) is enhanced as the plume mixes because additional ozone from the atmosphere is mixed into the plume, allowing equation (A-24) to proceed. When there are no reactions converting NO_2 to NO (e.g., at night), equation (A-24) proceeds until all of the NO in the plume is converted to NO_2 or until the ozone concentration in the plume drops to zero. Therefore, the rate of conversion of NO to NO_2 via equation (A-24) is limited by the rate of plume mixing that provides the necessary atmospheric ozone.

To complete the set of chemical reaction mechanisms, we must consider the photolysis of NO_2. When sunlight illuminates a plume containing nitrogen dioxide, short wavelength light and ultraviolet radiation are absorbed by the NO_2. As noted above, absorption of the shorter wavelength light produces the characteristic yellow-brown color associated with NO_2. Absorption of the more energetic ultraviolet light (UV) results in dissociation of the NO_2 molecule:

$$NO_2 + h\nu \rightarrow NO + O \quad . \tag{A-26}$$

$$O + O_2 \rightarrow O_3 \quad . \tag{A-27}$$

Leighton (1961) gave the rate of reaction (A-26) as

$$\frac{d[NO_2]}{dt} = -K_d\,[NO_2] \text{ ppm/s} \quad , \tag{A-28}$$

where K_d depends on the amount of light incident on the nitrogen dioxide. Davis, Smith, and Klauber (1974) gave the following expression for K_d as a function of the solar zenith angle Z_s:

$$K_d = 1 \times 10^{-2} \exp\left(-\frac{0.38}{\cos Z_s}\right) s^{-1} \quad . \tag{A-29}$$

With this set of chemical reactions, the chemical conversion of NO to NO_2 in the atmosphere can be calculated from background pollutant concentrations and from plume NO_x increments using the technique suggested by Latimer and Samuelsen (1975) and White (1977). Making the steady-state approximation, we have

$$[NO_2] = \frac{K_r}{K_d}[NO][O_3] \quad , \tag{A-30}$$

where

$$[NO] = [NO_x] - [NO_2] \qquad \text{(A-31)}$$

and

$$[O_3] = [O_3]_b - [NO_2] - [NO_2]_t - [NO_2]_b \quad . \qquad \text{(A-32)}$$

where $[NO_2]t$ signifies the concentration of NO_2 formed via the termolecular reaction (A-22) and $[NO_2]b$ signifies background concentrations. Substituting equations (A-28) and (A-29) into equation (A-27) we can solve for the concentration of NO_2:

$$[NO_2] = 0.5 \left[[NO_x] + [O_3]_b + [NO_2]_t + [NO_2]_b + \frac{K_d}{K_r} - \left\{ \left([NO_x] + [O_3]_b + [NO_2]_t + [NO_2]_b + \frac{K_d}{K_r} \right)^2 - 4[NO_x] \left([O_3]_b + [NO_2]_t + [NO_2]_b \right) \right\}^{1/2} \right] \quad .$$

(A-33)

Using this formulation to compute NO-to-NO_2 conversion in a hypothetical power plant plume, Latimer and Samuelsen (1978) studied the sensitivity of NO_2 formation to the rate of plume dilution, background ozone concentration, and solar radiation. The results of this analysis are presented in figure A-3. This figure shows that thermal oxidation (e.g., $[O_3] = 0$) converts up to 10 percent of the plume NO to NO_2, and additional conversion results when ambient ozone is mixed into the plume. A recent comparison of observations with calculations using equation (A-33) indicates good agreement, particularly if the diffusion of the plume is

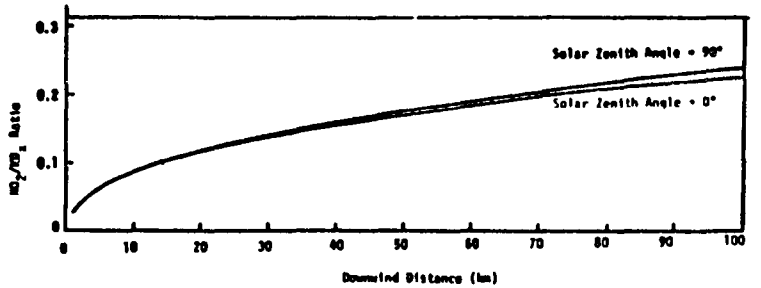

(a) Solar radiation

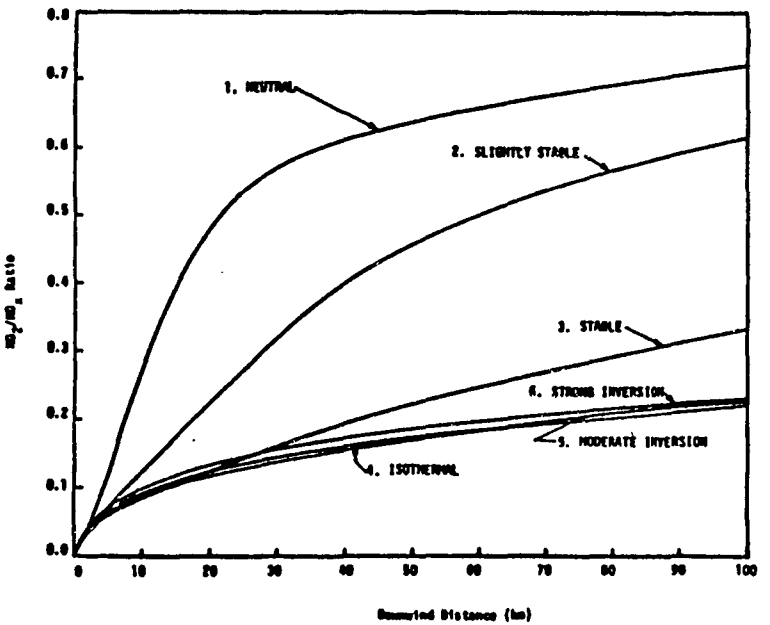

(b) Stability (TVA stability categories)

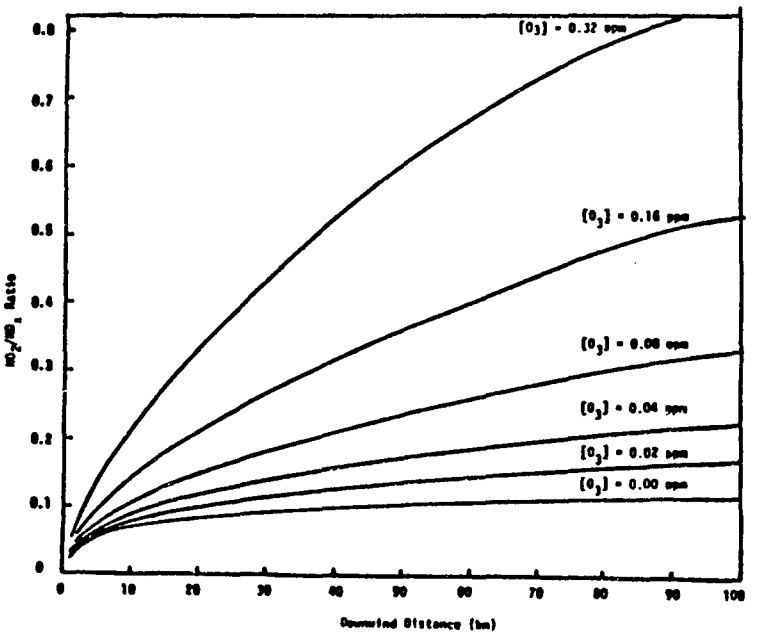

(c) Background ozone

Source: Latimer and Samuelsen (1978).

FIGURE A-3. SENSITIVITY OF NO-TO-NO_2 CONVERSION IN POWER PLANT PLUMES TO THE RATE OF PLUME DILUTION, BACKGROUND OZONE CONCENTRATION, AND SOLAR RADIATION

correctly calculated by using fitted diffusion coefficients based on plume diffusion measurements (see figure A-4).

A.2.2 Conversion of SO_2 to $SO_4^=$

It is critical to calculate the conversion of SO_2 emissions to sulfate ($SO_4^=$) aerosol, because the latter can effectively scatter light and cause reductions in visual range. The importance of SO_2 to $SO_4^=$ conversion can be seen from the schematic logic flow shown in figure A-1. The usual approach is to assume that sulfur dioxide (SO_2) gas is converted to sulfate ($SO_4^=$) aerosol at some constant rate; this approach employs a user-input value of a pseudo-first-order rate constant whose value is empirically determined.

There is considerable variation, however, in such measured SO_2-to-$SO_4^=$ conversion rates, which range from a few tenths of a percent to several percent per hour. Much of this variance in SO_2-to-$SO_4^=$ conversion observed in field measurement programs in recent years can be explained using a model that accounts for the reactions of plume SO_2 and NO_2 with the hydroxyl (OH•) radical. This chemical mechanism is incorporated in PLUVUE. In clean background areas, the gas-phase oxidation of SO_2 and NO_2 to sulfate aerosol and nitrate (nitric acid vapor) is due primarily to the reaction of these species with OH•. Previous assessments of homogeneous (gas-phase) oxidation of SO_2 to sulfate estimated the proportion assignable to the reaction with hydroxyl between about 75 percent in clean atmospheres (Calvert et al., 1978; Altshuller, 1979) and as low as 40 percent in polluted urban air (Isaksen, Hesstredt, and Hov, 1978), but more recent estimates place these values much higher. Kinetic models forming the basis of the early estimates used the value of $1.3 \times 10^{-12} cm^3 mol^{-1} s^{-1}$ for the rate constant of reaction for HO_2 and CH_3O_2 with NO. More recently, however, this rate has been measured at $8.1 \times 10^{-12} cm^3 mol^{-1} s^{-1}$ (Hampson and Garvin, 1978). This larger rate constant lowers the expected concentration of these peroxy radicals by a factor of 6 and, in turn, greatly reduces the SO_2 conversion resulting from reactions with these

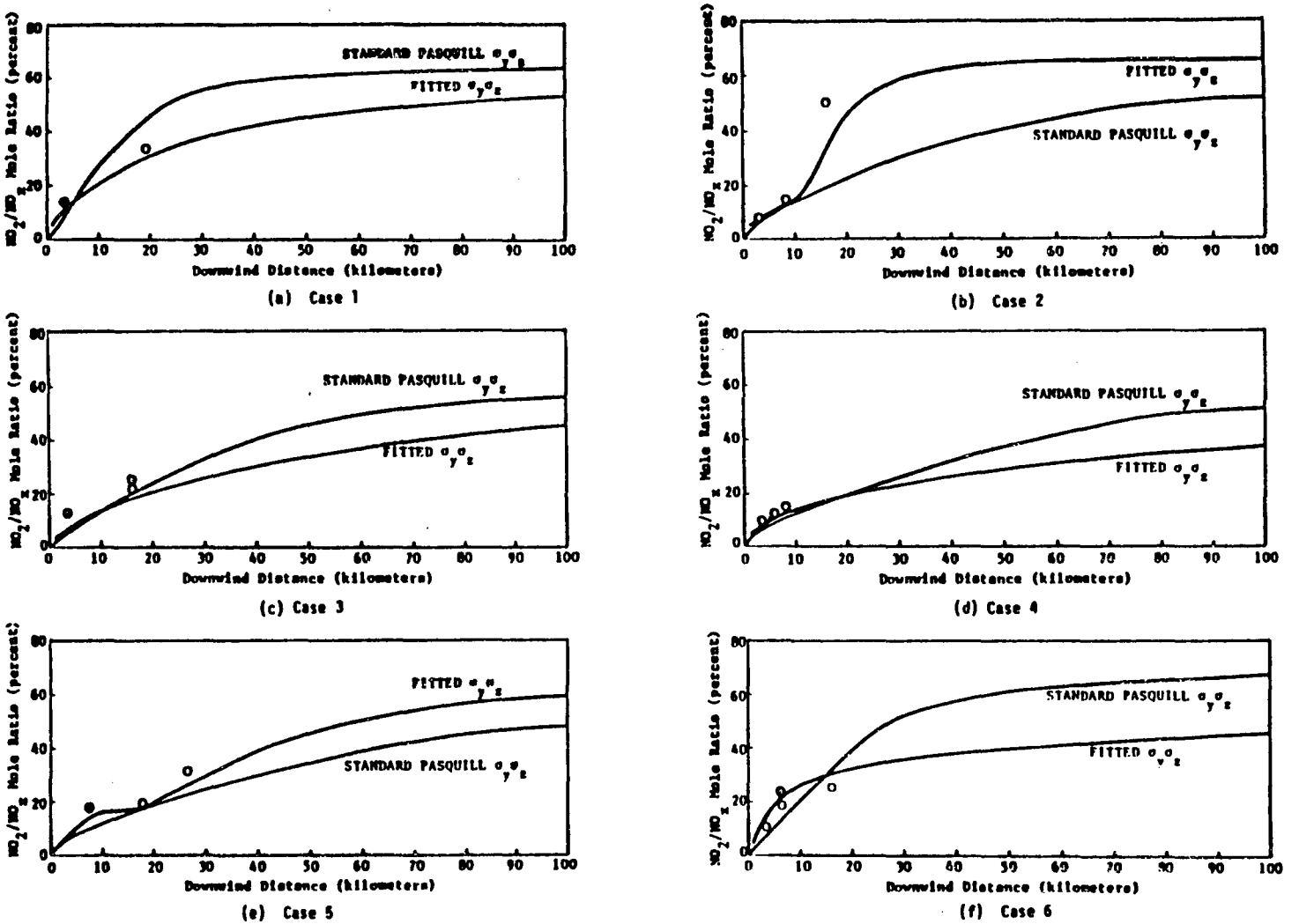

FIGURE A-4. COMPARISON OF MEASURED NO_2/NO_x MOLE RATIOS (CIRCLED POINTS) IN THE PLUME CENTERLINE DOWNWIND OF A COAL-FIRED POWER PLANT WITH COMPUTER-CALCULATED VALUES (SOLID LINES) USING STANDARD PASQUILL AND FITTED $\sigma y \sigma z$

radicals. When recalculated using the new rate constant, the fraction of SO_2-to-sulfate conversion that results from reaction with the hydroxyl radical is approximately 95 percent for clean atmospheres and 70 percent for the extremely polluted case.

These estimates are supported by the work of Miller (1978), who found that the SO_2 oxidation rate was not dependent on the absolute concentrations of hydrocarbons and nitrogen oxides but on the ratio of nonmethane hydrocarbon to nitrogen oxides.

The rate of sulfate (and nitric acid) formation can be estimated by calculating the steady-state concentration of OH• within a plume. This steady-state plume OH• concentration is calculated by balancing the rate of OH• production with the rate of OH• destruction. The following reactions are used:

> OH• production*

- $O_3 + h\nu \rightarrow O(^1D) + O_2$

$$\left[\left(K_{34} = 1.3 \times 10^{-3} (\cos Z_s)^{2.74} min^{-1}\right)\right] \quad \text{(A-34)}$$

- $O(^1D) + M \rightarrow O(^3P) + M \quad (K_{35} = 4.45 \times 10^{10} min^{-1})$ (A-35)

- $O(^1D) + H_2O \rightarrow 2\ OH• \quad (K_{36} = 3.4 \times 10^{5} ppm^{-1} min^{-1})$ (A-36)

> OH• destruction (major sinks in plumes)

- $OH• + SO_2 \rightarrow HSO_3 \ldots \quad (K_{37} = 2.0 \times 10^{3} ppm^{-1} min^{-1})$ (A-37)

- $OH• + NO_2 \rightarrow HNO_3 \quad (K_{38} = 1.4 \times 10^{4} ppm^{-1} min^{-1})$. (A-38)

---

* See Latimer et al. (1980) for a discussion of other sources of OH•. Rate constants are based on Whitten and Killus (1980), private communication.

With the assumption of steady-state concentrations of O('D) and OH• in the plume, we can write the following equations:

$$\frac{d[OH\bullet]}{dt} = \frac{d[O'(D)]}{dt} = 0 \quad , \tag{A-39}$$

$$\frac{d[O('D)]}{dt} = K_{34}(h\nu)[O_3] - K_{35}[O('D)] - K_{36}[O'(D)][H_2O] \quad , \tag{A-40}$$

$$[O('D)] = \frac{K_{34}(h\nu)[O_3]}{K_{35} + K_{36}[H_2O]} \quad , \tag{A-41}$$

$$\frac{d[OH\bullet]}{dt} = 2\,K_{36}[O('D)][H_2O] - K_{37}[OH\bullet][SO_2] - K_{38}[OH\bullet][NO_2] \quad , \tag{A-42}$$

$$[OH\bullet] = \frac{2\,K_{36}[O('D)][H_2O]}{K_{37}[SO_2] + K_{38}[NO_2]} \quad . \tag{A-43}$$

With this steady-state concentration, plume pseudo-first-order SO_2-to-SO_4 and NO_2-to-HNO_3 conversion rates can be calculated as follows:*

$$-\frac{1}{[SO_2]}\frac{d[SO_2]}{dt} = K_{37}[OH\bullet] \quad , \tag{A-44}$$

$$-\frac{1}{[NO_2]}\frac{d[NO_2]}{dt} = K_{38}[OH\bullet] \quad . \tag{A-45}$$

Note from equations (A-41) and (A-42) that plume OH• concentrations are reduced below background tropospheric values for two reasons:

---

* The user is given the option in PLUVUE of supplementing the SO_2-to-$SO_4^=$ conversion rate calculated on the basis of steady-state plume OH• concentrations with a user-input pseudo-first-order rate constant, which can be varied as a function of downwind distance.

- Plume ozone (O_3) concentrations are reduced below background values because of the reaction $NO + O_3 \rightarrow NO_2 + O_2$ (eq. A-24).
- Plume concentrations of NO_2 and SO_2 are high, thus reducing steady-state OH• concentrations.

It should be pointed out that at night there is no production of OH• from ozone photolysis; also, in early morning and late afternoon and in winter OH• production is diminished because ultraviolet flux decreases as solar zenith angles approach 90°. Thus, sulfate and nitrate are not formed at night and are formed only very slowly in concentrated plumes. Nitrate is expected to remain as HNO_3 vapor and without visual effects until it is eventually deposited. Ammonium nitrate could exist in aerosol form; however, sulfate competes for available atmospheric ammonia.

PLUVUE was run, with this OH• chemical mechanism included, for a plume from a 1600 Mwe coal-fired power plant. On the basis of this case study, the effect of the following on sulfate formation rate was studied:

- Plume dilution, corresponding to neutral and stable light-wind conditions at various downwind distances.
- Time of day.
- Season.

The history of sulfate formation in a plume parcel based on this case study is shown in figure A-5. Note that time of day, season, and plume concentration all affect the rate of sulfate formation. This effect is explained by the formulations shown in equations (A-41), (A-43), and (A-44).* The SO_2-to-$SO_4^=$ conversion rate is directly proportional to the

* It should be noted that sulfate can form not only by reactions with OH• but also on existing, catalytic fly ash particles. However, this sulfate coating on existing particles is not expected to significantly add to aerosol surface area, which is important for light scattering.

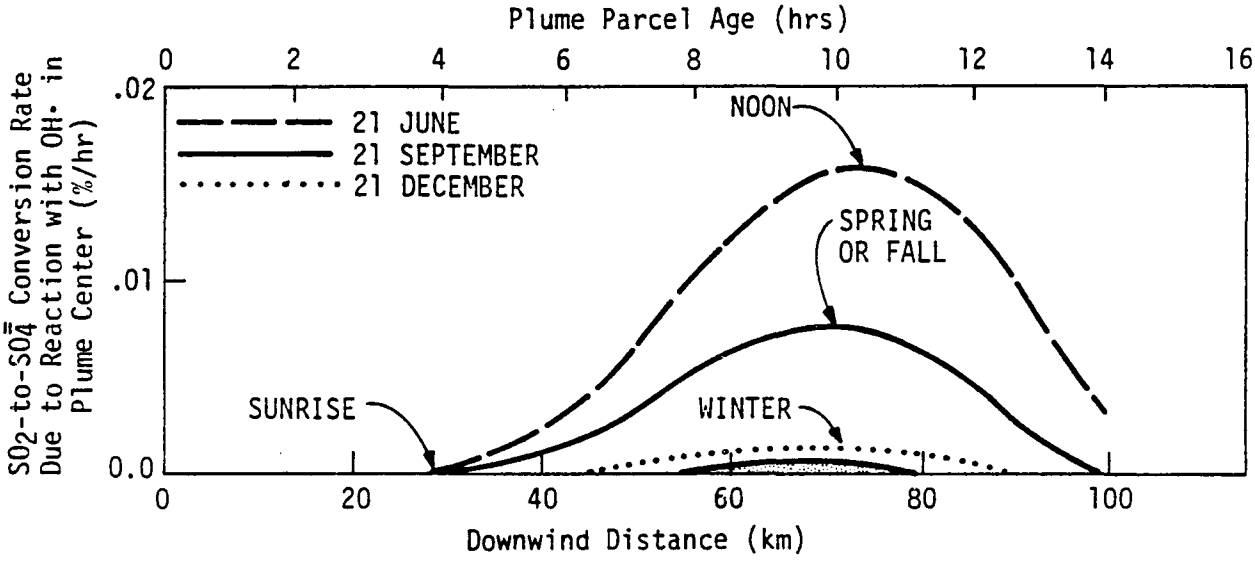

Notes:

(1) Time-dependent SO_2-to-$SO_4^{=}$ conversion rates for the history of a parcel in the center of a well-mixed plume (neutral stability) which is observed 100 km downwind at 1500 (in the afternoon) are plotted for indicated seasons in Figure 5(a).

(2) Comparable conversion rates for a well-mixed plume observed 160 km downwind at 1500 are plotted in Figure 5(b).

(3) Conversion rates for stable plumes (isothermal stability) are considerably less than 0.01 percent/hr. See shaded areas at the bottom of graphs.

(a) Life history of a plume parcel observed 100 km downwind at 1500 hours.

FIGURE A-5. CALCULATED TIME DEPENDENCE OF SULFATE FORMATION IN THE CENTER OF PLUMES FROM A 1600 Mwe COAL-FIRED POWER PLANT, 2 m/s WINDS, NEUTRAL AND STABLE CONDITIONS

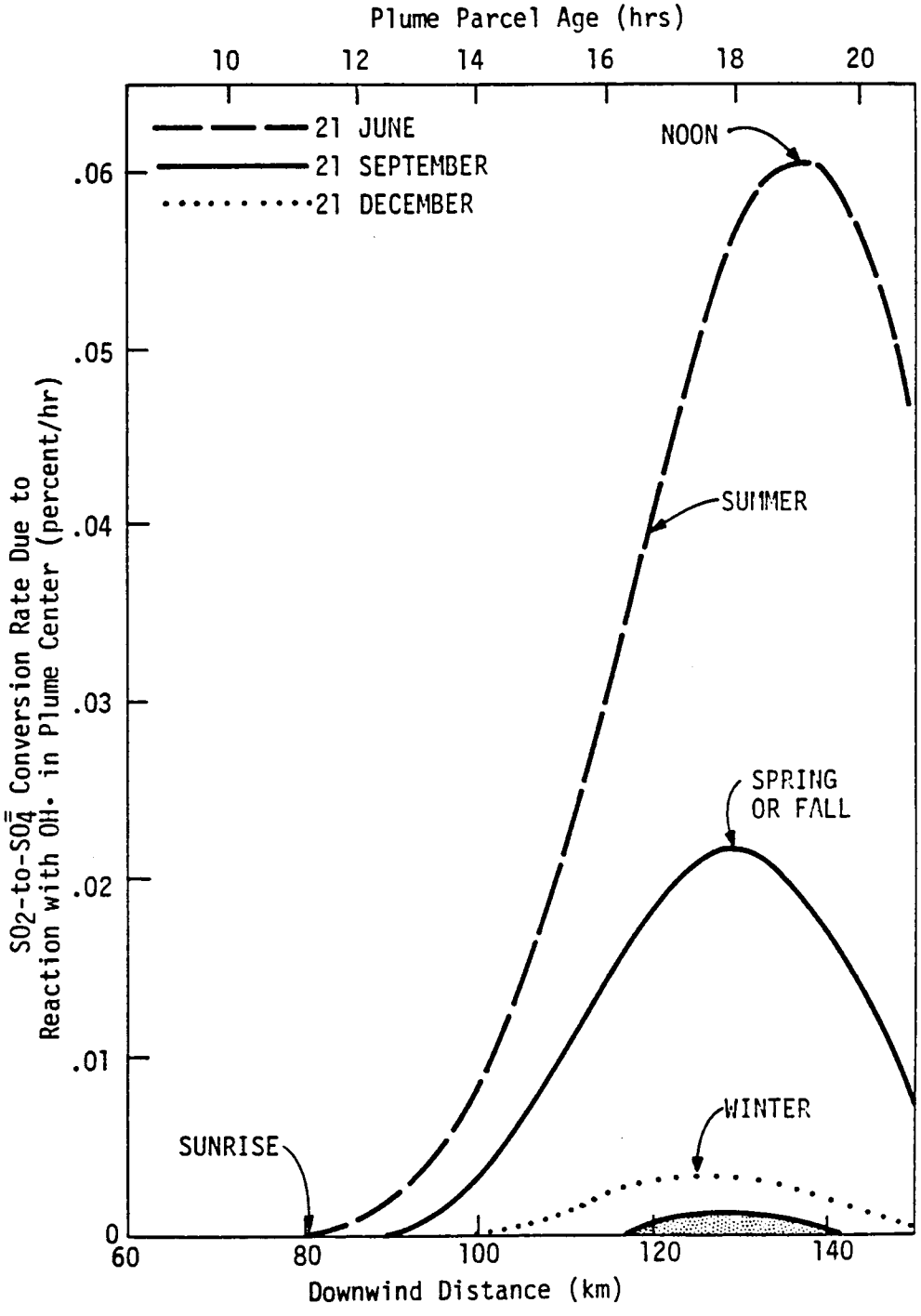

(b) Life history of a plume parcel observed 160 km downwind at 1500 hours.

FIGURE A-5 (Concluded)

plume ozone and water vapor concentrations and to ultraviolet (UV) flux, and it is inversely proportional to plume SO_2 and NO_2 concentrations.

The effect of UV flux is noted in both the seasonal and time-of-day dependence of the sulfate formation rate. Note from figure A-5 that no conversion of SO_2 to sulfate occurs at night. Sulfate formation starts after sunrise, reaches its maximum rate at noon (when ultraviolet flux reaches a maximum), and then begins to decrease. Thus, a plume parcel observed at a given distance downwind from a power plant may have undergone sulfate formation during only a fraction of its journey. For example, a plume parcel 160 km downwind of its source, when winds are 2 m/s, would require a transit time of more than 22 hours. During this period sulfate would be formed only during the sunlight hours (see figure A-5[b]).

The effect of plume SO_2 and NO_2 concentrations on the steady-state $OH\cdot$ concentration and hence on sulfate formation is also shown in figure A-5. Note, by comparing figure A-5(a) with A-5(b), that sulfate formation is much more rapid when plume parcels are more dilute (at farther downwind distances). In the dilute, neutral-stability plumes at downwind distances greater than 100 km, sulfate formation rates reach noon peaks of about 0.06, 0.02, and 0.004 percent per hour, respectively, for the summer, fall, and winter simulations for this latitude. In the less dilute, neutral-stability plumes at downwind distances of less than 100 km, the sulfate formation rates peak at 0.016, 0.008, and less than 0.002 percent per hour for summer, fall, and winter, respectively. However, formation rates in stable plumes are considerably less than 0.01 percent per hour even at noon on a summer day.

These model calculations support the argument made by Latimer (1980) that the atmospheric discoloration of stable power plant plumes (where particulate emissions are controlled) is caused primarily by nitrogen dioxide (NO_2) gas, not by secondary sulfate aerosol. Sulfate aerosol is not formed in plumes during nighttime transport, and formation is minimal during daytime transport when plumes are concentrated (as they would be

during stable conditions). After plumes have become well mixed, significant rates of sulfate formation can occur in the daytime, though these rates approach zero with low sun angles. Thus, sulfate formation is a long range (greater than 100 km), multiday phenomenon, not a near-source problem.

A.3 AEROSOL SIZE DISTRIBUTION

The aerosol size distribution is characterized by a series of aerosol modes, each having a log-normal distribution of mass (or volume). Each of the following modes is treated separately in PLUVUE:

- Background accumulation mode (submicron) aerosol (typically having a mass median diameter of about 0.3 μm and a geometric standard deviation of 2).
- Background coarse mode (> 1 μm) aerosol (typically having a mass median diameter of about 6 μm and a geometric standard deviation of 2).
- Plume primary particulate aerosol (e.g., fly ash emissions).
- Plume secondary sulfate ($SO_4^=$) aerosol (typically having a mass median diameter of 0.1 to 0.3 μm and a geometric standard deviation of 2).

The expression developed by Winkler (1973) is used to calculate the amount of liquid water associated with submicron background and plume sulfate aerosol as a function of relative humidity.

Secondary aerosol is assumed to form in the submicron plume secondary aerosol mode. A time delay equal to the time between successive downwind distances is introduced to account for coagulation and condensation time delays.

A.4 ATMOSPHERIC OPTICS

In the atmospheric optics component of the plume visibility model, the light scattering and absorption properties of the aerosol and the resultant light intensity (spectral radiance) for various illumination and viewing situations are computed. The details of these calculations are given in appendix B of Latimer et al. (1978); the major points are summarized in this section.

A.4.1 Calculation of the Scattering and Absorption Properties

After the concentrations of the pollutants are specified by the transport and chemistry subroutines, their radiative properties must be determined. For NO_2, the absorption at a particular wavelength is a tabulated function (Nixon, 1940) multiplied by the concentration. For aerosols, however, the procedure is more complicated.

In general, a particle's ability to scatter and absorb radiation at a particular frequency is a function of size, composition, shape, and relative humidity. The flexibility to specify the size distribution of both primary and secondary particles was desired. Therefore, the effect of particle size on the wavelength dependence of the extinction coefficient and the phase function, the solution of Maxwell's equations for scattering by a sphere, and the so-called Mie equations were used in PLUVUE. These calculations are appropriate for atmospheric aerosol; comparisons of Mie calculations, with empirical correlations of scattering-to-mass indicate substantial agreement.

The Mie calculations in PLUVUE are performed using an IBM subroutine written by J. V. Dave (Dave, 1970). The required inputs are the particle size parameter (ratio of the circumference to the wavelength of radiation), the index of refraction (real and imaginary part), and the number and location of absorption cross sections and the Stokes transformation matrix (Van De Hulst, 1957), which can be simply converted to the scattering distribution assuming randomly polarized light. The scattering and

absorption properties per particle are then summed over the particular log-normal size distribution for the given aerosol mode.

A.4.2 Calculation of Light Intensity

The light intensity, or radiance (watts/m^2/steradian) at a particular location in the atmosphere is a function of the direction of observation Ω and the wavelength λ. Calculation of the light intensity in a medium follows from the radiative transfer equation. This equation is a conservation of energy statement that accounts for the light added to the line of sight by scattering and the light lost because of absorption and scattering. Approximations and solution techniques applicable to planetary atmospheres have been discussed by Hansen and Travis (1974) and Irvine (1975).

The physical situation that we are concerned with is shown schematically in figure A-6. To compute the spectral light intensity at the observer, we sum (integrate) the scattered and absorbed light over the path, r, associated with the line of sight Ω. The resultant general expression for the background sky intensity at a particular wavelength is

$$I_b(\Omega) = \int_0^{\tau_\infty} \frac{\omega(\tau)}{4\pi} \int_{\Omega'=4\pi} I(\Omega', \tau') p(\Omega' \rightarrow \Omega, \tau') \, d\Omega' \, e^{-\tau'} \, d\tau' \quad , \quad \text{(A-46)}$$

where

τ = the optical depth ($\tau \equiv \int_0^r b_{ext} \, dr$, where b_{ext} is the extinction coefficient),

ω = the albedo for single scattering ($\omega \equiv b_{scat}/b_{ext}$ where b_{scat} is the scattering coefficient),

$p(\Omega' \rightarrow \Omega)$ = the scattering distribution function for the angle $\Omega' \rightarrow \Omega$),

I = the spectral intensity at τ' from direct and diffuse solar radiation.

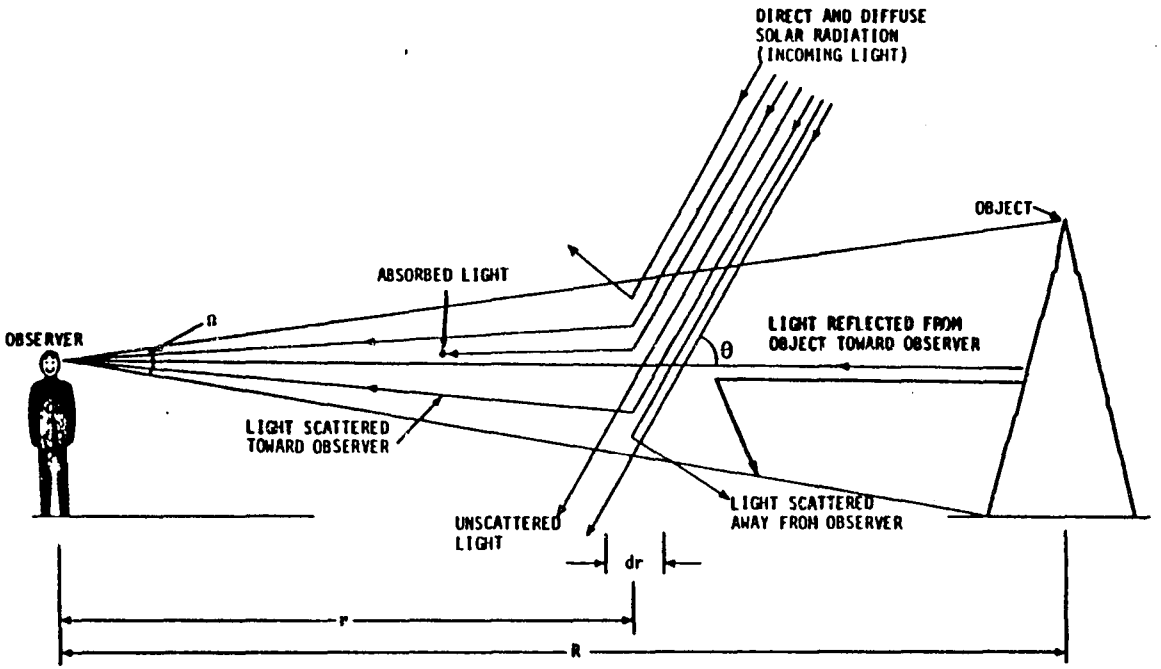

FIGURE A-6. LIGHT SCATTERING AND ABSORPTION IN THE ATMOSPHERE

The intensity seen by an observer in direction Ω of a background viewing object of intensity I_0 at distance R is

$$I_{obj}(\Omega) = I_0(\Omega)e^{-\tau_R}$$

$$+ \int_0^{\tau_R} \frac{\omega(\tau')}{4\pi} \int_{\Omega'=4\pi} I(\Omega', \tau)\, p(\Omega' \rightarrow \Omega, \tau')\, d\Omega'\, e^{-\tau'}\, d\tau' \quad . \tag{A-47}$$

Equations (A-46) and (A-47) then completely describe the spectral intensity of the sky and a background object. Once these two quantities are known, the visual effects of the intervening atmosphere can be quantified. In evaluating equations (A-46) and (A-47), we encounter two main difficulties: First, the quantity in the integral is a fairly complicated function, and accurate specification is tedious. Second, the atmosphere is inherently inhomogeneous; thus, the radiative properties ω, p are somewhat complicated functions of r and Ω. The following approximations are therefore made in PLUVUE:

- Plane parallel atmosphere
- Two homogeneous layers
- Average solar flux approximation
- Average diffuse intensity approximation.

The equation for the background intensity at the surface becomes, for a given viewing direction,

$$I_b = I_{sky}e^{-\tau_{OD}} + \frac{\bar{\omega}_{OD}}{4\pi} \bar{p}_{OD}(\theta)\, F_{s,av}\left(1 - e^{-\tau_{OD}}\right)$$

$$+ \bar{\omega}_{0D} \, I_{av}^{dif} \left(1 - e^{-\tau_{0\infty}}\right) \quad , \tag{A-48}$$

and for the intensity in the direction of an object in the planetary boundary layer,

$$I_{obj} = I_o e^{-\tau_R} + \frac{\bar{\omega}_{0D}}{4\pi} \bar{p}_{0D}(\Theta) \, F_{s,av} \left(1 - e^{-\tau_R}\right)$$

$$+ \bar{\omega}_{0D} \, I_{av}^{dif} \left(1 - e^{-\tau_R}\right) \quad , \tag{A-49}$$

where

$\bar{\omega}_{0D}$, $\bar{p}_{0D}(\Theta)$ = the average albedo and phase function, respectively;

τ_{0D} = the optical depth of the path in the boundary layer;

$F_{s,av}$, I_{av}^{dif} = the average solar direct intensity and diffuse intensity, respectively;

I_{sky}, I_o = the intensities from the upper atmosphere and object, respectively.

Thus, the background intensity and the intensity in the direction of an object at distance R from the observer can be computed given the following inputs:

- Background radiative properties (e.g., size distribution, visual range).
- Solar zenith angle.
- Scattering angle.
- Viewed object intensity.
- Direction of observation.
- Planetary boundary layer height.

The plume is treated as a homogeneous layer with a given optical thickness and mean properties $\overline{\omega}_{plume}$ and $\overline{p}_{plume}(\Theta)$. We also assume that the plume does not affect the solar radiation illumination (an optically thin plume).

Diffuse radiation (I_{av}^{dif}) is computed using an approximation discussed in appendix B of Latimer et al. (1978).

Spectral radiance, or light intensity $I(\lambda)$, is calculated for 39 wavelengths spanning the visible spectrum (0.36 μm < λ < 0.74 μm, in 0.01 μm increments).

A.5 GEOMETRY OF PLUME, OBSERVER, AND SUN

For performing as many as four different types of optics calculations at selected points along the plume trajectory, PLUVUE has two modes: plume-based and observer-based calculations. The calculations for plume transport, diffusion, and chemistry are identical for calculations in both modes. The major difference between the two types of calculations is the orientation of the position of the viewer to the source and the plume.

Plume-based calculations are repeated for several combinations of plume-observer-sun geometries. Because of the repetitions, these plume-based calculations are more expensive and produce more printed output than the observer-based calculations, which are performed for only the specific line-of-sight orientations corresponding to the given observer position, the portions of the plume being observed, and the specific position of the sun relative to these lines of sight.

There are four types of optics calculations: (1) horizontal views through the plume with a sky viewing background; (2) nonhorizontal views through the plume with a sky viewing background; (3) horizontal views through the plume with white, gray, and black viewing backgrounds; and

(4) horizontal views along the axis of the plume with a sky viewing background.

Figure A-7 illustrates the geometry of the plume-based optics calculations for horizontal views through the plume. This figure depicts schematically the variety of distances from the observer to the plume and the variety of horizontal azimuthal angles between the line of sight and the plume trajectory.* Calculations for all these geometries are repeated for up to six different scattering angles.

Plume-based calculations for nonhorizontal views through the plume are shown in figure A-8. For one azimuthal angle (α), figure A-8(a) shows the range of vertical elevation angles (β) of the line of sight. The observer position is determined by the intersection of the line of sight with flat terrain. For one elevation angle (β) of the line of sight, figure A-8(b) shows the range of four azimuthal angles (α) between the plume centerline and the line of sight. Again, these calculations are repeated for as many as six different scattering angles at each point of analysis along the plume trajectory.

Figure A-9 shows the geometry for the optics calculation for horizontal views perpendicular to the plume with white, gray, and black viewing backgrounds. For each point on the plume trajectory and each scattering angle, the calculations are executed for a range of distances from the observer to the background object, starting at the plume centerline and ending at 80 percent of the background visual range. The distances, from the observer to the plume, range from 2 percent to 80 percent of the background visual range.

Figure A-10 illustrates the configuration used for the plume-based calculation for views along the axis of the plume. The calculations are made from the second through the final downwind distances. At each point,

---

* These azimuthal angles are measured from the plume centerline to the line of sight such that the angles range from 0° to 90°.

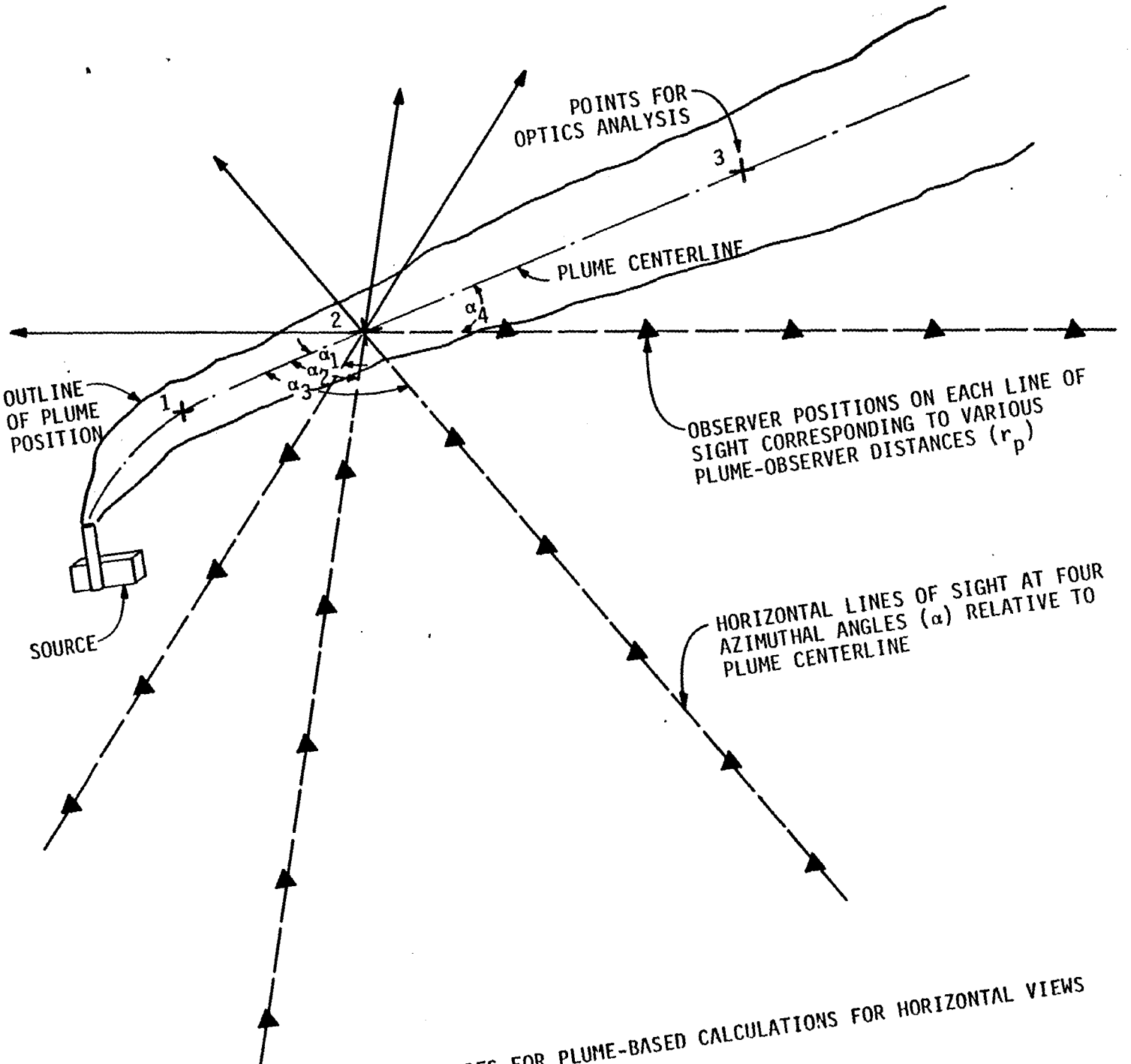

FIGURE A-7. GEOMETRIES FOR PLUME-BASED CALCULATIONS FOR HORIZONTAL VIEWS WITH A SKY BACKGROUND

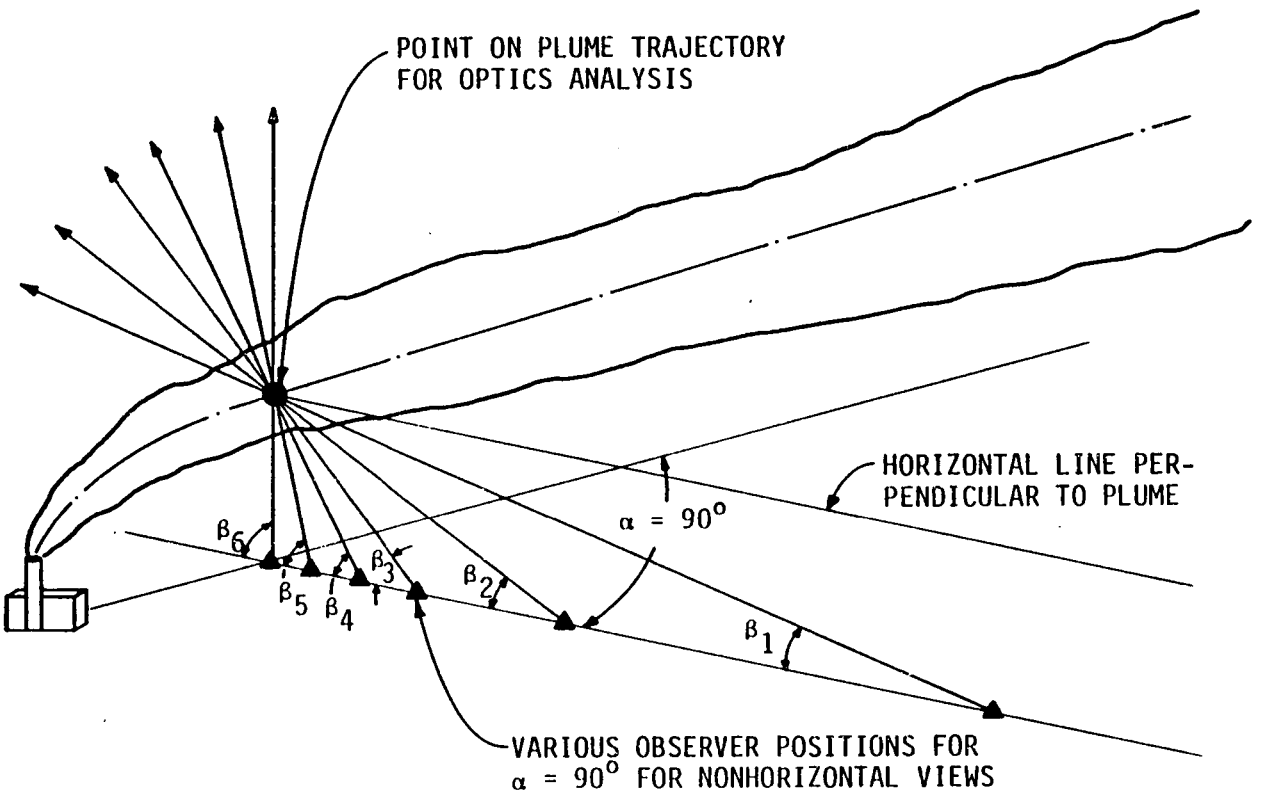

(a) Variation in elevation angle (β) for a fixed azimuthal angle (α = 90°) between the plume trajectory and the line of sight.

FIGURE A-8. GEOMETRIES FOR PLUME-BASED CALCULATIONS FOR NONHORIZONTAL VIEWS WITH A SKY BACKGROUND

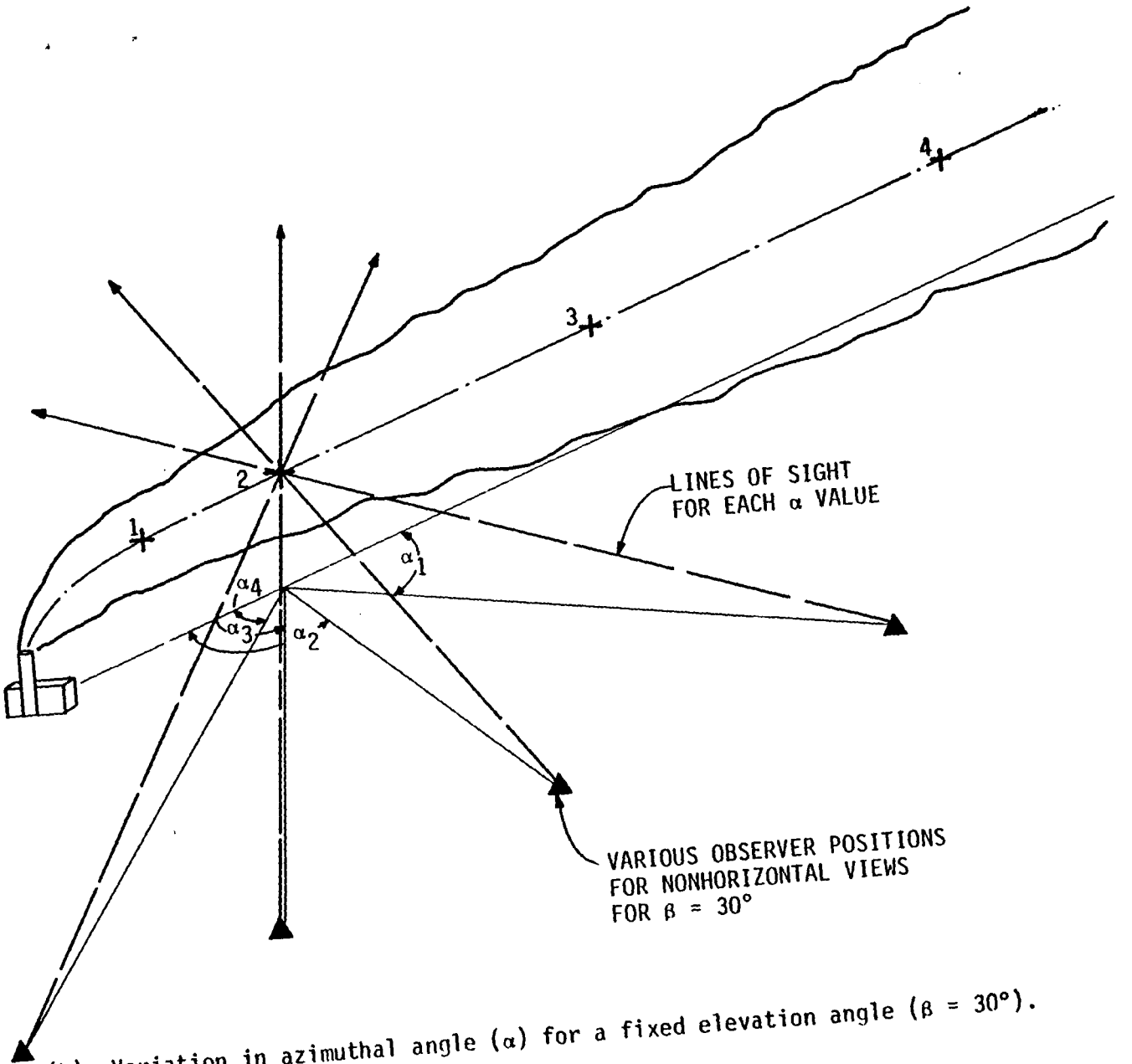

(b) Variation in azimuthal angle (α) for a fixed elevation angle (β = 30°).

FIGURE A-8 (Concluded)

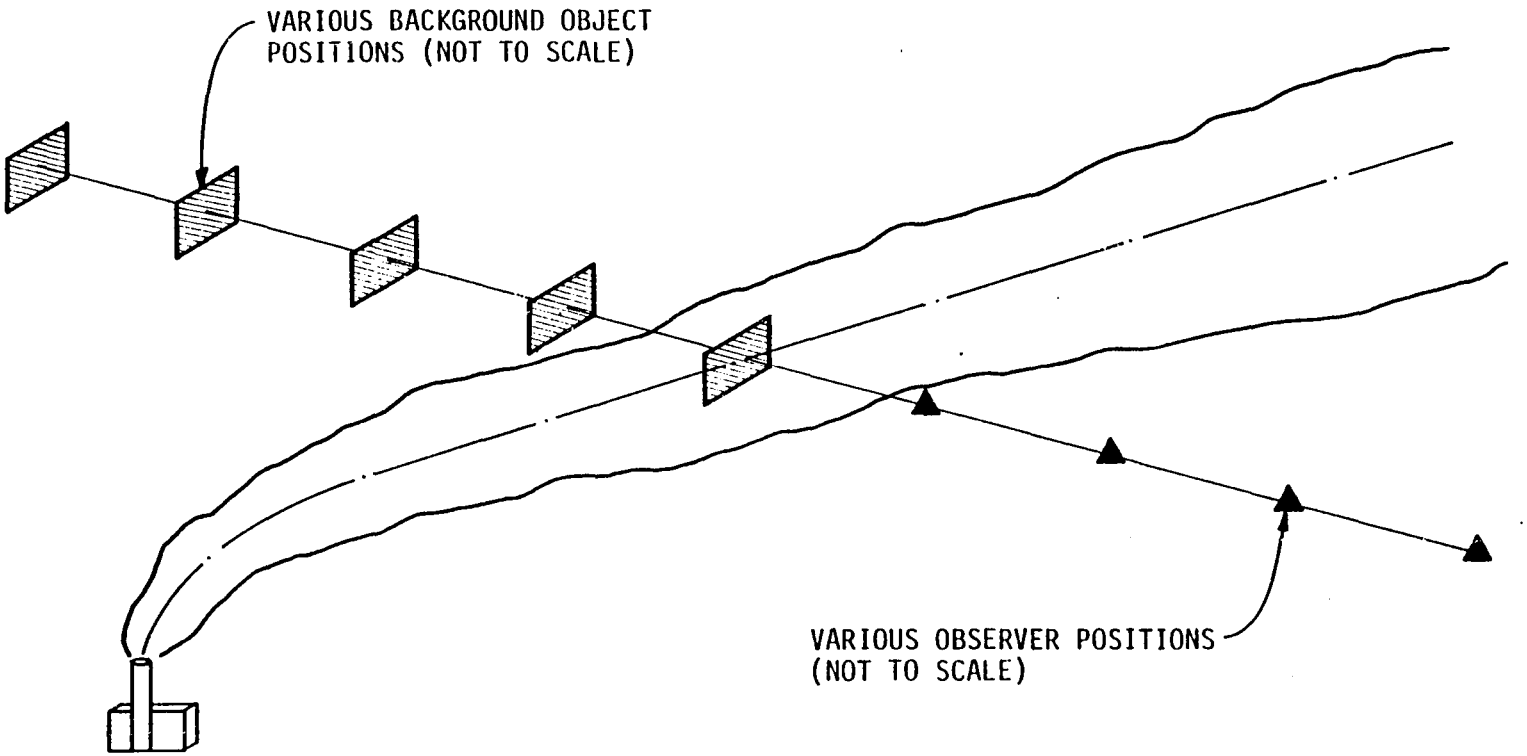

FIGURE A-9. GEOMETRIES FOR PLUME-BASED CALCULATIONS FOR VIEWING OF WHITE, GRAY, AND BLACK OBJECTS FOR HORIZONTAL VIEWS PERPENDICULAR TO THE PLUME

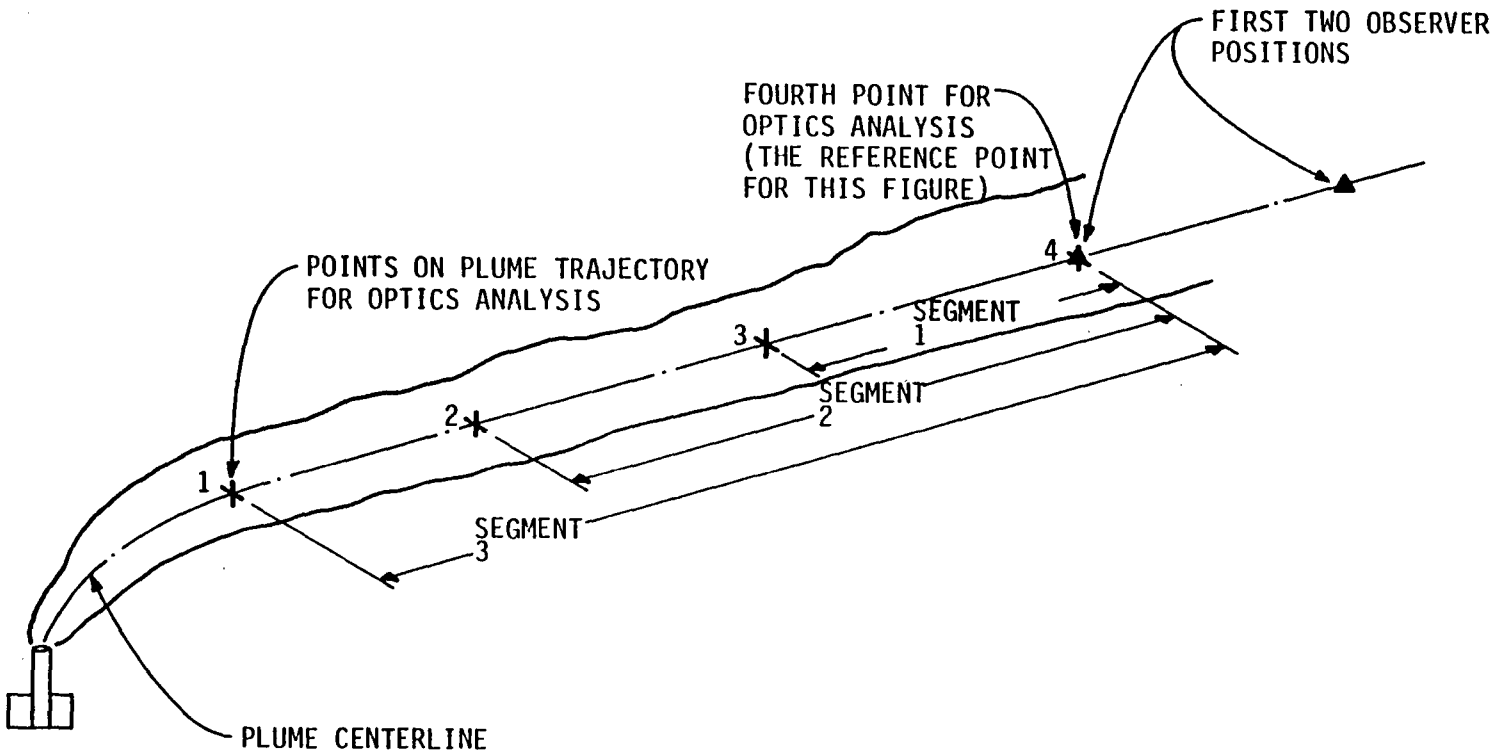

FIGURE A-10. GEOMETRIES FOR PLUME-BASED CALCULATIONS FOR HORIZONTAL VIEWS ALONG THE AXIS OF THE PLUME

the observer is looking toward the emissions source with a sky background. The calculations are made for views through plume segments defined by the particular point of analysis, as well as successive analysis points upwind. The calculations are repeated for observer positions at a range of distances from the downwind point at which the plume segment is assumed to end.

The observer-based geometry used for views through the plume center with a clear sky background is shown in figure A-11. At each point of analysis along the plume trajectory, the optics calculation is made for only one scattering angle, one plume-observer distance, and one azimuthal angle specific for the source position, observer position, wind direction, date, and time of day used as input.

For calculations with white, gray, and black viewing backgrounds, the geometries are the same as those for horizontal views with a sky background (figure A-11), with the addition of the specific background object distance, along each line of sight, from the observer through the points on the plume trajectory.

Figure A-12 is a plan view of the geometry for an observer-based calculation for views along the plume. At each analysis point along the plume trajectory, the centerline concentration is integrated along a segment on the line of sight that would correspond to a Gaussian distribution. The line of sight is always horizontal. The calculation is performed for a clear sky background and for white, gray, and black viewing objects at the specific distance for each line of sight.

It should be noted that if the distance (r_p) and azimuthal angle (α) are such that the observer is within the plume, the total plume optical thickness along the line of sight is reduced accordingly. The calculated distance r_p is the distance between the observer and the centroid of plume material viewed by him.

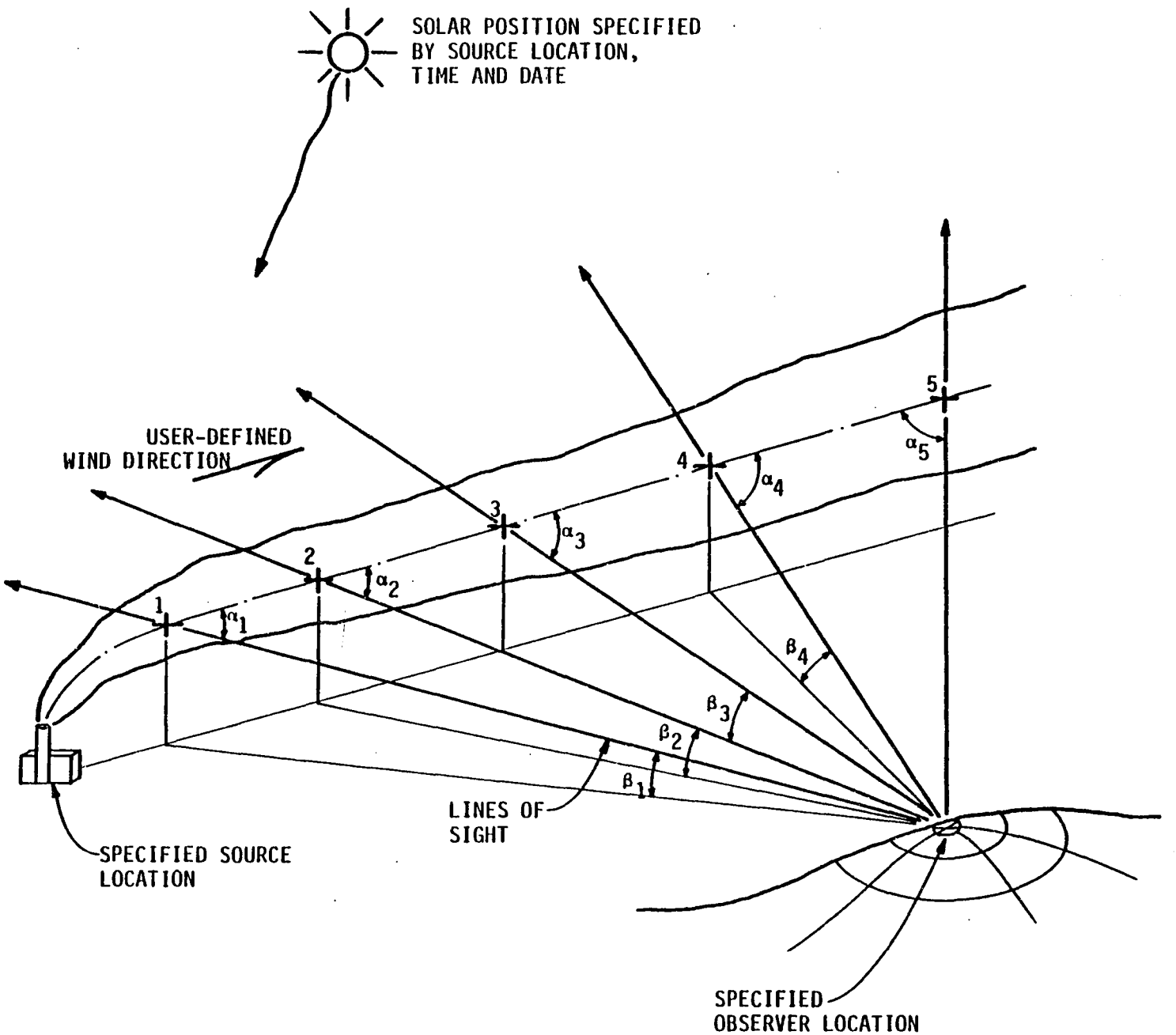

FIGURE A-11. GEOMETRY USED FOR OBSERVER-BASED CALCULATIONS FOR NONHORIZONTAL VIEWS THROUGH THE PLUME FOR CLEAR-SKY BACKGROUNDS

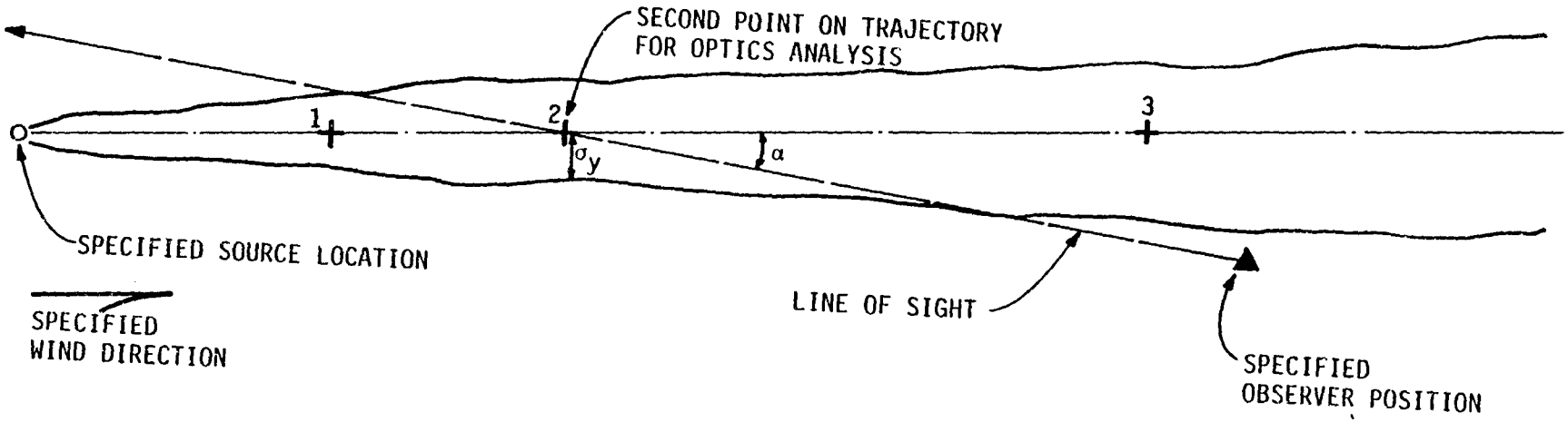

FIGURE A-12. PLAN VIEW OF GEOMETRY FOR OBSERVER-BASED CALCULATIONS FOR VIEWS ALONG THE PLUME

REFERENCES

American Society for Testing and Materials (1974), "Standard Method of Specifying Color by the Munsell System," D1535-68, Philadelphia, Pennsylvania.

Bergstrom, R. W., et al. (1980), "Comparison of the Observed and Predicted Visual Effects of Power Plant Plumes," paper accepted for presentation at the Conference on Plumes and Visibility: Measurements and Model Components, 12-14 November 1980.

Briggs, G. A. (1972), "Discussion on Chimney Plumes in Neutral and Stable Surroundings, "Atmos. Environ., Vol. 6, pp. 507-610.

Briggs, G. A. (1969), "Plume Rise," U.S. Atomic Energy Comission Critical Review Series, TID-25075, National Technical Information Service, Springfield, Virginia.

Briggs, G. A. (1971), "Some Recent Analyses of Plume Rise Observations," in Proc. of the Second International Clean Air Congress, H. M. Englund and W. T. Berry, eds., pp. 1029-1032 (Academic Press, New York, New York).

Bury, J. R., et al. (1980), "Applicant's Response to Attachment 1 of the Commission's Order Accepting Notice of Intention with Conditions," California Coal Project, D. Visibility, pp. I-28-I-39, Docket No. 79-NOI-3, California Energy Resources Conservation and Development Commission, Sacramento, California.

Committee on Colorimetry (1963), "The Science of Color," Optical Society of America, Washington, D.C.

Holzworth, G. C. (1972), "Mixing Heights, Wind Speeds, and Potential for Urban Air Pollution Throughout the Contiguous United States," AP-101, Office of Air Programs, Environmental Protection Agency, Research Triangle Park, North Carolina.

Horvath, H. (1971), "On the Brown Colour of Atmospheric Haze," Atmos. Environ., Vol. 5., pp. 333-344.

Husar, R. B., and W. H. White (1976), "On the Color of the Los Angeles Smog," Atmos. Environ., Vol. 10, pp. 195-204.

Johnson, C. D., et al. (1980), "User's Manual for the Plume Visibility Model (PLUVUE), 28-ES80-160R, Systems Applications, Incorporated, San Rafael, California.

Latimer, D. A., and R. G. Ireson (1980), "Workbook for Estimating Visibility Impairment," 65-ES80-105R, Systems Applications, Incorporated, San Rafael, California.

Latimer, D. A., and G. S. Samuelsen (1978), "Visual Impact of Plumes from Power Plants," Atmos. Environ., Vol. 12, pp. 1455-1465.

Latimer, D. A., and G. S. Samuelsen (1975), "Visual Impact of Plumes from Power Plants," UCI-ARTR-75-3, UCI Air Quality Laboratory, School of Engineering, University of California, Irvine, California.

Latimer, D. A., et al. (1978), The Development of Mathematical Models for the Prediction of Anthropogenic Visibility Impairment," EPA-450/3-78-110a, b, and c, EF78-63A and B, Systems Applications, Incorporated, San Rafael, California.

Middleton, W.E.F. (1952), Vision Through the Atmosphere (University of Toronto Press, Toronto, Canada).

Singh, H. B., F. L. Ludwig, and W. B. Johnson (1978), "Tropospheric Ozone: Concentrations and Variabilities in Clean Remote Areas," Atmos. Environ., Vol 12, pp. 2185-2196.

1. Report No.	2. Government Accession No.	3. Recipient's Catalog No.
NASA CR-163103		

4. Title and Subtitle	5. Report Date
ASSESSMENT OF THE VISIBILITY IMPAIRMENT CAUSED BY THE EMISSIONS FROM THE PROPOSED POWER PLANT AT BORON, CALIFORNIA	December 1980
	6. Performing Organization Code

7. Author(s)	8. Performing Organization Report No.
R. W. Bergstrom, J. R. Doyle, C. D. Johnson, H. Y. Holman, and M. A. Wojcik	H-1143
	10. Work Unit No.

9. Performing Organization Name and Address	11. Contract or Grant No.
Systems Applications, Incorporated 950 Northgate Drive San Rafael, California 94903	NAS4-2745
	13. Type of Report and Period Covered
12. Sponsoring Agency Name and Address	Contractor Report - Final
National Aeronautics and Space Administration Washington, D.C. 20546	14. Sponsoring Agency Code

15. Supplementary Notes

NASA Technical Monitor: Victor W. Horton, Dryden Flight Research Center

16. Abstract

A site about 20 kilometers northeast of Edwards Air Force Base has been chosen as one possible location for a 1500 megawatt coal-fired power plant. The plant would consume about 20,000 metric tons of coal per day when operating at maximum capacity.

The Naval Weapons Center at China Lake, California, NASA Dryden Flight Research Center at Edwards, California, and the Air Force Flight Test Center at Edwards Air Force Base are concerned that the power plant plume could have a detrimental effect upon flight test operations and optical tracking of targets in the test ranges within a 100 kilometer radius of the plant.

The current atmospheric conditions and visibility were modeled, and the effect of the power plant effluent was then added to determine its influence upon the prevailing visibility--the actual reduction in visibility being a function of meteorological conditions and observer-plume-target geometry. In the cases investigated, the perceptibility of a target was reduced by a minimum of 10 percent and a maximum of 100 percent. This significant visual impact would occur 40 days per year in the Edwards area with meteorological conditions such as to cause some visual impact 80 days per year.

17. Key Words (Suggested by Author(s))	18. Distribution Statement
Visibility Visual impact of air pollution Visibility modeling	Unclassified - Unlimited Subject category 45

19. Security Classif. (of this report)	20. Security Classif. (of this page)	21. No. of Pages	22. Price*
Unclassified	Unclassified	161	$11.00

For sale by the National Technical Information Service, Springfield, Virginia 22161

End of Document